The Co-Combustion Performance of South African Coal and Refuse Derived Fuel

---

Prepared by

Kerina Isaac (672563)

Submitted to

School of Chemical and Metallurgical Engineering, Faculty of Engineering and the Built Environment, University of the Witwatersrand, Johannesburg, South Africa, in fulfillment of the requirements for the degree of Master of Science in Engineering.

Supervisor(s): Dr. S. Bada and Emeritus Professor. R. Falcon

November 2019

DECLARATION

I declare that this dissertation is my own unaided work, unless otherwise stated and acknowledged. It is being submitted for the degree of Master of Science in the School of Chemical and Metallurgical Engineering, to the University of Witwatersrand, Johannesburg. It has not been submitted before for any degree or examination to any other university.

Signed: ……on this …… day of …….. Year……..

ABSTRACT

This research focuses on the co-firing of low-quality coal with refuse derived fuel (RDF) as a means to utilise some of the abundant high-ash coal available in South Africa as a fuel co-fired with RDF in existing pulverised fuel boilers. The use of RDF is also a means to reduce the volume of waste dumped in landfill sites. The physicochemical characteristics of the RDF, run of mine coal (ROM) and discard coal were investigated, along with the co-combustion behaviour and kinetics of the RDFs, coal and their blends at different weight ratios. The blends tested contained 85%, 70%, 50% and 25% coal with the remaining proportion made up of RDF. The gaseous emissions and ash residue from the combustion of coal, RDF and coal/RDF blends were also analysed to determine the environmental impact of co-firing with RDF.

The physicochemical analysis revealed that the run-of-mine and discard coal have relatively low calorific values of 21.7 MJ/kg and 16.7 MJ/kg, respectively. The RDF samples were comprised of plastic and paper, as well as smaller amounts of other materials. The RDF sample containing mostly plastic (PL) and the other containing mostly paper (PB) were found to have higher energy contents of 31.2 MJ/kg and 22.4 MJ/kg, respectively. The thermogravimetric analysis was performed in an atmosphere of air, over a temperature range of 25 – 850°C, and the results showed that the RDF samples had lower ignition, devolatilisation, and burnout temperatures compared to the coals. The ignition temperatures for the blended fuel occurs in the lower temperature region when RDF is added to the blend, likewise the peak temperatures and burnout temperatures shifted to a lower temperature zone. The activation energies (E_a) were determined using the Coats-Redfern method. The E_a for the ROM coal of 104.4 kJ/mol, was found to reduce to 31.4 kJ/mol for 75% PB + 25% coal and 35 kJ/mol for 75% PL + 25% coal blends, respectively. The discard coal which had an E_a of 109.9 kJ/mol was reduced to 30.9 kJ/mol with the (paper blend) and 33.5 kJ/mol with the (plastic blend) for the 75% RDF + 25% coal discard blends.

The analysis of the ash for the chloride and alkali metal content in the RDFs, coal samples and their blends were determined with the use of ion chromatography and X-ray fluorescence (XRF) techniques. The co-combustion ash of discard coal and RDF showed a decrease in chloride and alkali metal content as the ratio of coal was increased in the blend. The calculated slagging and fouling indices showed that as the coal ratio in the blend increases, the propensity of the fuel to slag and foul the boiler surfaces decreases. The propensity to slag was found to

be low for the ash obtained from the co-fired blends, while the propensity to foul decreased from high to medium range for all the blends with less than 75% of the RDF PB.

The concentration of gases emitted from the combustion and co-combustion test was determined with the aid of an MGA 11 mobile gas analyzer connected online at 1 scan per second. The co-combustion of RDF with coal showed a decrease in SO_2 emissions from (387 ppm) for the discard coal to within the legislated maximum emission for South African new coal fired plants. This was attained with samples containing > 15% PL and > 30% PB RDF. The lowest SO_2 emission of 50 ppm was achieved for the blend of 25% discard coal (C2) + 75% PL. The RDF sample (PL) emitted the highest NO_x emission of 143 ppm. The peak concentration of NO_x emitted was increased with the addition of RDF during co-combustion, however, the duration of the emission was greatly reduced and all samples were within the South African standard limits. There was also an increase in the emissions of CO and CO_2 which could be due to the high volatile matter content of the RDF. The lowest CO_2 emissions was 6000 ppm and this was achieved with the blend of 85% C2 + 15% PB.

It was established in this study that the most favourable fuel blend that could be used for power generation is that of discard coal (70%) and PL (30%). This was based on the activation energy obtained from this blend, with the lowest apparent activation energies of 55.8 kJ/mol and 54.2 kJ/mol for the volatile and char combustion, respectively. This makes this blend the preferred alternative fuel to be fired in the existing pulverised fuel boilers, or other type of industrial boilers, in South Africa.

ACKNOWLEDGEMENTS

I would like to thank my supervisor Dr S.O Bada for all his help and direction throughout this research study. I would also like to thank my co-supervisor Prof R.M.S Falcon for her supervision.

To my family, thank you for your support and encouragement.

I give thanks to Interwaste, South Africa for providing the refuse derived waste used in this study. As well as valuable information on the RDF material used in this study.

I gratefully acknowledge with thanks the financial support of National Research Foundation of South Africa's SARChI Clean Coal Technology Grant (Grant Number: 86421). In addition. Opinions, findings and conclusions expressed are those of the authors and NRF accepts no liability whatsoever in this regard.

TABLE OF CONTENTS

LIST OF FIGURES

LIST OF TABLES

CHAPTER 1: INTRODUCTION

1.1. BACKGROUND AND MOTIVATION

According to Eskom, the major power utility company in South Africa, the amount of electricity generated from the coal-fired power plants in the country increased to 91% in 2018, out of the total 221 936 GWh of electricity produced (Eskom, 2018). The Koeberg nuclear power plant generated 6.4%, and the remaining 2.6% of all South Africa's electricity was from hydro power and other renewable energy sources (Eskom, 2018). The integrated resource plan (IRP) foresees that this high percentage is likely to remain the same over the next 30-40 years in order to prevent the negative impact its decline would have on the South African economy (Lilley, 2015).

The electricity price in South Africa has greatly increased in the past years and coal shortages are also being experienced, with the shortfall ranging between 60 to 120 Mt (Jeffrey, et al., 2014). Some of the other challenges associated with coal are the increasing ash content of coals for domestic use, coalfields for future use are located further away and require infrastructure and development before they can be used, and there is also the challenge of transport of coal from the remote coalfields to the points of use (Jeffrey, et al., 2014). There is more than a billion tons of coal discard in the country and this is required to be utilized (DME, 2001; Belaid, et al., 2013), In addition, the production of acid mine drainage and the CO_2, SO_x and NO_x emissions associated with coal combustion are of great environmental concern for the future utilization of coal (Jeffrey, et al., 2014). In 2014, South Africa's greenhouse gas emissions amounted to 510 million tonnes and was one of the Top 20 GHG emitting countries in the world (WRI, 2014).

Over 2.01 billion tonnes of waste was produced worldwide in 2016, which is expected to increase to 3.4 billion tonnes by 2050 (WorldBank, 2019). South Africa produces about 54.2 million tons of waste per year, of which only 38.6% is recycled and 61.4% is dumped in landfills (DEA, 2018). In South Africa, landfilling remains the dominant choice for both general and hazardous waste management. South Africa's waste management strategy aims at shifting the focus from collection and disposal of municipal solid waste (MSW) to waste minimisation (DEA, 2012). It is highly important that research into the utilization of this resource, with a view of separating out the combustible fractions for power generation should

be conducted. Refuse derived fuel (RDF) is made up of combustible materials derived from MSW, commercial, or industrial waste, through sorting (Vekemans & Chaouki, 2016). It is a more homogenous fuel with a higher calorific value and energy density compared to the municipal solid waste. The co-firing of coal with RDF could be an option which can be implemented in the existing infrastructure of coal power plants to supplement the declining coal supply and reduce the costs of energy production, as waste is abundant and renewable (Aderoju, et al., 2017). Surveys have indicated that the discharge of greenhouse gas (GHG) could be brought down with the co-firing of this fuel with coal, thereby, reducing the gases and leachate from landfill sites, as considerably as the amount of waste at these sites (Vekemans & Chaouki, 2016).

In this investigation, the physicochemical properties of the coal and RDF samples were analysed and the estimated potential energy content in the RDF produced in SA for power generation, through combustion, was calculated by using the lower heating value (LHV) of the RDF fractions involved in this study. The combustion and co-combustion characteristics of RDF with coal at different percentage ratios were reported and the activation energy from the co-combustion of each blend was determined using the model-fitting Coats-Redfern method. The impact of coal on the reduction of chlorine and alkaline content of ash from RDF combustion was determined through ash analyses and the concentration of CO_2, CO, SO_2 and NO_x gases emitted during the co-firing was also reported.

1.2. AIM AND OBJECTIVES

This study seeks to utilize South African high ash coal, as well as reduce the volume of waste dumped on landfills, by co-firing coal with RDF. The aim is to determine the co-combustion blends which produce the most favourable combustion characteristics, as well as minimise harmful gaseous and ash emissions. The objectives of this research are to determine:

- The physicochemical properties of the RDF and coal samples.
- The energy potential of the RDF resource in South Africa.
- Combustion characteristics of RDF, coal and RDF-coal blends.
- Kinetics of the combustion and co-combustion using the Coats-Redfern method.

- Evaluate the slagging and fouling tendency of the ash produced from the co-combustion of RDF and coal
- Evaluate the concentration of the CO_2, CO, SO_2 and NO_x emitted from the RDF, coal and RDF-coal blends combustion

1.3. HYPOTHESIS

RDF will ignite and burnout completely at a lower temperature compared to the coal. It is also expected that the slagging and fouling tendency of the ash will reduce with co-firing compared to RDF combustion alone and that the concentration of the NO_x, SO_2, CO and CO_2 emitted during combustion will be less with co-firing than with coal combustion alone.

1.4. RESEARCH QUESTIONS

The research questions presented below will be addressed through achieving the objectives of this research.

- What is the heat content of RDF in South Africa?
- What are the physicochemical properties of the RDF and coal?
- How does the proximate analysis of RDF compare to that of coal?
- How does the ultimate analysis of RDF compare to that of coal?
- How does the combustion performance of RFD and RDF-coal blends differ from that of coal?
- What is the reaction kinetics for the combustion of RDF, coal, and RDF-coal blends?
- What percentage of RDF in the blended fuel results in the best co-combustion performance?
- What is the concentration of the SO_2 and NO_x, CO_2, CO from the combustion of RDF, coal and RDF-coal blends?
- How do the ash constituents change for coal, RDF and RDF-coal blends?

1.5. LAYOUT OF THE DISSERTATION

This dissertation is comprised of five chapters which cover the following:

1. Chapter One introduces the topic of this research with a background and motivation for the study. The research aim, objectives and hypothesis of the study are also included and the list of research questions which will be answered with this research are presented.
2. Chapter Two is a literature review which gives an overview of the electricity generation and use of coal in South Africa. Refuse derived fuel and its uses are explained in greater detail and published literature on the co-combustion of coal and RDF, as well as the gaseous emissions and ash emissions associated with it are explored.
3. Chapter Three outlines the materials and methodology used in this research. The detailed experimental procedure, equipment and standards used are covered in this chapter.
4. Chapter Four presents the results of the experimental work outlined in Chapter 3, as well as the discussion of the significance of the results. The results include the characterization of the raw materials, the combustion and co-combustion performance of the coal and RDF samples and their reaction kinetics. The gaseous emissions analysis and the ash characterization from the co-combustion is also discussed.
5. Chapter Five gives the conclusions of the research as well as the recommendations for future research.

CHAPTER 2: LITERATURE REVIEW

This research investigates the co-combustion performance of South African coal and refuse derived fuel (RDF) in order to determine the possibility of co-firing these fuels for power generation. As such, this chapter covers an overview of electricity generation in South Africa from coal, other uses of coal and the available coal quality in South Africa. In addition, refuse derived fuel is explained in greater detail and published literature on co-combustion and environmental concerns is explored. The significance of thermogravimetric analysis for determining the reactivity of the fuels utilized and the reaction kinetic model applied is also discussed.

2.1 ELECTRICITY GENERATION IN SOUTH AFRICA

Coal contributed about 88.3% (215 691 gigawatt-hours) to the total energy mix in South Africa according to the 2013 report by the "*Electricity, gas and water supply industry"* (StatsSA, 2018). The dominance of coal decreased slightly to 85.7% (203 114 gigawatt-hours) of electricity generated in 2016, before increasing to 91% (202 106 gigawatt-hours) in 2019 (StatsSA, 2018; Eskom, 2019). In 2016, the contribution from coal-fired power stations was followed by 5.2% from nuclear power and 3.2% from natural gas, with the full breakdown depicted in Figure 2.1. In 2019, the nuclear power share increased to 6.4% of the total electricity (14 193 GWh) (Eskom, 2018). Wind power contributed 2 126 gigawatt-hours in 2016, this was reduced to 331 gigawatt-hours in 2019 (StatsSA, 2018; Eskom, 2019). Solar power did not feature as a source of electricity production in 2013, but in 2016 it contributed about 2 151 gigawatt-hours (StatsSA, 2018).

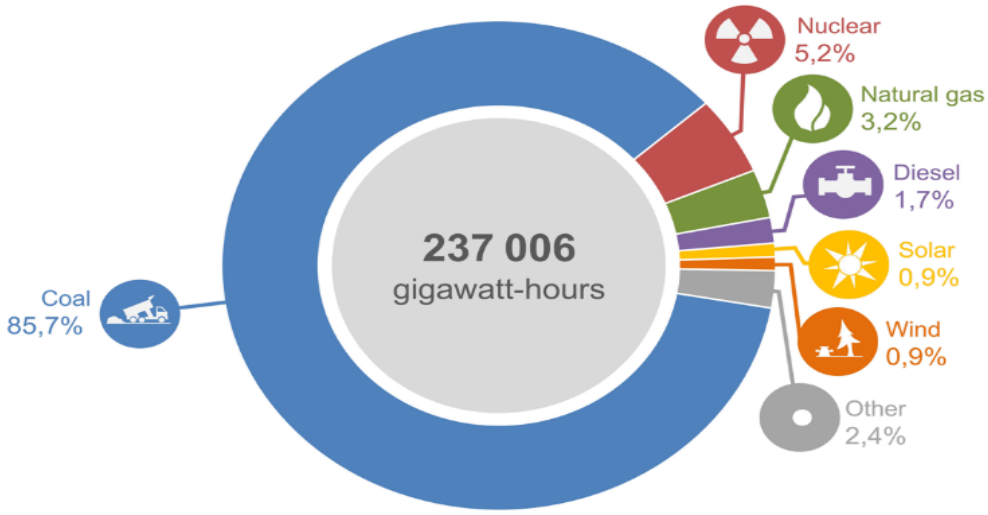

Figure 2. 1: South Africa's total electricity generated in 2016 (StatsSA, 2018)

Coal is a dominant fuel for electricity production in South Africa and this is due to the abundant reserves of coal in the country, and the relatively low production costs compared to other energy sources. The use of coal also contributes to the economy; in 2008 its surpassed gold in its contribution to the gross domestic profit (StatsSA, 2018). In addition, in 2013, it contributed approximately R51 billion to South Africa's economy, in comparison to gold which contributed R31 billion. In the same year, it became the highest foreign exchange earning commodity with an overall value-added contribution of 22.5%, compared to PGM (platinum group metals) at 21.0% and gold at 18.5% (StatsSA, 2014). Coal is the leading mining commodities revenue generator for the country with a total of R119 billion total revenue in 2017, followed by the platinum group metals, gold and iron ore (PWC, 2017). In addition, nearly 100% of the country's carbon reductants in the metallurgical industry, and heat and power for up to 6 000 industrial users such as pulp and paper, cement, sugar, mining and agriculture, are produced from coal (FFF, 2017).

2.2 THE COAL RESOURCE IN SOUTH AFRICA

The formation of coal, which occurs through a process known as coalification, determines the quality of the coal. Coal in South Africa was formed in cold swamps in glacial valleys, lakes and shallow seas during the Permian period, around 300 million years ago (Falcon & Ham, 1988). Plant matter which was either present in the swamps or was washed there by floods, including cold climate deciduous forest plants to warm climate woodland plants and reeds were involved in the formation of the coal (Falcon & Ham, 1988). The plant matter in a peat mire undergoes chemical and physical changes as it is degraded by oxygen and microorganisms (Schweinfurth, 2009). When oxygen is depleted, further degradation is achieved with anaerobic microorganisms (Schweinfurth, 2009). Once the plant matter has been converted to peat and has been buried, the coalification process continues through the increase in temperature and pressure (Schweinfurth, 2009). Higher temperatures are known to eliminate moisture and volatile matter, thereby producing higher ranked coals with higher calorific values (Schweinfurth, 2009). In southern Africa the coal seams were not buried very deeply and are easier to mine in comparison to coal seams in the northern hemisphere (Falcon & Ham, 1988). In the southern hemisphere hot volcanic lava has made intrusions into the coal seams, which has resulted in a wide variety of coal qualities within localised areas (Falcon & Ham, 1988). In Africa, the sequence of sediments which occurred is known as the Karoo System, this was divided into four series; the Stormberg, Beaufort, Ecca and Dwyka Series (Rensburg, et al., 1969). The main vegetation and coal development occurred during the Middle Ecca Stage (Rensburg, et al., 1969).

South Africa possesses around 30 billion tonnes of coal, of which the greatest proportion is bituminous coal, which is 3.5% of the world's total coal resources, in addition, 3.3% of the worlds annual coal production comes from South Africa (CoM, 2018). The country has 19 coalfields, which can be found in the Kwa-Zulu Natal, Mpumalanga, Limpopo and the Free State provinces (Jeffrey, 2005). Almost 83% of the coal mined in South Africa comes from Mpumalanga (CoM, 2018). With the depleting coal reserves in the Mpumalanga region, most of the major mining houses, including the junior miners are now shifting their operations to the Waterberg region (Jeffrey, 2005).

In South Africa, the majority of coal mined is utilised in three major sectors; power generation, liquid fuels and chemical production, and the metallurgical industry, as depicted in Figure 2.2. South Africa exports around 30% of the domestic coal produced, in 2016 this amounted to 69

Mt, making South Africa sixth in the world in terms of volume of coal exported (CoM, 2018). Coal exports from South Africa have seen a shift from the European markets to the Asian markets, with India accounting for around half of the volume of the total exports from SA (CoM, 2018). The exportation of coal to the European market began declining with the implementation of the Kyoto Protocol imposing strict greenhouse gas emission targets (CoM, 2018).

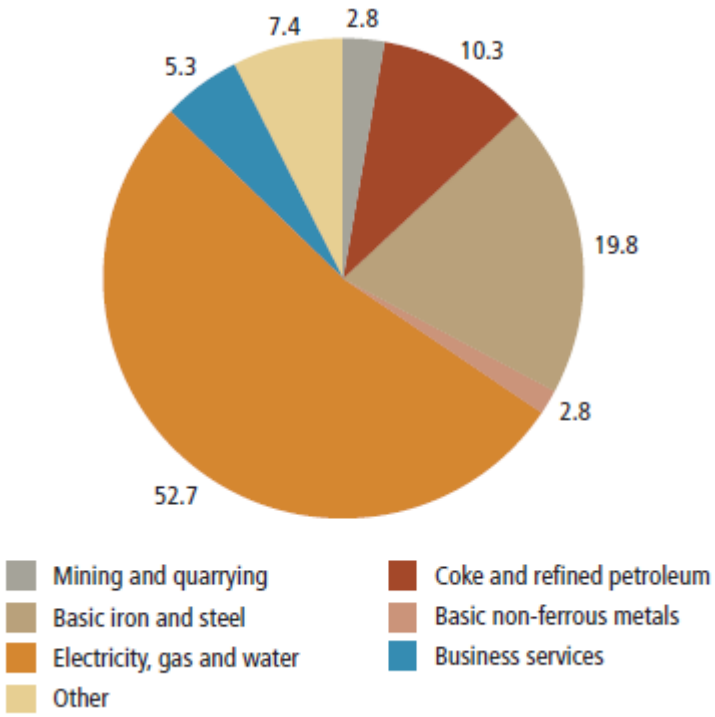

Figure 2. 2 Coal Demand from Industries in 2015 (CoM, 2018)

In 2016, the SA coal industry was responsible for 17% of the total employment in the mining sector, which amounted to R21 billion in wages and salaries (CoM, 2018). The importance of the coal industry is highlighted by the 173 093 jobs created indirectly, through the procurement of goods and services (CoM, 2018). These jobs were mainly created in the transport and storage industries (CoM, 2018). The major constraints on the growth of the coal industry in South Africa include policy and regulations which aim to reduce carbon emissions, access to capital due to regulations, and reductions in the credit extended for the purposes of building new coal-fired power stations (CoM, 2018). In addition, there is a lack of water and adequate rail infrastructure in the Waterberg region, which is limiting investment in coal mining in that region (CoM, 2018).

2.3 COAL QUALITY

Coal quality is influenced by the minerals and macerals present in the coal as well as the coal rank, porosity, moisture content, surface area, weathering, particle size and degree of oxidation (Falcon & Ham, 1988). These factors affect the combustion of coal and are inherent characteristics of the coal which developed as the coal was formed. In South Africa, various boiler designs are utilised for electricity production, therefore it is important to ensure that the coal quality being utilised is well suited to the boiler type (Wagner, et al., 2018). For instance, fluidised bed combustion (FBC) operates at lower temperatures and is more flexible to coal quality than pulverised fuel boilers (Wagner, et al., 2018). Coal quality is also important when coal is used in other applications such as gasification, liquefaction and carbonization. There are a variety of gasification processes which can be used and each requires different fuel quality. For instance, the fixed-bed-dry-bottom gasification process can be used for all coal qualities, while the Winkler and Koppers-Totzek process uses only medium ranked bituminous coals (Wagner, et al., 2018). Coal beneficiation technologies are used in South Africa to upgrade the relatively low-grade and high-ash coal that is mined in the country to produce coal of different qualities for different applications (Prevost, 2003). Some of the liquid fuel and chemical production plants in the country make use of run-of-mine (ROM) coal, while other local users such as the metallurgical industry and industrial small boilers wash coal to improve its quality (Prevost, 2003).

2.3.1 COAL MINERALS

Minerals in coal can either be intrinsic or extrinsic, the former are minerals which were present in the plant matter before the formation of the coal, while the latter are minerals deposited through percolating water into fractures or cavities long after the formation of peat (Wagner, et al., 2018). The mineral content of coals from the Mpumalanga coalfields can range between 8 - 35% of the coals weight (Wagner, et al., 2018). The inorganic minerals present in coal have an effect on the ash and the gases produced when the coal is burned (Schweinfurth, 2009).

The most abundant minerals present in Southern African coals are minerals from the clay group, which can amount to up to 80% of the minerals contained in the coal (Wagner, et al., 2018). Other common minerals present in coal include pyrite, quartz and carbonate group minerals; such as calcite, ankerite and siderite (Falcon, 2013). Less common minerals in coal include phosphorous bearing minerals such as apatite, uranium bearing minerals such as zircon,

and antimony bearing minerals such as rutile (Falcon, 2013). The slagging and fouling tendency of the ash produced from the coal is dependent on the minerals present in the coal (Schweinfurth, 2009). Coal ashes contain mostly alumina, silica and iron oxides, as well as smaller amounts of calcium and magnesium oxides (Sharma, et al., 2014). The alumina, silica and titanium oxides increase the ash fusion temperature as they have melting points between 1600 and 1900°C (Sharma, et al., 2014). Other oxides and alkalis reduce the AFT, for instance SO_3 has the highest propensity to reduce the AFT, this is followed by CaO, MgO, Fe_2O_3 and Na_2O respectively (Ji, et al., 2016). Quartz (SiO_2) and pyrite (FeS_2) can also form abrasive ash deposits due to their non-spherical structure (Sharma, et al., 2014).

2.3.2 COAL MACERALS

Macerals are particles of organic matter present in the coal. Macerals can be grouped into three types, namely, vitrinite, liptinite and inertinite (Schweinfurth, 2009). The inertinite group of macerals can be further broken down into fusinite and semi-fusinite maceral groups. The type of coal is determined from the majority of the maceral groups present, as can be seen in Table 2.1.

Table 2. 1 Classification of coal by maceral type (Falcon, 2013)

Coal type	Vitrinite macerals	Liptinite macerals	Inertinite macerals
Vitric coal	> 65%	-	-
Fusic coal	-	-	> 65%
Intermediate-fusic coal	< 65%	< 17.5%	17.5 - 55%
Liptic coal	-	> 65%	-
Intermediate-liptic coal	< 65%	< 17.5%	17.5 - 25%

The importance of the maceral groups contained in a coal is due to the difference in reactivity and rate of oxidation of the different macerals (Falcon & Ham, 1988). Vitrinite macerals come from wood deposited in shallow waters and they appear grey and homogenous (Falcon, 2013). These macerals are oxidised easily, they have considerable volatile matter content and are easy to combust with a short burnout time (Falcon, 2013). Liptinite macerals are formed from spores, pollen, leaf cuticles, wood resins and algae deposits and they contain more hydrogen

than vitrinite or fusinite (Falcon, 2013). These macerals oxidise at a more rapid rate and is more reactive and volatile-rich than both vitrinite and inertinite (Falcon & Ham, 1988). The inertinite macerals of the fusinite sub-group appear white and come from the cell walls of wood that have been oxidised or burned to some degree (Schweinfurth, 2009). These macerals are not very volatile and oxidise at a slower rate than vitrinite or liptinite, they are difficult to combust and have a long burnout time (Falcon, 2013). The inertinite macerals of the semi-fusinite subgroup appear pale grey and come from the cell walls of woody tissue, from wood which was deposited in semi-wet conditions (Falcon, 2013). These macerals are moderately volatile with a moderate burnout time, they also combust more easily than the macerals of the fusinite sub-group (Falcon, 2013).

The macerals of coal can range between mainly vitrinite to mainly fusinite (Schweinfurth, 2009). Coals with primarily vitrinite macerals are shiny and black, whereas coals with mainly fusinite macerals are dull and dusty (Schweinfurth, 2009). A band of macerals, greater than 50 μm, containing one or more types of macerals is termed a microlithotype (Falcon & Ham, 1988). The microlithotypes in a coal influence the properties of the coal such as the strength and density as well as the suitability of the coal for combustion, gasification or coking (Falcon & Ham, 1988). For instance, a coal with microlithotypes which are heterogenous can contain too many contaminants which prevent the formation of pores in the coal and thereby negatively affect the behaviour of the coal for combustion and metallurgical application (Falcon & Ham, 1988).

2.3.3 COAL RANK

Coal rank is a measure of the coals maturity and is a factor used to determine the quality of coal. (Rensburg, et al., 1969). The coal ranks from lowest to highest are peat, lignite, sub-bituminous, bituminous coal, and anthracite (Rensburg, et al., 1969). The rank of a coal is determined by the amount of fixed carbon, total moisture and volatile matter content in the coal (Schweinfurth, 2009). Coals which have been buried deeply for a long period of time, will tend to have a higher rank as it was subjected to higher temperatures during the coalification process (Schweinfurth, 2009). The characteristics of coal depend on its rank on a pure basis (moisture-free and mineral-free coal) (Rensburg, et al., 1969).

- Higher ranked coals have a higher carbon content.
- Oxygen content increases with increasing rank.
- Hydrogen content and volatile matter decreases in higher ranked coal, this is termed 'low-volatile coals'.
- Moisture content decreases with increasing rank, but increases slightly in anthracite.
- The calorific value increases as rank increases, however calorific value decreases slightly in anthracite.
- Chemical reactivity increases as rank increases.

Coal strength is relatively constant until it matures up to the medium volatile bituminous stage where the strength decreases, then increases again in the anthracite stage (Rensburg, et al., 1969). The rank of the coal has an effect on the ignition and peak temperature of the coal during combustion, as well as the devolatilization rate and the reactivity of the char produced from the combustion (Falcon & Ham, 1988). Therefore, the rank of coal must be considered when selecting a coal in regard to the operating temperature of the furnace or fluidised bed reactor (Falcon & Ham, 1988).

2.4 COAL COMBUSTION

Coal combustion is the generation of thermal energy due to the oxidation of the combustible matter in the coal in the presence of heat (Falcon & Ham, 1988). Coal is made up of mainly carbon, water, hydrogen and oxygen, with much smaller amounts of nitrogen, sulfur and various minerals (Shen, n.d.). When coal is heated moisture is driven off at around 100°C, this is followed by a two-stage process; the release and combustion of the volatile matter which is referred to as pyrolysis and the combustion of the char (Wagner, et al., 2018). The heating of the coal to release the volatile matter is referred to as devolatilization, and the temperature at which this begins is called the initiation temperature of the volatile matter (IT_{VM}) (Cumming & McLaughlin, 1982). The weight loss rate of the volatile release is roughly linear until around 450°C when the combustion of the fixed carbon begins and the weight loss rate accelerates. The temperature at which the char combustion begins is referred to as the initiation temperature of the fixed carbon (IT_{FC}). During char combustion oxygen diffuses into the char particles; combusting the char and releasing gases, as can be seen in Equation (2.1) (Wagner, et al., 2018).

$$C + O_2 \rightarrow CO_2 \qquad \text{Equation 2.1}$$

The carbon within coal is mostly bound by single bonds, the energy required to break this bond is about 83 kcal/mole (Hossain, 2018). In order for the carbon to react with the oxygen, the double bond between the two oxygen molecules must be broken and this requires about 119 kcal/mole (Hossain, 2018). The total energy required for the reaction between carbon-oxygen is about 202 kcal/mole, on the other hand, the release of energy amounts to 354 kcal/mole which is a net energy release of 152 kcal/mole if there is sufficient oxygen for complete combustion (Hossain, 2018). The main by-product of coal combustion is carbon dioxide. Nitrogen in coal is generally released as N_2 or NO_2 gas and sulfur as SO_2 gas (Hossain, 2018). In cases where there is insufficient oxygen for combustion, CO gas will be produced as a by-product as shown by the reaction below (Hossain, 2018).

$$C + CO_2 \rightarrow 2CO \qquad \text{Equation 2.2}$$

2.5 IMPACT OF LOW-QUALITY COAL ON PULVERISED FUEL BOILERS

A pulverised fuel boiler is designed according to the expected quality of the coal to be used. When the coal supplied to the boiler does not meet these standards it results in challenges such as requiring increased supply, ash removal constraints, and damage to equipment (Umraw, 2019). Ash causes a change in the thermal behaviour inside the boiler, as the ash consumes energy as it is heated and begins to change phase (Jayanti, et al., 2007). The presence of large amounts of ash act as a barrier to the oxygen as it attempts to reach the char surface, thus it impedes the coal combustion. This effect is worsened when the ash begins to slag and soften (Jayanti, et al., 2007). In addition to these effects the ash formed in the boiler can slag and foul the boiler surfaces leading to negative effects on heat transfer and increasing the potential for corrosion.

Ash removal from the boiler is of great importance, failure to remove ash effectively results in partial load losses, and downtime due to planned and unplanned maintenance (Yelland, 2019). The high volume of ash produced from firing high-ash coal in pulverised boilers results in ash handling challenges which can become an environmental problem as emission limitations are exceeded (Yelland, 2019). The build-up of slag on boiler tubes can also result in tube leaks and the formation of large clinkers which can cause damage to the bottom of the boiler (Yelland,

2019). With the addition of RDF, some of the ash related issues being faced by pulverised fuel boilers in South Africa can be improved.

2.6 REFUSE DERIVED FUEL

2.6.1 COMPOSITION OF REFUSE DERIVED FUEL

A waste hierarchy produced by Vekemans and Chaouki (2016) according to the financial, environmental, social and management concerns, is depicted in Figure 2.3. The figure shows that waste reduction, reuse, recycling and recovery of waste are all preferable to waste disposal. Waste quantities can be reduced to a point, but there will always be some remaining. The reuse of waste is sometimes based on the availability of techniques to process the waste and the monetary value of recycling waste for different end products and materials (Vekemans & Chaouki, 2016). Some paper types are difficult to recycle due to the chemicals they contain, this includes waterproof paper, wax or polyethylene (PE) coated paper, and paper with adhesive layers; these papers can be co-combusted and used for energy production instead of being discarded (Malaťák, et al., 2018).

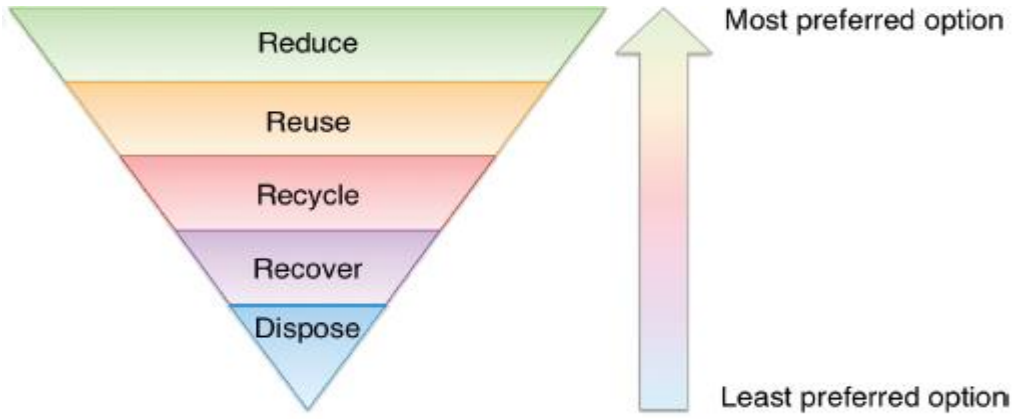

Figure 2. 3: Hierarchy of waste management options (Vekemans & Chaouki, 2016)

Refuse derived fuel (RDF) is made up of combustible materials, derived from municipal, commercial or industrial waste. The waste is transformed into a more homogenous fuel with a higher calorific value by sorting the waste and separating out the incombustible materials. The grade of the fuel can be improved by blending RDF with known calorific values through shredding, milling, and blending at different percentage ratios (Vekemans & Chaouki, 2016).

The high calorific value fraction of the RDF can generally be separated into a biogenic fraction and a plastic fraction (Vekemans & Chaouki, 2016). The biogenic materials include wood, paper and cardboards. These materials may contain a variety of additives used in their production such as pigments and binders (Vekemans & Chaouki, 2016). The various pigments, coatings and binders used in wood, paper and cardboard have an effect on the ash volume and composition produced from combustion (Tappi, 2007). The most common types of plastics found in RDF include polyethylene (PE), polypropylene (PP), polystyrene (PS), polyvinylchloride (PVC), polyethylene terephthalate (PET) and nylon (Cozzani, et al., 1994). Multi-material elements can also be found in RDF such as packaging containing both plastic and paper with an aluminium foil. The components in RDF has an effect on the combustion characteristics as well as the gaseous emissions and ash constituents. The biogenic materials in the RDF emit as much CO_2 when combusted as they have captured in their life cycle (Vekemans & Chaouki, 2016). Princeton (2014), also indicated that co-firing leads to the reduction in methane emissions from landfill sites, which has a heat trapping potential 30 times greater than carbon dioxide. The plastic fraction generally contains some chlorine, which can be harmful to the environment, on the other hand, the combustion of the biogenic fraction results in a high ash residue (Febrero, et al., 2015).

The different components contained in the RDF have an effect on its combustion performance. Akdag et al. (2016) compared the combustion performance characteristics of two RDF samples which were made up of approximately 60% textiles, 20% paper and 20% plastics. It was found that both the RDF samples displayed multiple peaks on the DTG plot which were due to the combination of the decomposition of the cellulose and the plastic in the samples (Akdag, et al., 2016). In a study conducted by Cozzani et al. (1994) three main components of RDF were identified, namely; paper containing cellulose, plant material containing cellulose, hemicellulose and lignin, and polyethylene plastic. This study found that the pyrolysis behaviour of cellulose occurred as a distinct weight loss step around 350°C while the degradation of plastic (PE) occurred as the second weight loss step between 450 and 500°C (Cozzani, et al., 1994).

A more recent pyrolysis study was conducted by Porshnov et al. (2018) on RDF components, the author found that paper, cardboard and natural rubber (latex) exhibited a three-stage degradation. The first stage was the decomposition of hemicellulose, followed by the decomposition of cellulose and lignin respectively (Porshnov, et al., 2018). The decomposition

of hydrocarbon waste plastics occurred at higher temperatures in comparison to the biogenic components and generally exhibited a single stage of decomposition (Porshnov, et al., 2018). The synthetic polymers; latex, vinyl and PS showed two stages of decomposition whereas the PP, PE, PET, nylon and nitrile rubber all exhibited one stage of decomposition (Porshnov, et al., 2018). The decomposition of halogenated waste plastics, such as PVC and vinyl rubber, takes place as a two-stage process (Porshnov, et al., 2018). In the decomposition of PVC, the first stage is due to the release of the corrosive HCl gas, which evolved between 260 to 300°C (Porshnov, et al., 2018).

2.6.2 USE OF RDF IN CEMENT PLANTS

One of the more common uses for RDF is an additive fuel in cement kilns. In Austria, Germany and Italy, MSW is mechanically and biologically treated to produce a refuse derived fuel, while in Belgium and Denmark MSW undergoes sorting to produce the RDF used in the cement plants (Gendebien, et al., 2003). In the Netherlands the MSW is sorted for paper and plastic which is compressed and pelletized before use in cement kilns (Kara, et al., 2008). The conditions of combustion in cement kilns are favourable for alternative fuels such as RDF, with temperatures up to 1450 $^{\circ}$C with little to no incineration wastes (Kara, et al., 2008). The long residence time in which waste is subjected to incineration in the cement kilns also allows for the disposal of hazardous waste (Kara, et al., 2008). An advantage of burning RDF in a cement kiln is that no adaptations need to be made to the kilns, the only modification required is the addition of the RDF handling system (Kara, et al., 2008). The use of RDF with a higher calorific value and a lower moisture content than coal has significant advantage such as the reduction of CO_2 emissions and ash residue (Chatziaras, et al., 2016). The economic advantage of using RDF in cement plants depends on the investment costs as well as the cost of coal compared to the cost of landfill disposal. Reducing the volume of MSW in landfill sites is an advantage which government may provide funding for in order to make use of RDF in cement plants more economically attractive (Kara, et al., 2008).

Chen et al. (2018) conducted a study in which the co-combustion characteristics of anthracite and RDF were tested in the environment of a precalciner which is used to heat up the raw material before it enters the cement kiln. The precalciner cement environment includes different temperature distribution as a result of the coal combustion endothermic reaction and the exothermic process of $CaCO_3$ decomposition (Chen, et al., 2018). It is also characterised

by two gas flows, one in which oxygen has a 21% concentration, and the other being the flue gas from the kiln, where O_2 is between 2 – 4% concentration (Chen, et al., 2018). The combustion profile for both RDF and anthracite show three reaction stages, namely; the moisture evaporation and preheating stage, the devolatilization stage and finally the char combustion (Chen, et al., 2018). The ignition temperature for the co-fired fuel was 318 °C which was lower than the predicted value, indicating that the RDF lowered the ignition temperature of the mixture (Chen, et al., 2018). The presence of RDF in the fuel mixture also enhanced the combustion rate of the anthracite and shortened the burn out time (Chen, et al., 2018).

The concentrations of the flue gases were measured with a MGA 5 mobile gas analyser, which measures CO and NO_x electrochemically and uses an infrared cell to measure the O_2 and CO_2 concentrations (Chen, et al., 2018). The co-combustion of anthracite and RDF showed that during the first stage of combustion a linear additive effect was observed for CO and CO_2 emissions (Chen, et al., 2018). Furthermore, the same samples were tested at 800°C and it was found that the combustion rate was slower which resulted in higher concentrations of CO and lower concentrations of CO_2 (Chen, et al., 2018). During co-combustion of the fuels at a 1:1 ratio, the NO_x was released in both stages of combustion (Chen, et al., 2018). From the char combustion stage, the NO_x concentrations were lower than the average of the emissions of the separate fuels, which the author suggested could be due to the high CO concentration inhibiting the NO_x formation (Chen, et al., 2018). The SO_2 emissions were lower than the average of the emissions from the two separate fuels in the devolatilization stage and the emissions were close to the average of the two fuels emissions in the char combustion stage, showing a synergistic effect (Chen, et al., 2018).

The ash from the combustion of RDF in the precalciner contained mostly SiO_2, with smaller concentrations of Fe_2O_3, $CaSO_4$ and $CaCO_3$ (Chen, et al., 2018). The co-combustion of this fuel with anthracite resulted in the formation of some new oxides in the ashes, including $CaAl_2Si_2O_8$ and CaO (Chen, et al., 2018). One of the major concerns with the use of RDF in cement production is the chlorine content of the fuel as chlorine weakens the product and increases the risk of corrosion of steel bars in reinforced concrete (Chatziaras, et al., 2016). Plastics like PVC which contain high amounts of chlorine must be limited in the fuel mix in order to prevent negative impacts on the product (Chatziaras, et al., 2016). Other concerns with the use of RDF include maintaining a continuous supply of RDF to the kiln, the combustion

characteristics of the RDF, the effect of the chemical composition of the RDF on the cement produced, the long-term effects of the use of RDF on the kilns operation and the effect on the atmospheric emissions (Kara, et al., 2008).

2.6.3 GASIFICATION OF RDF

Gasification is a process used to produce a syngas with small amounts of liquid and solids, this is performed by heating the fuel under a controlled amount of oxygen (Dalai, et al., 2009). Syngas is a mixture of H_2 and CO gas, along with water, methane and CO_2, which can be used in many applications, such as in engines and generators, fuel cells or as a feed to produce hydrogen or methanol and ammonia (Dalai, et al., 2009). The products produced from gasification and the yield of the gas is dependent on the type of feed used, the reaction temperature and pressure, the reactor configuration, the gasifying agent and the reaction catalyst (Dalai, et al., 2009).

RDF can be used as a substitute for fossil fuels in gasification. The conversion of RDF to syngas is dependent on the RDF composition, process design and the operating conditions of the process (Materazzi, et al., 2016). The process for RDF conversion to syngas starts with the heating of the RDF in the gasifier to 100 - 150°C and the drying of the RDF with heat from other parts of the gasifier (Materazzi, et al., 2016). The drying is dependent on the temperature, the gas velocity, the surface area of the RDF, the diffusivity, and bonding of the moisture in the RDF components (Materazzi, et al., 2016). The first conversion step is known as pyrolysis, in this step the water vapour and non-condensable gases are driven off and the carbon and ash remain in the gasifier (Materazzi, et al., 2016). In the second step of the conversion, the volatiles and char become the final syngas (Materazzi, et al., 2016). The stand-alone fluidised bed gasifiers present various problems when operated with refuse derived fuel (Materazzi, et al., 2016). This includes the high volatile matter and ash content of the RDF which decreases the thermal output, the forming of ash clinkers and increased tar and CO_2 emissions (Materazzi, et al., 2016). A two-stage process for RDF gasification which separates the primary gasification, and the tar and ash conversion can be achieved by using a plasma converter (Materazzi, et al., 2016).

Steam gasification makes use of steam as the catalyst and as the source of oxygen (Dalai, et al., 2009). Steam gasification results in a high-grade syngas which has minimum amounts of

N_2 (Dalai, et al., 2009). In the study by Dalai et al. (2009) two types of refuse derived fuel were used to study the syngas production in a fixed-bed reactor (Dalai, et al., 2009). The major products from the process was H_2 and CO, together with CO_2 and other hydrocarbons (Dalai, et al., 2009). The study found that the optimum temperature for H_2 and CO production was 725 °C, and the calorific value of the gas is higher when lower gasification temperatures are used (Dalai, et al., 2009). It was also found from the ultimate analysis carried out on the RDF that the total carbon and hydrogen are the major elemental components of the RDF. The gasification studies showed that the higher the C and H content in the RDF, the larger the amount of CO and H_2 produced (Dalai, et al., 2009).

2.6.4 COMBUSTION OF RDF

Refuse derived fuels can be incinerated using a variety of different technologies in waste-to-energy (WtE) plants. High priority is given to the fuel's particle size when selecting the type of boiler for RDF incineration. For solid recovered fuel (SRF) which is similar in composition to RDF but is produced in accordance with the European standard EN 15359, it was noted that power plants require a particle size less than 20 mm (Iacovidou, et al., 2018). The largest particle size of SRF can be utilised in fluidised bed combustion (< 10 - 200 mm) and boiler grate firing (< 300 mm) (Iacovidou, et al., 2018). The size of the fuel particles generally used in pulverised fuel boilers is much smaller, around 75 μm.

One of the most common technologies used in WtE plants is fluidised bed combustion (FBC). The major advantage of this technology is its ability to accommodate low quality and high moisture content fuel, such as biomass and waste derived fuels (Abdul, et al., 2012). One of the major challenges of firing waste derived fuels in fluidized bed boilers, as experienced by Foster-Wheeler, in their 20 waste-fired boilers, include the increased bed agglomeration and fouling of the convective heat surfaces (Zabetta, et al., 2008). The waste fired in these boilers contained recycled wood, industrial sludge and biogenic waste from the food industry, which has a high propensity for fouling and an extremely high propensity to corrode the boiler surfaces when fired without any countermeasures in place (Zabetta, et al., 2008). Fouling of the convective heat surfaces is due to the presence of alkali metals, such as Na and K, combined with Si, S and most often, Cl (Febrero, et al., 2015).

Some of the countermeasures which can be employed to reduce the problems of bed agglomeration include increasing the frequency of bottom ash removal to reduce the amount of alkali metal deposits in the bed (Zabetta, et al., 2008). Agglomeration, fouling and corrosion can also be managed by reducing the operating temperatures below the level at which the unwanted reactions become unmanageable, however this leads to less efficiency in the process (Zabetta, et al., 2008). Other countermeasures include alternative bed materials that are inert to alkalis, additives which can react with the alkalis and produce compounds with high melting points and co-combustion (Zabetta, et al., 2008). The use of co-combustion allows the problematic elements from the waste to be counteracted, for instance some coals can reduce the alkalis from waste and therefore reduce the corrosive alkali deposits (Zabetta, et al., 2008). In a study conducted on the co-combustion of wood-pellets and anthracite it was found that the fouling and slagging indices calculated for the co-combustion blends were lower than those for 100% biomass (Guo & Zhong, 2018). This was due to compounds with higher melting points being formed when coal is blended with 20% biomass, on the other hand more alkali metals were found in the 100% biomass ash which resulted in a greater propensity for slagging (Guo & Zhong, 2018). This was also supported by the research conducted by Zhang et al. (2018), where it was found that increasing the coal ratio in the co-combustion blend with simulated MSW resulted in an increase in the ash fusion temperatures.

A study was conducted by Rotheut and Quicker (2017) in which previously landfilled municipal solid waste was excavated and treated in a mechanical waste treatment facility to produce a refuse derived fuel. The RDF was then fired in a four-pass boiler in a modern WtE plant that previously incinerated both MSW and commercial waste (Rotheut & Quicker, 2017). The incineration of the landfilled RDF caused temporary blockages in the feeding hopper to the boiler and frequent fluctuations in the steam production (Rotheut & Quicker, 2017). The gaseous emissions analysis showed that the HCl concentration was increased significantly with the incineration of the previously landfilled RDF (Rotheut & Quicker, 2017). In addition, much higher volumes of lime milk, which is an additive used to capture the acidic gaseous components from the flue gas were required when incinerating the RDF from the landfill site (Rotheut & Quicker, 2017).

2.7 CO-COMBUSTION OF COAL AND REFUSE DERIVED FUEL

Some of the benefits achieved through utilising RDF in co-combustion include the reduction of waste in landfill sites, which in turn reduces the leachates and greenhouse gases emitted from the landfill sites. The high alkali and alkali earth metal content, and the Cl content of RDF are some of the drawbacks of pure RDF incineration as these constituents have a negative effect on the ash and gaseous emissions (Akdag, et al., 2016). Co-firing coal with RDF can assist in reducing the aforementioned impacts of RDF on the environment when combusted alone. RDF is also considered to be a renewable fuel as waste is continuously produced in large amounts, which indicates the long-term security of feedstock for energy generation. The abundance of this resource could lead to RDF being a cheaper alternative fuel, which can reduce the costs of electricity production. RDF co-combustion is a technology which can be retrofitted onto existing power stations with minimal to no modifications. There is also an opportunity for job creation through the growth of a resource recovery industry (Interwaste, 2018). Coal combustion results in NO_x and SO_2 emissions which are precursors for acid rain, these emissions could be reduced by co-firing with refuse derived fuel as RDF has a lower nitrogen content and a negligible sulfur content (Vekemans & Chaouki, 2016; Malaťák, et al., 2018).

An investigation was reported by Muthuramen et al. (2010), which investigated the co-combustion performance of hydrothermally treated municipal solid waste and Indonesian coal with high ash Indian coal. The hydrothermal treatment process allowed the MSW to be converted to a powder which could more easily be blended and combusted with coal, the treatment also reduced the moisture content of the raw MSW and increased the density to four times that of the raw MSW (Muthuraman, et al., 2010). The hydrothermal treatment had no effect on the calorific value of the fuel, which remained at 18 MJ/kg after treatment (Muthuraman, et al., 2010). Thermogravimetric analysis (TGA) was carried out on all samples, i.e. Indian coal, Indonesian coal, municipal solid waste and MSW-coal blends to determine their combustion performance (Muthuraman, et al., 2010). The author observed that as the percentage of the treated MSW in the blends increases, the temperature at which the volatile matter was initiated and released, reduces to a lower temperature region. More so, the ignition temperature was also found to be decreasing with increasing amounts of MSW in the fuel which is desirable for low volatile coals (Muthuraman, et al., 2010). The pre-exponential factor and the activation energy of the reactions decreased as the percentage of the MSW in the blend increases, and the blends with the lower percentage ratios (10% and 20%) of MSW possesses similar kinetics to coal combustion (Muthuraman, et al., 2010).

The co-firing combustion performance of paper mill sludge and municipal solid waste was studied by Hu et al. (2015). In this study it was found that the combustion of MSW could be divided into two stages; the release and combustion of the volatile matter, followed by the combustion of the fixed carbon and ash residues (Hu, et al., 2015). The comprehensive combustion characteristic index showed that the MSW index was much higher than that of the paper mill sludge, indicating that the combustion was more vigorous in MSW (Hu, et al., 2015). Comparing the theoretical mass loss curves with the experimental data showed that there are other interactions between the MSW and paper mill sludge as there were deviations between the calculated weighted average and the experimental data (Hu, et al., 2015). This was more prevalent at higher temperatures where it was noted that the experimental mass change over time was lower than the calculated values (Hu, et al., 2015). The apparent activation energy for the reactions were calculated using the Ozawa-Flynn-Wall and the Starink Methods. The values obtained from both methods were consistent and a wider range of E_a values were calculated for MSW which could be due to the varied composition of the MSW (Hu, et al., 2015).

The combustion behaviour of different types of wastes and their blends with lignite was studied by Iordanidis et al. (2018). Paper, plastic, textile and composites of organic materials were separated out of MSW, and the fuels were combusted in a TGA with lignite to study their combustion performance (Iordanidis, et al., 2018). The author found that due to the higher volatile matter content of the wastes, the ignition of the wastes and their blends occurs at a lower temperature than the ignition temperature for lignite alone (Iordanidis, et al., 2018). The reaction of the co-combusted coal and waste was more intense, the thermal profile shows the co-combusted fuel with a higher peak temperature than the lignite and with a lower burnout temperature (Iordanidis, et al., 2018).

In Italy, municipal solid waste (MSW) undergoes mechanical-biological treatment to produce a refuse derived fuel which is then co-combusted with coal in the Fusina coal-fired power station (Rigamonti, et al., 2012). RDF co-combustion in the Fusina plant began in 2005 at 18 400 tons per year and increased significantly in use, to 58 000 tons per year (Gasperetti, 2013). In 2013, a new agreement was signed to allow the increase in RDF combustion in the Fusina plant to up to 70 000 tons per year (Gasperetti, 2013). A saving of 40 000 tons per year of coal was achieved, along with 55 000 tons per year of CO_2 emissions avoided (Gasperetti, 2013). Various tests were carried out to compare the environmental impact of firing coal alone compared to the co-combustion of coal and RDF in power plant. It was found that with up to

5% RDF combustion, no significant negative impacts on the boiler were observed (Gasperetti, 2013). In addition, there were no significant impacts on the gaseous emissions, and the emissions were found to be in accordance with the limits of the Legislative Decree 133/05 of Italy (Gasperetti, 2013). The emissions of SO_x, Mn, Ni and V were also found to be lower as a result of co-combustion (Rigamonti, et al., 2012).

2.8 ENVIRONMENTAL IMPACTS

2.8.1 ATMOSPHERIC EMISSIONS FROM THE CO-COMBUSTION OF COAL AND RDF

Coal combustion for electricity production is one of the major sources of air pollution due to the emissions of particulate matter, carbon dioxide, sulfur dioxide and oxides of nitrogen from coal-fired power stations (Iacovidou, et al., 2018). The negative effect these air pollutants have on the environment and human health has resulted in many new regulations being put in place with the aim to reduce the use of fossil fuels for energy generation. Table 2.2 details the emission limits for South Africa according to the National Environmental Management: Air Quality Act of South Africa, 2004, while Table 2.3 shows the emission limits of a few countries for comparison with South Africa.

Table 2. 2: Emission limits for solid fuel combustion and solid biomass combustion (DEA, 2010) (IEA, 2015)

Substance	Plant status	mg/Nm^3 under normal conditions of 10% O_2, 273 K and 101.3 kPa
Particulate matter (PM)	New	50
	Existing	100
Sulfur dioxide (SO_2)	New	500
	Existing	3 500
Oxides of Nitrogen NO_x represented as NO_2	New	750
	Existing	1 100

Table 2. 3 Emissions limits for new and existing power stations in different regions (Belaid, 2017) (IEA, 2015)

Region	SO_2 mg/m^3		NOx (as NO_2) mg/m^3		Particulate matter (PM) mg/m^3	
	Existing	New	Existing	New	Existing	New
China	200-400	100-200	200	100	30	30
European Union	200-400	150-400	200-300	150-300	20–30	10–20
United States	160-640	160	117-640	117	23	23
India	200-600	100	300-600	100	50–100	30
Indonesia	750	750	850	750	150	100
Japan	-	-	200-300	200-300	30-100	30-100
Mexico	550-2 200	30-2 200	110-375	250-375	60 - 450	60-450
Philippines	1 000-1 500	200-700	1 000-1 500	500-1 000	150-200	150-200
Korea	286	229	308	164	40	20-30
Thailand	700-1 300	180-360	400	200	180-320	80
Vietnam	1 500	500	1 000	650-100	400	200

In the study conducted by Akdag et al. (2016) the gaseous emissions from the co-combustion of RDF and coal were measured in a cylindrical batch reactor at a temperature of 900°C. It was found that as the RDF combusted there was quick formation of CO_2 and CO which corresponded to a sharp drop in oxygen, this was attributed to the high volatile matter content of the RDF (Akdag, et al., 2016). The emissions of CO from the RDF combustion were very large, with 1000 - 5000 ppm of CO being formed when the RDF in the co-combustion blend was between 3 – 5%. When the RDF content was increased in the blend, below 20%, CO measured up to 6000 ppm (Akdag, et al., 2016). This study also found that there was a decrease in the SO_2 emissions as the RDF in the co-combustion blend increased, however there was no obvious effect on the emissions of NO_x (Akdag, et al., 2016).

Combustion is known to lead to the formation of nitrogen oxides, collectively called NO_x. The majority of nitrogen oxides are emitted as nitric oxide (NO) with a lesser amount of nitrogen dioxide (NO_2). A study on the co-combustion emissions of RDF and coal in a fluidised bed have shown a reduction in NO_x which could be due to the reduced nitrogen content and the nature of the nitrogenous compounds in the RDF (Vekemans & Chaouki, 2016). With an increase in RDF ratio above 30% in a particular fuel blend, an increase in NO_x emissions was observed by Vekemans and Chaouki, (2016). The author indicated that this could be as a result of the decreased in amount of char formed from coal for the reduction of NO to N_2 (Vekemans

& Chaouki, 2016). In another test using a cyclone fired combustor and an entrained flow reactor, a reduction in NO_x emissions was observed (Vekemans & Chaouki, 2016). The entrained flow reactor showed a reduction in NO_x with increased RDF ratio in the fuel (above 30%), contrary to the results from the fluidised bed reactor studies (Vekemans & Chaouki, 2016). In the research conducted by Zhang et al. (2018), percentage blends of MSW (7.5 – 25%) were co-combusted with coal and the gaseous emissions were analysed. It was found that NO_x emissions showed a downward trend with increasing MSW content, up to 15%, thereafter an upward trend was experienced, however all blends had lower NO_x emissions than coal combustion alone (Zhang, et al., 2018).

The co-combustion of RDF and coal in a vortexing fluidised bed combustor was conducted by Chyang et al. (2010). The author observed an increase in NO_x emissions, i.e. NO and NO_2 emission increases as the proportion of RDF in the blend increases. The author claimed this could be as a result of the form of nitrogen in RDF being NH_3, which can form NO at the temperatures used in fluidised bed combustion (Chyang, et al., 2010). In addition, the author reported that the lesser quantity of coal in the fuel might be responsible, as NO can be destroyed by char as shown in the following reaction steps (Chyang, et al., 2010).

$$C + 2NO \rightarrow CO_2 + N_2 \qquad \text{Equation 2.3}$$

$$C + NO \rightarrow \frac{1}{2}N_2 + CO \qquad \text{Equation 2.4}$$

$$NO + CO \rightarrow \frac{1}{2}N_2 + CO_2 \qquad \text{Equation 2.5}$$

In the study conducted on the co-combustion of RDF and anthracite it was found that during the RDF combustion alone, NO_x was released quickly and was formed mainly during the devolatilization stage according to the reaction in Equation (2.6) (Chen, et al., 2018).

$$N\ (Volatile) + O_2 \rightarrow NO + CO/CO_2 \qquad \text{Equation 2.6}$$

Co-firing with RDF has also been shown to decrease the SO_2 emissions during combustion, and this can be attributed to the reduced sulfur content in RDF compared to coal (Vekemans & Chaouki, 2016). In the study conducted by Zhang et al. (2018) the SO_2 emissions increased at first and then decreased with increasing MSW content in the fuel. The author suggested that this could be due to the higher adsorption rate of SO_2 onto the fly ash particles which became

irregular and had a large surface area due to the addition of MSW (Zhang, et al., 2018). In addition, the SO_2 emission might have been reduced and absorbed by the increased content of alkaline oxides (calcium oxide) in RDF; as seen in Equation (2.7) (Vekemans & Chaouki, 2016).

$$CaO + SO_2 + 0.5O_2 \rightarrow CaSO_4 + heat \qquad \text{Equation 2.7}$$

The majority of chlorine from the RDF fuel, is found as HCl in the flue gasses of the furnace (Vekemans & Chaouki, 2016). The HCl from the flue gas can cause corrosion at high temperatures as the HCl oxidises the tubes (Vekemans & Chaouki, 2016). Chyang et al. (2010) indicated that the HCl concentration increases with increasing proportions of RDF in the fuel when combusted in a vortexing fluidised bed reactor. HCl can also react with organic molecules to form polychlorinated dioxins (PCDD) and furans (PCDF) (Vekemans & Chaouki, 2016). PCDD and PCDF are formed at temperatures around 250 - 400°C in MSW incinerators, however they have not been detected in the co-combustion of MSW and coal (Vekemans & Chaouki, 2016). Cl_2 is formed when HCl reacts with oxygen during the gas cooling process, as shown by the Deacon reaction below.

$$2HCl + 0.5O_2 \leftrightarrow H_2O + Cl_2 \qquad \text{Equation 2.8}$$

Cl_2 is the major chlorination agent in the formation of PCDD and PCDF, however Cl_2 is decomposed by the reaction with sulfur as shown in Equation (2.9) (Vekemans & Chaouki, 2016). It can therefore be seen that the higher content of sulfur from co-combustion with coal suppresses the formation of PCDD and PCDF to very low concentrations (Vekemans & Chaouki, 2016).

$$Cl_2 + SO_2 + H_2O \leftrightarrow 2HCl + SO_3 \qquad \text{Equation 2.9}$$

A year-long co-combustion test was conducted in a 65 MW circulating fluidised-bed boiler in which RDF was co-combusted with peat and coal and the efficiency of the combustion as well as the corrosion inside the boiler was examined (Manninen, et al., 1997). In addition, five different types of packaging derived fuel (PDF), which is the dry, combustible portion of MSW was also co-combusted in the same plant (Manninen, et al., 1997). This study found that both the PDF and the RDF performed well in the co-combustion with low emissions. Both CO and

SO_2 emissions decreased as a result of the co-combustion (Manninen, et al., 1997). The HCl emission concentration increased as the chlorine content of the fuel increased and the co-combustion of a 10% RDF and peat/coal blend did not cause high temperature chlorine-induced corrosion in the boiler (Manninen, et al., 1997).

2.8.2 ASH EMISSIONS FROM THE CO-COMBUSTION OF COAL AND RDF

Ash produced from the combustion of coal can be divided into bottom ash, which falls to the bottom of the furnace, and fly ash, which leaves the furnace with the exhaust gases. The composition of the fly ash can vary considerably depending on the composition of the coal being burned. Fly ash generally consists of the following trace elements; arsenic, beryllium, boron, cadmium, chromium, hexavalent chromium, cobalt, lead, manganese, mercury, molybdenum, selenium, strontium, thallium, and vanadium, with much lower concentrations of dioxins and PAH compounds (RTI, 2007).

In coal, a large fraction of the ash forming elements are present within the coal minerals such as Si, Al, Fe and Mn (Vekemans & Chaouki, 2016). In municipal solid waste and refuse derived fuels, most of the inorganic minerals are present as free ions and simple salts rich in alkalis and alkali earth metals such as K, Na, Ca and Mg (Vekemans & Chaouki, 2016). The ash produced from RDF incineration has a high slagging tendency due to the large proportions of alkaline elements in the ash, the fouling tendency of RDF ash is also high due to the presence of volatile inorganic oxides such as Na_2O and K_2O (Akdag, et al., 2016). The alkali metals contained in the RDF are released at lower temperatures, under 600°C, and once vaporized, they can react to form alkali silicates, sulfates and chlorides (Vekemans & Chaouki, 2016). These species can soften at lower temperatures and cause slagging, fouling and corrosion of the furnace walls. The most abundant elements contained in RDF ash include Si and Ca, this is followed by Cl which originates from the plastic and waste paper components in the RDF (Akdag, et al., 2016). In addition to this, Fe, Al and S are also found in high concentrations in the ash from RDF (Akdag, et al., 2016). Higher concentrations of S and P in RDF also increases the slagging and fouling indices for the ash (Akdag, et al., 2016). A high viscous melt may be produced if the ash contains large amounts of silica which melts and forms a glassy phase (Teixeira, et al., 2012).

One of the drawbacks of RDF combustion is the chlorine content of the waste. Chlorine is present in an inorganic form, as a salt (NaCl), as well as organic chlorine from PVC. MSW has a higher chlorine content than coal, which reacts during combustion to form HCl vapour or chlorides which condense on the furnace walls causing corrosion (Vekemans & Chaouki, 2016). Chlorides formation in the furnace lowers the softening temperature of the furnace deposits and damages the protective oxide layer of the furnace surface when the deposits melt (Vekemans & Chaouki, 2016). Corrosion also occurs below the softening temperature of the deposits due to the presence of gaseous chlorine from chloride containing deposits (Vekemans & Chaouki, 2016). The ash produced from PVC can also be hazardous due to the use of barium, cadmium, lead and zinc as stabilizers in the product (Porshnov, et al., 2018).

Slagging is caused by depositions of molten ash in the high temperature zones of the boiler where radiative heat transfer is dominant (Teixeira, et al., 2012). Fouling occurs in the convective zones of the boiler as ash deposits form while the gases cool down (Teixeira, et al., 2012). Numerous researchers have developed different equations to help predict the behaviour of the ash formed during the combustion of different fuels. The base-to-acid ratio equation is utilised to determine the likelihood of slagging of the ash deposits using the weight concentration of each compound (James, et al., 2012). When the value of $R_{B/A}$ is in the range of 0.4 - 0.7 the slagging potential of the ash is high or severe, whereas when the value is less than 0.4 or greater than 0.7 the slagging propensity is low to medium (Miller, 2011).

$$R_{b/a} = \frac{Fe_2O_3 + CaO + MgO + K_2O + Na_2O}{SiO_2 + TiO_2 + Al_2O_3} \qquad \text{Equation 2.10}$$

The fouling index is shown by the equation below. The fouling potential is low when F_u is less than 0.6, medium when F_u is between 0.6 and 1.6, high when F_u is between 1.6 and 40 and extremely high when the index is above 40 with a tendency for the deposits to sinter (Teixeira, et al., 2012).

$$F_u = R_{B/A} \times (Na_2O + K_2O) \qquad \text{Equation 2.11}$$

A study was conducted by Norton et al. (1988) to compare the ash constituents from coal and refuse derived fuel (RDF) after combustion. The analysis of the ash samples was done using X-ray florescence, atomic absorption and neutron activation. The analysis of the bottom ash

from a 35 MW boiler where a blend of RDF and coal was co-fired showed that the concentration of Br, Cr, Ga, Na, Ni, Pb, Sb, Sn, Ti and Zn were 2-5 times higher than when coal was combusted alone (Norton, et al., 1988). The fly ash collected from the electrostatic precipitator, was found to have a high concentration of As, Br, Cr, Ga, Ge, Pb, Sn, and Zn when RDF was co-combusted with coal (Norton, et al., 1988). The most significant increases in the stack fly ash were seen for Br, Cd, Pb, Sb, Se, Sn, and Zn (Norton, et al., 1988).

In the study conducted by Zhang et al. (2018), a simulated MSW, made up of PVC and PE plastic, paper, textiles, biomass and kitchen waste, was combusted with a mixture of brown and bituminous coal (Zhang, et al., 2018). The SEM analysis of the ash showed that the coal ash particles were spherical and smooth, however with increasing simulated MSW content in the fuel, the ash became more irregular (Zhang, et al., 2018). The ash fusion temperature showed a decrease with increasing MSW content; however, the decrease was not significant at less than 20°C (Zhang, et al., 2018). The elemental analysis of the ash was done using XRF and it was found that the Si and Al content of the ash decreased with increasing amounts of simulated MSW in the fuel, while the Fe, Cl and S content increased (Zhang, et al., 2018).

2.9 THERMOGRAVIMETRIC ANALYSIS

The combustion behaviour of all the samples utilized in this study was determined using thermogravimetric analysis (TGA). This is a thermal analysis, which is used to examine the change in mass of a sample against the change in temperature. An oxidative atmosphere of air is used and the fuel samples are combusted at a specified heating rate in order to determine their reaction kinetics. The weight loss of the sample is recorded as a function of temperature to give the TG plot. The derivative of these results gives the DTG plot which shows the rate of weight loss (%/min) of the sample which can be used to evaluate the combustion performance. The first peak noted on a DTG plot, at a temperature between 80°C and 150°C depending on the sample, denotes the loss of inherent moisture. As the reaction temperature increases, and the DTG curve crosses the zero point on the Y/X-axis the volatile matter is released. This point is called the initiation temperature (IT_{VM}) (Cumming & McLaughlin, 1982). With the initiation of the volatile matter, the slope of the combustion curve increases as combustion begins and the point of inflection on the curve is known as the initiation temperature of fixed carbon (IT_{FC}) (Cumming & McLaughlin, 1982). The peak temperature (PT) is the point of maximum weight

loss and the burnout temperature (BT) is the point at which the curve falls back to zero (Cumming & McLaughlin, 1982).

In order to determine the ignition and burnout temperatures of the combustion from the TG and DTG plots the 'Intersection Method' can be used. In this method two points on the TG plot must be identified. The first point (labelled A in Figure 2.4) is the point at which a vertical line drawn from the first peak on the DTG plot intersects with the TG plot. The second point (labelled B in the same figure) is the point at which devolatilization begins, a horizontal line is then drawn through point B and a tangent is drawn from point A, the point at which these two lines intersect will give the ignition temperature of the fuel (T_i) (Lu & Chen, 2015). In order to determine the burnout temperature of the fuel a vertical line is drawn from the second peak on the DTG plot to the point where it intersects with the TG plot (labelled point C on the diagram). The point at which the TG plot becomes steady (labelled D in the diagram) is determined and a horizontal line is drawn from that point. A tangent is drawn from point C and the burnout temperature (T_b) will be found at the intersection of the tangent and the horizontal line from point D (Lu & Chen, 2015). In the case of two peaks being present on the DTG plot, the second peak should be used for the determination of the burnout temperature (Lu & Chen, 2015). An alternative, and simpler method of determining the burnout temperature is the 'Conversion Method'. In this method the burnout temperature is identified as the temperature when the conversion reaches 99% (Lu & Chen, 2015).

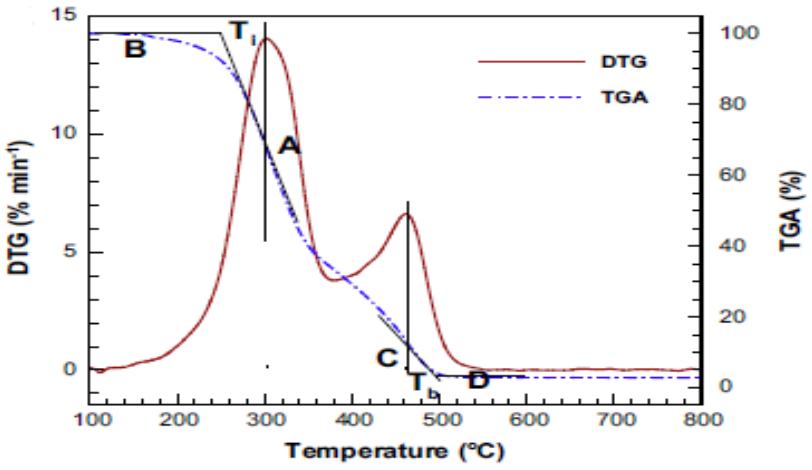

Figure 2. 4: The Intersection Method for Determining T_i and T_b (Lu & Chen, 2015)

2.10 REACTION KINETICS

Reaction kinetics can be determined by using either model-free (isoconversional) methods or model-fitting methods. Model-free methods, such as Kissinger-Akahira-Sunose (KAS), Friedman and Ozawa-Flynn-Wall (OFW), use multi-heating rate data to determine the reaction kinetics and are not based on a reaction order or model (Alvarez, et al., 2016). Model-fitting methods, such as Coats-Redfern, use single-heating rate data in their application and choose a reaction model to fit the experimental data. The rate equation generally used for kinetic studies is shown in the equation below (Blaine & Kissinger, 2012).

$$\frac{d\alpha}{dt} = k(T)f(\alpha) \qquad \text{Equation 2.12}$$

The term $\frac{d\alpha}{dt}$ is the rate of conversion, $k(T)$ is the rate constant, $f(\alpha)$ is a function representing the reaction model, and α represents the conversion which can also be expressed as shown below.

$$\alpha = \frac{m_0 - m_t}{m_0 - m_f} \qquad \text{Equation 2.13}$$

Where m_0 is the initial mass of the sample, m_t is the mass of the sample at time *t* and m_f is the final mass of the sample. The rate constant, *k*, can be expressed by the Arrhenius equation as shown below.

$$k = Ae^{-\frac{E_a}{RT}} \qquad \text{Equation 2.14}$$

Where A is the pre-exponential factor (min^{-1}), E_A is the apparent activation energy $(\frac{kJ}{mol})$, R is the gas constant $(\frac{J}{K.mol})$, and T is the temperature (K). Combining Equation (2.12) and (2.14) results in the general rate equation (Blaine & Kissinger, 2012).

$$\frac{d\alpha}{dt} = Ae^{-\frac{E_a}{RT}}f(\alpha) \qquad \text{Equation 2.15}$$

The heating rate, used in the thermogravimetric analysis can be expressed as β, shown below.

$$\beta = \frac{dT}{dt} \qquad \text{Equation 2.16}$$

Using this equation with Equation (2.15) will result in the following:

$$\frac{d\alpha}{dT} = \frac{A}{\beta} e^{-\frac{E_a}{RT}} f(\alpha) \qquad \text{Equation 2.17}$$

Rearranging this equation results in Equation (2.18) below.

$$\frac{d\alpha}{f(\alpha)} = \frac{A}{\beta} e^{-\frac{E_a}{RT}} dT \qquad \text{Equation 2.18}$$

From this equation, the integral below is obtained, which is referred to as $g(\alpha)$.

$$g(\alpha) = \int_0^{\alpha} \frac{d\alpha}{f(\alpha)} = \frac{A}{\beta} \int_{T_0}^{T} e^{-\frac{E_a}{RT}} dT = \frac{AE_a}{\beta R} p\left(\frac{E_a}{RT}\right) \qquad \text{Equation 2.19}$$

The term $p\left(\frac{E_a}{RT}\right)$ has no solution and is solved using approximations or numerical methods (Alvarez, et al., 2016).

2.10.1 THE COATS-REDFERN METHOD

In order to approximate the solution to the integral expressed in Equation (2.19), the Coats-Redfern approximation uses the asymptotic series expansion to obtain the equation below.

$$ln\left[\frac{g(\alpha)}{T^2}\right] = ln\left[\frac{AR}{\beta E_a}\left(1 - \frac{2RT}{E_a}\right)\right] - \frac{E_a}{RT} \qquad \text{Equation 2.20}$$

Assuming that the term $\frac{2RT}{E_a}$ is much smaller than one, it can be ignored which results in Equation (2.21) which is used to plot $ln\left(\frac{g(\alpha)}{T^2}\right)$ versus $\frac{1}{T}$ (Gil, et al., 2010). The slope of the plot will give the apparent activation energy of the reaction. In order to determine the correct solid-state reaction model for $g(\alpha)$ various reaction models are tested, some of the common models are presented in Table 2.4. The model which results in the linear regression closest to one is the model deemed to best describe the reaction (Alvarez, et al., 2016).

$$ln\left(\frac{g(\alpha)}{T^2}\right) = ln\left(\frac{AR}{\beta E_a}\right) - \frac{E_a}{RT}$$ Equation 2.21

Table 2. 4: Solid state reaction models (Gil, et al., 2010)

Solid-state reaction model	$f(\alpha)$	$g(\alpha)$
Reaction order models		
First order reaction	$(1-\alpha)$	$-\ln(1-\alpha)$
Second order reaction	$(1-\alpha)^2$	$(1-\alpha)^{-1}-1$
Diffusion models		
One-dimensional diffusion	$\frac{1}{2}\alpha^{-1}$	α^2
Two-dimensional diffusion	$[-ln(1-\alpha)]^{-1}$	$(1-\alpha)ln(1-\alpha)+\alpha$
Jander's diffusion control	$2(1-\alpha)^{\frac{2}{3}}\left[1-(1-\alpha)^{\frac{1}{3}}\right]^{-1}$	$\left[1-(1-x)^{\frac{1}{3}}\right]^2$
Ginstling and Brounshtein's diffusion control	$\frac{3}{2}\left[(1-\alpha)^{\frac{-1}{3}}-1\right]^{-1}$	$1-\frac{2}{3}\alpha-(1-\alpha)^{\frac{2}{3}}$
Phase boundary-controlled models		
Contracting area	$2(1-\alpha)^{\frac{1}{2}}$	$1-(1-\alpha)^{\frac{1}{2}}$
Contracting volume	$3(1-\alpha)^{\frac{2}{3}}$	$1-(1-\alpha)^{\frac{1}{3}}$

In a study done on the kinetic parameters of various biomass fuels it was found that the two model-free methods tested, KAS and OFW, were not suitable for the determination of the activation energy in biomass due to the assumption for these two methods that $\frac{E_a}{RT}$ be greater or equal to 20 and smaller or equal to 60 (Alvarez, et al., 2016). This condition was not met during the combustion of lignin making these methods unsuitable for biomass when lignin combustion takes place (Alvarez, et al., 2016). On the other hand, the Coats-Redfern method was applied to determine the kinetic parameters of all the biomass fuels with success (Alvarez, et al., 2016). This finding was also supported in a study by Anca-Couce, *et al*., (2015), in which the reaction kinetics of biomass pyrolysis was compared using isoconversional methods, as well as model fitting methods. It was found that the model-fitting method more accurately estimated the activation energy for the wood species that were studied, when compared to the KAS and Kissinger methods (Anca-Coucea, et al., 2014).

2.11 CONCLUSION

It is evident that coal is likely to remain the top contributor for energy production in South Africa for the next 30 - 40 years, due to the economic importance of coal in the country. The quality of coal available for use is decreasing and coals with higher ash contents and lower calorific values are becoming more abundant. Therefore, it is necessary to find ways in which low quality coal can be utilised for energy production while reducing the atmospheric emissions of CO_2, SO_x and NO_x, as well as reducing the reliance on coal and the cost of energy production.

The literature indicates that municipal solid waste is abundant and many studies have been carried out on co-combustion using MSW, this indicates that there is an abundant supply of waste for refuse derived fuel. This cheap resource has a high calorific value and can reduce the cost of producing electricity and provide a renewable fuel for coal-fired power stations. The waste in landfill sites across the country is vast and produces emissions such as the greenhouse gases methane and CO_2, as well as leachate which can seep into the groundwater. Using material from these landfill sites to produce refuse derived fuel for coal-fired power stations will lead to a reduction of these emissions and reduce the strain on space in landfill sites.

There is a lot of literature on the use of RDF in cement plants and as a feedstock for gasification. The use of RDF for cement production can weaken the cement and cause corrosion to the steel bars in reinforced concrete due to the chlorine content from plastics like PVC. When RDF is used as a feedstock in gasification there are various problems which are encountered which include the high volatile matter and ash content decreasing the thermal output of the gasifier and the formation of ash clinkers and increased tar and CO_2 emissions. Two-stage processes for gasification of RDF are therefore required to overcome these issues.

There are also some problems associated with the incineration of RDF on its own in waste-to-energy plants, this includes the corrosive and fouling deposits produced as a result of the alkali metal content in the ash residue. In addition to this, HCl emissions produced from RDF incineration is corrosive to the boiler surfaces. A counter-measure which can reduce these negative effects is the co-combustion of RDF with coal. This can reduce the alkali metal content of the fuel and produce less corrosive ash deposits while still gaining the benefits of RDF such as the reduced CO_2, NO_x and SO_x emissions.

CHAPTER 3: RESEARCH METHODOLOGY

3.1 SOURCE OF RDF FOR THIS RESEARCH

The refuse derived fuel (RDF) used in this study was sourced from Interwaste in Germiston. Interwaste is an environmental solutions company which specialises in integrated waste management and provides services such as waste classification and separation, collection and compaction of waste, and material recovery (Interwaste, 2018). The tasks outlined in the flow chart below show the sequence of activities and procedures followed in this research.

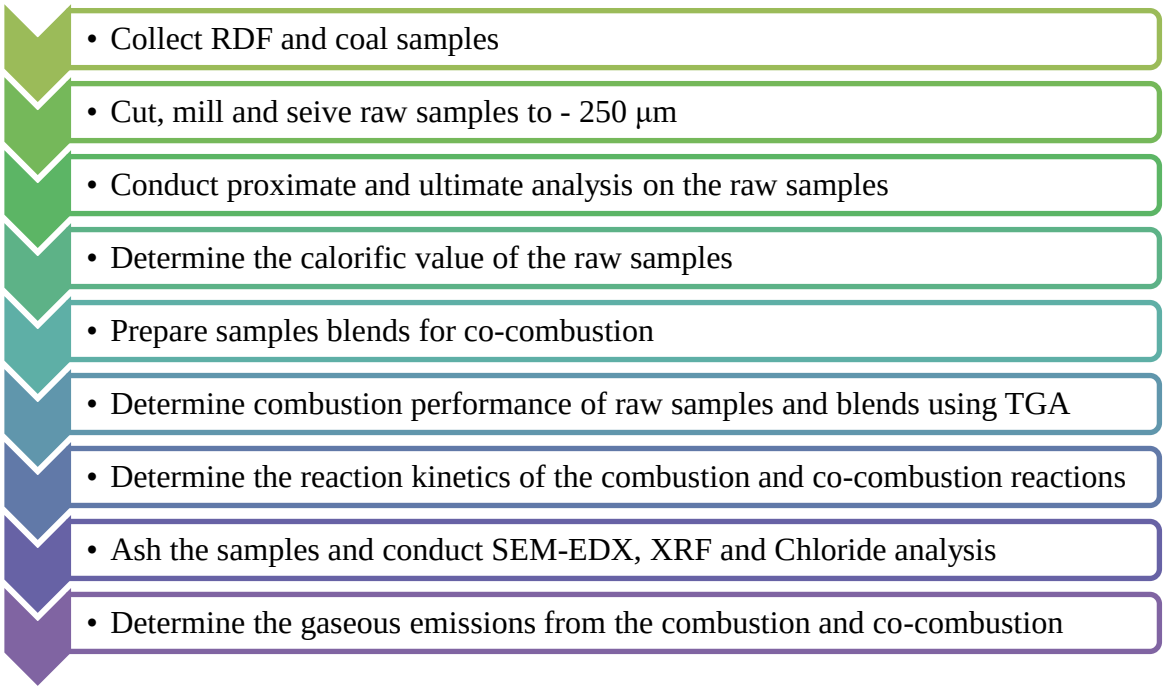

Figure 3. 1: Experimental flow chart procedure.

The waste utilized was collected from different industries and includes cardboard, paper, wood, textiles and plastics. At the waste management plant, the refuse is shredded in a primary and secondary shredder to reduce the size of the materials before being sorted into different grades (Interwaste, 2018). The sorted waste is then densified into different bales, depending on the intended use (Interwaste, 2018). The samples utilized in this study are taken from the various waste bales present on site to make up 15 kg of samples containing cardboard, paper, plastic and textiles. The majority of the waste was made up of multi-component packaging such as soup and spice packaging, soap packaging, ice cream packaging, wax paper, lotion containers,

margarine containers, nitrile gloves, boxes, polypropylene film, and small amounts of textiles such as gauze. Overall, the composition of the materials making up the RDF is divided into four categories, as seen below:

- 40% Plastic
- 40% Paper
- 15% Cardboard
- 5% Textile

The RDF samples collected from Interwaste for this research were composed of three different types, with the main components listed below. Sample P1, seen in Figure 3.2., was mostly made up of brown paper, it also contained considerable amounts of plastics from soap and washing powder packaging. Sample P2, seen in Figure 3.3, was mostly made up of yellow paper with a glossy coating and nitrile gloves. It also contained foil backed brown paper and other papers and plastics. Sample PL, seen in Figure 3.4, was mostly made up of plastic from soap and spice packages. The spice packages were a combination of paper, plastic film and aluminium foil lining, with a small amount of textile materials.

- Sample P1: 85% brown paper and cardboard, 10% plastic and 5% textiles
- Sample P2: 65% yellow paper, 20% brown paper, 10% plastic and 5% textiles
- Sample PL: 85% plastic, 10% paper and 5% textiles

Figure 3. 2: Sample P1 (Paper 1)

Figure 3. 3: Sample P2 (Paper 2)

Figure 3. 4: Sample PL (Plastic)

The Retsch SM 200 was used to mill the RDF samples to - 250 µm. The elastic nature of the plastic packaging in the RDF prevented a further reduction in size as the material was not brittle enough to be cut through by the mill. A blend of the two RDF samples which were mostly made up of paper (P1 and P2) was then prepared by mixing the samples in a 1:1 ratio, this sample is hereafter referred to as sample PB (paper blend). Run-of-mine (ROM) coal (sample C1) and discard coal (sample C2) from Mpumalanga province was used in this research. The ROM coal is defined as the raw mined coal, which is beneficiated in a coal washing plant (Ramani & Evans, 1998). While the discard coal, is the mineral (inorganic) containing coal

component separated from the coal organics during beneficiation from the washing plant. The ROM and discard coal samples were milled in the Retsch SM 200 to - 250 μm. A representative sample from each coal was prepared for all the analyses, including the combustion test. All samples were stored in sealed polyethylene sample bags with clear labelling in a cool and dark area to prevent interactions with light and heat.

3.2 EQUIPMENT

Table 3. 1: Table of Equipment

The Retsch SM 200 is a cutting mill with removable bottom sieve which was used for the milling of the coal and all RDF samples. Image: (Retsch, n.d.)	
The Leco TGA 701 was utilized for the proximate analysis, as well as the combustion and co-combustion tests. Image: (MARC, n.d.)	
The heat content/calorific values of all the samples was determined using a Leco AC 500 oxygen bomb calorimeter. Image: (LECO, n.d.)	

A Malvern Mastersizer 2000 particle size analyser with a Hydro 2000MU dispersion unit was used to determine the sample's particle size distribution (PSD).
Image: (MalvernPanalytical, n.d.)

The Elementar vario EL cube was used for the ultimate analysis and total sulfur determination.
Image: (Elementar, n.d.)

The Carl Zeiss Sigma Field Emission Scanning Electron Microscope (FE-SEM) was used to determine the external morphology and semi-quantitative chemical composition of the ash samples.
Image: (I&M, 2012)

A Metrohm Eco analyser was utilised to determine the chloride concentrations in the ash samples through ion chromatography.
Image: (Metrohm, n.d.)

The Ametek SPECTRO XEPOS HE analyser from the was utilised for XRF (X-ray fluorescence) analysis to determine the elemental composition of the ash samples. This is an energy dispersive XRF which can

hold up to 12 samples and covers elements from Na to U.

A horizontal tube combustion reactor from South Africa which has an internal mullite tube of 40 mm inner diameter and 750 mm length, was used for the gaseous emissions tests. A EUROTHERM 2216e temperature controller maintained the reactor at the set temperature.

The schematic of this equipment can be seen in Section 3.6 below.

An MGA 11 analyser was used for the combustion gas concentration determinations. This is a mobile, multi-gas analyser capable of measuring up to seven different gas concentrations simultaneously. Image: (Fodisch, 2017)

3.3 ANALYTICAL TECHNIQUES

3.3.1 PROXIMATE ANALYSIS

The proximate analysis was conducted in a Leco TGA 701 in accordance with ASTM D5142 (ASTM, 2009). This method involved the following steps:

- Approximately 1 g of each sample was measured into a ceramic crucible for this analysis.
- For the moisture determination, the samples were analysed at a temperature of 25°C to 107°C at a ramp rate of 6°C/min in a nitrogen atmosphere. The uncovered samples were held at 107°C for 15 minutes, until the final sample weight remained constant.
- For the volatile matter determination, the crucibles were covered and the temperature was increased from 107°C to 950°C at a ramp rate of 43°C/min in an atmosphere of nitrogen and held at this temperature for 7 minutes.

- The temperature was immediately reduced below 600°C, and the covers were removed. For the ash determination, the temperature was increased from 600°C to 750°C at a heating rate of 3°C/min in an atmosphere of oxygen. The non-combustible residues remaining after this step, is denoted as the sample's ash content.
- The fixed carbon content was determined from the following equation:

$$FC = 100 - VM - Ash \qquad \text{Equation 3.1}$$

Where FC is the fixed carbon content (%), VM is the volatile matter content (%) and, Ash is the ash content (%).

3.3.2 ULTIMATE ANALYSIS

The ultimate analysis for all the raw samples were conducted in the Elementar vario EL cube analyser, as seen in Figure 3.5. About 50 mg of each sample was weighed into tin foil capsules and loaded into the equipment's carousel which can house up to 80 samples. The sample was then automatically transferred to the combustion vessel where the samples were first flushed with helium (He), which acts as a carrier gas to remove atmospheric nitrogen (Elementar, n.d.). The combustion of the samples is then carried out at 1150°C. The gases for analysis; N_2, CO_2, H_2O and SO_2 are separated into their components in the gas separation columns before they are sent to the thermal conductivity detector (TCD) for elemental concentration detection (Elementar, n.d.). The percentage concentrations of C, H, N and S are determined with the analyser and the percentage concentration of O is determined by difference according to Equation (3.2).

$$O\ (\%) = 100 - (C + H + N + S + Ash) \qquad \text{Equation 3.2}$$

Where O represents the total oxygen, C is the total carbon, H represents the hydrogen, N is the nitrogen, and S is the total sulfur.

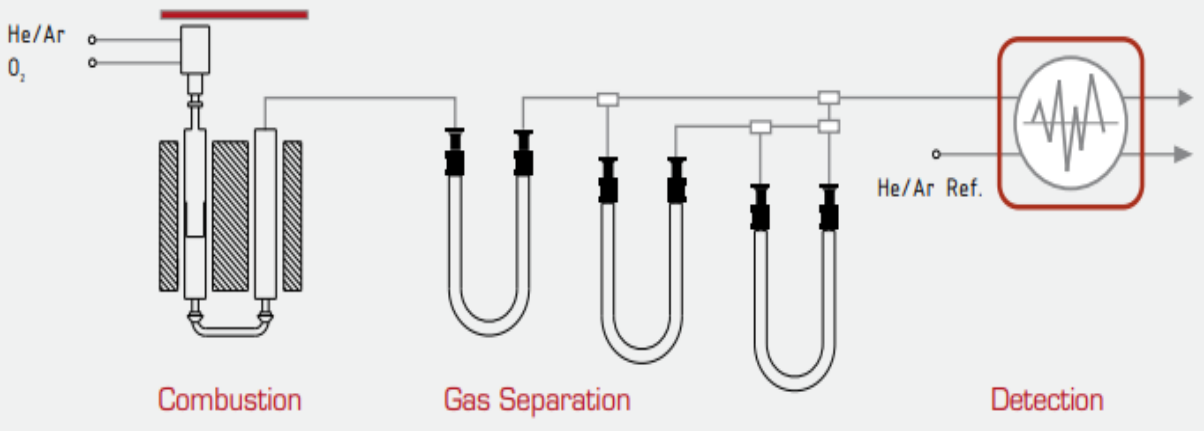

Figure 3. 5: Experimental setup in the Elementar vario EL cube analyser (Elementar, n.d.)

3.3.3 CALORIFIC VALUE

The calorific value test was conducted in a Leco AC500 bomb calorimeter in accordance with the ASTM D5865 standard (ASTM, 2019). Approximately 1 g of sample was used for the test and a repeat run was done to confirm the reproducibility of the result. This test was conducted for each RDF and coal sample according to the following steps:

- 1 g of sample was measured and loaded into the crucible.
- A 10 cm fuse wire was connected to the combustion vessel electrodes above the sample and the crucible was then placed in a combustion vessel.
- The combustion vessel was closed and the needle valve was tightened before the vessel was charged with oxygen to 28.96 bars.
- The oxygen filled combustion vessel/bomb was then placed into the combustion vessel bucket, filled with 2 L distilled water from the water reservoir.
- The analysis of the sample started after the two combustion vessel fuse leads were connected to the combustion vessel electrodes.
- After the analysis was complete, the combustion gases were discharged and the remaining fuse wire fragments were measured to correct the calorific value determined.

3.3.4 PARTICLE SIZE DISTRIBUTION

The particle size distribution was determined for each raw sample using the Malvern Mastersizer 2000 with the Hydro 2000MU dispersion unit. This was done according to the following steps:

- Approximately 800 ml of distilled water was measured into a beaker and placed into the sample dispersion unit.
- The pump speed was set at 3000 rpm to prevent the sample from settling out in the liquid and the pump arm was lowered into the beaker.
- A background measurement was taken before any sample was added to the water.
- The sample was added until the lazer obscuration range was between 10 – 20% (the sample was pumped to the flow cell in the optical bench, where it was measured before returning to the beaker via the tubing).
- The ultrasonic probe was set to a displacement of 20 μm and this was used to assist in dispersing the RDF samples when agglomerates formed.

3.3.5 COMBUSTION AND CO-COMBUSTION PERFORMANCE

The samples for the co-combustion tests were made up by blending the coal and RDF samples at different percentage weight ratios. PL was mixed with sample C1 (ROM) at 15%, 30%, 50% and 75% to make a blend of PL and C1 at different ratios. The same procedure was applied in making the blends of PL and C2 (discard), as well as for the blended paper RDF sample (PB) with both the coal samples. The full set of co-combustion tests (88 samples) can be seen in Table 3.1 below. The number in brackets of the sample ID represents the mass percentage of the raw material in the blend. Four different heating rates were used for the co-combustion tests in order to compare the combustion profiles under different heating rates.

Table 3. 2: Combustion tests experimental procedure

Sample ID	Heating rate 1 (°C/min)	Heating rate 2 (°C/min)	Heating rate 3 (°C/min)	Heating rate 4 (°C/min)
100% C1	5	7	10	14
100% C2	5	7	10	14
100% PL	5	7	10	14
100% PB	5	7	10	14
85% C1 + 15% PL	5	7	10	14
70% C1 + 30% PL	5	7	10	14
50% C1 + 50% PL	5	7	10	14
25% C1 + 75% PL	5	7	10	14
85% C1 + 15% PB	5	7	10	14
70% C1 + 30% PB	5	7	10	14
50% C1 + 50% PB	5	7	10	14
25% C1 + 75% PB	5	7	10	14
85% C2 + 15% PL	5	7	10	14
70% C2 + 30% PL	5	7	10	14
50% C2 + 50% PL	5	7	10	14
25% C2 + 75% PL	5	7	10	14
85% C2 + 15% PB	5	7	10	14
70% C2 + 30% PB	5	7	10	14
50% C2 + 50% PB	5	7	10	14
25% C2 + 75% PB	5	7	10	14

The co-combustion tests were conducted in the Leco TGA 701 in an oxidative atmosphere using air according to the following steps:

- Approximately 150 mg of each sample of raw RDF, coal and their blends were loaded into ceramic crucibles and loaded in the TGA carousel
- The samples were heated from 25°C to 850°C at the specified heating rate. The temperature was then held at 850°C for 20 minutes to complete the combustion.

The DTG and TG curves were plotted from the data obtained from the analysis, and the thermographs plotted (DTG) from these data were used to evaluate the combustion performance, including initiation temperature of the volatile matter (IT_{VM}), initiation temperature of fixed carbon (IT_{FC}), peak temperature (PT) and burnout temperature (T_b) of the

samples. The intersection method and the conversion method, as explained in Section 2.9, was used to determine the ignition and burnout temperatures of the samples, respectively.

3.4 COATS-REDFERN REACTION KINETICS

The Coats-Redfern method is a non-isothermal, model-fitting kinetic modelling approach which was used to calculate the apparent activation energy for the combustion of the raw samples and their blends. For this model-fitting method the samples were co-combusted in the Leco TGA 701 at a constant heating rate of 10°C/min. Various solid-state reaction models, as presented in Table 2.4, were then fitted to the data and the linear regression was calculated for the data set by plotting $\ln\left[\frac{g(\alpha)}{T^2}\right]$ versus $\frac{1}{T}$. The solid-state reaction model with a linear regression constant closest to 1 was deemed to be the model controlling the reaction rate. The apparent activation energy was then determined from the slope of the trend line through the data. A single global reaction was considered for the combustion of the samples and this was split into different stages in order to determine the apparent kinetic energy in the different phases of the reaction.

3.5 ASH ANALYSES

3.5.1 ASHING OF THE SAMPLES

The ash from the blends of discard coal, the paper blend RDF and the plastic RDF were chosen for further analysis. This research focused on the combustion and co-combustion performance of low-quality coal and RDF; therefore, the discard coal ash samples were chosen as these samples had a lower quality when compared to the run-of-mine coal. Approximately 15 g of ash of each sample was prepared using the Leco TGA 701. The RDF (samples PB and PL) and RDF-coal blends with larger proportions of RDF, up to 50%, were ashed in accordance with the BS EN 14775:2009 standard for '*Solid biofuels - Determination of ash content*' (BSI, 2009). The following steps were carried out in the Leco TGA 701 in an oxidative atmosphere of air.

- Approximately 1 g of sample was measured into the ceramic crucibles and placed in the TGA.
- The samples were heated from 25° to 250°C at a heating rate of 7°C/min and held for a period of 1 hour at this temperature.

- The samples were then heated from 250°C to 570°C at a heating rate of 10°C/min, and held at this temperature for a period of 2 hours until the weight became constant.

The 100% coal discard samples (C2) and the RDF-coal blends with higher proportions of coal were ashed in an atmosphere of air according to the standard ISO 1171:2010 for *'Solid mineral fuels - Determination of ash*', as unburned carbon remained in these samples when ashed at lower temperatures (ISO, 2010). The following steps were carried out in the Leco TGA 701.

- Approximately 1 g of each sample was measured into the ceramic crucibles and placed in the TGA.
- The samples were heated from room temperature to 500°C at a heating rate of 7°C/min and the samples were held at this temperature for 30 minutes.
- The samples were then heated from 500°C to 815°C at a heating rate of 10°C/min and the samples were held for 2 hours at this temperature until the weight became constant.

3.5.2 SEM/EDX

The following ashed samples were selected for SEM/EDX analysis: 100% C2, 100% PL, 100% PB, 70% C2 + 30% PL, 70% C2 + 30% PB, 25% C2 + 75% PL and 25% C2 + 75% PB. The physicochemical properties, as well as the combustion performance of the two coal samples showed that the discard coal was of lower quality than the ROM coal. This research is focused on improving the combustion parameters of low-quality coal while achieving acceptable ash characteristics and gaseous emissions, hence the samples containing discard coal were chosen for further investigation. Two blends with each RDF type were chosen in order to determine the trends with increasing RDF content. The preparation of the ash samples for SEM-EDX involved the following steps.

- The samples were mounted by sticking carbon tape onto stainless steel stubs.
- A small amount of ash (about 20 mg) was then stuck onto the carbon tape and the excess was dusted off with an air duster.
- The mounted samples were then sputter coated with one coat of carbon and two coats of Au/Pd in order to make the samples conductive.

The samples were then analysed using the Carl Zeiss Sigma FE-SEM. The prepared samples were magnified to different degrees and images of the ash particles were taken. The semi-quantitative elemental composition of the overall sample, as well as several selected areas of interest was determined.

3.5.3 XRF ANALYSIS

The XRF analysis for the seven selected ash samples were conducted using an Ametek SPECTRO XEPOS HE analyser which uses He gas to purge the instrument before running the samples in an environment of Helium. There was no sample preparation required for this method, and approximately 5 g of each ash sample was loaded into a sample cup for this analysis. The sample cups are made with Prolene thin-film, to create a sample cup with a clear film bottom. These sample cups are placed into the metal inserts of the sample carousel. The samples are analysed by the X-ray tube emitting X-rays to excite the samples, as seen in Figure 3.6, while the silicon drift detector (SDD) is used in detecting the fluorescent X-rays. Each sample analysis took approximately 15 minutes to complete and covered a range of elements from Na to U.

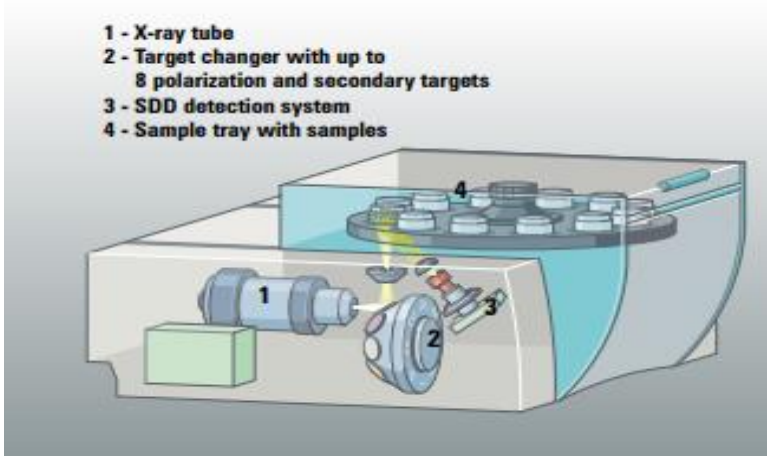

Figure 3. 6: Internal diagram of the Ametek SPECTRO XEPOS HE analyser

3.5.4 CHLORIDE ANALYSIS

The chloride analysis was conducted on all eleven ash samples using the Mertohm Eco IC analyser with an aqueous multi-element standard. Approximately 3 g of ash was utilised for this analysis according to the following steps.

- The ash samples were weighed into two 50 ml centrifuge tubes and diluted with deionised water.
- The centrifuge tubes were then shaken at 150 rpm for a period of 1 hour and thereafter the pH and electrical conductivity of the samples were measured.
- Acetic acid was then added to the centrifuge tubes which were shaken at 50 rpm for a period of 18 hours.
- The samples were then syringe filtered at 22 μm and the pH and electrical conductivity of the samples were measured again after letting the samples stand for 18 hours.
- Samples with high electrical conductivity were further diluted and then measured in the Metrohm Eco IC.

3.6 GASEOUS EMISSIONS ANALYSIS

The gaseous emissions analysis was conducted on the 100% RDF samples, both 100% ROM and discard coal, as well as the blends of discard coal with PB and PL. The horizontal tube combustion reactor was utilised for these tests, a diagram of the reactor can be seen in Figure 3.7. The horizontal tube reactor was first set to 850°C and all samples were combusted at this temperature and their gaseous emissions were recorded. The reactor was then set to 950°C and the discard coal was combusted and the gaseous emissions were recorded for comparison. The Dr Födisch MGA 11 analyser was connected to the gas outlet, labelled 10 in the diagram, to measure the combustion emissions. From the gas outlet, the analyser extracted a partial volume of the flue gas. The flue gas was then conditioned by an integrated condensate trap and the CO, SO_2, NO and NO_2 gas concentrations were measured by an electrochemical cell. The CO_2 gas concentration was measured by an infrared photometer.

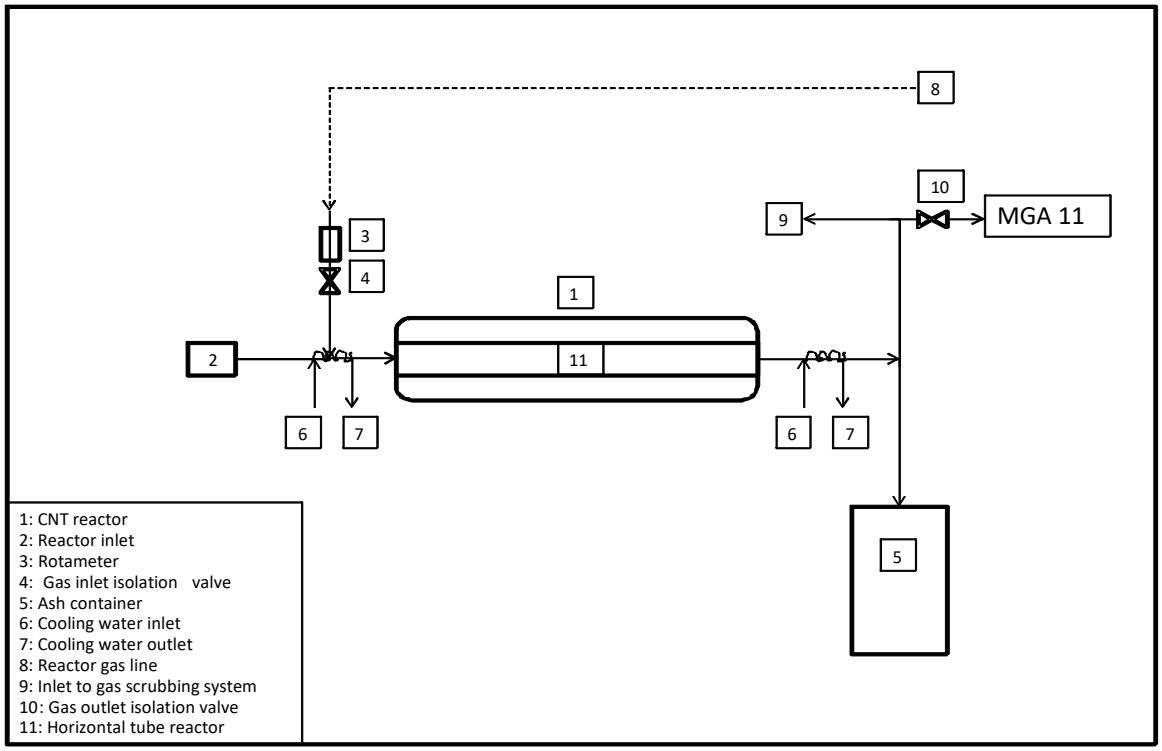

Figure 3. 7: Horizontal tube combustion reactor diagram

The combustion reactor was flushed with air to remove any gases from the furnace and the outlet gas line before each gaseous emission test was conducted. The flushing of the system was carried out prior to each test according to the following steps:

- The reactor inlet was closed and the gas inlet and outlet isolation valves (labelled 4 and 10, respectively) were opened.
- The rotameter needle valve was opened to allow the flow of air through the reactor.
- The system was flushed for approximately 5 minutes or until the gaseous emissions reading from the MGA 11 came down to zero.

The below-mentioned procedure was then followed to analyse the gaseous emissions in a batch test, from the combustion and co-combustion of all samples in an air environment. Before the commencing of the test, the reactor was heated from room temperature to the set temperature of 850°C or 950°C. A blank test was then conducted with an empty crucible inserted into the reactor and the MGA 11 recorded the gases emitted at a rate of one scan per second in order to achieve a baseline for the tests to follow.

- 250 mg of sample was measured into a ceramic crucible and the sample was inserted into the reactor through the reactor inlet.
- The rotameter needle valve was opened to allow air to flow at 160 $\frac{ml}{s}$ through the reactor tube for the combustion of the sample.
- The gaseous emissions from the sample were recorded for a ten-minute period, with measurements taken every second with the MGA 11 analyser.
- The sample was then removed from the tube and the reactor inlet was closed to flush the system for the next measurement.

To conclude, the refuse derived fuel used in this research was sourced from Interwaste, while the ROM and discard coal was sourced from Mpumalanga province. These raw samples were then prepared by milling the samples to -250 μm and blending the samples for the co-combustion and ashing tests to follow. The analytical techniques used were explained in detail and the equipment used for each analysis was also mentioned. The following chapter, Chapter 4: Results and Discussion, will give a detailed discussion of the results obtained from each of the analytical tests referred to in this chapter.

CHAPTER 4: RESULTS AND DISCUSSION

This chapter discusses the results of all the experimental investigation conducted in this research. This includes the physicochemical properties of the RDF samples (PL and PB), the run-of-mine coal and discard coal, the combustion and co-combustion performance of the samples, as well as the reaction kinetic parameters for all samples. The gaseous emission, along with the elemental composition of the ash obtained from the combustion and co-combustion tests were included in this chapter.

4.1 CHARACTERISTICS OF RAW RDF AND COAL SAMPLES

The physicochemical properties of the two RDFs and coal samples utilized in this study is presented in Table 4.1. The total mass of general waste produced in South Africa for the year 2017, with the percentage proportion of plastic and paper generated in the same year are also depicted in the same table. This data was extracted from the South Africa State of Waste Report, (DEA, 2018).

Table 4. 1: Physicochemical properties of raw materials used in this study

Parameters	Plastic RDF (PL)	Paper blend (PB)	C1 (ROM)	C2 (DISCARD)
Proximate analysis				
Fixed Carbon (wt%, db)	6.07	9.30	46.51	36.58
Volatile Matter (wt%, db)	82.68	83.82	23.40	20.59
Ash content (wt%, db)	11.25	6.66	30.09	42.83
Moisture (wt%: Ar)	1.23	3.19	2.24	2.06
Ultimate analysis (wt%, db)				
Hydrogen	9.38	8.63	3.26	2.73
Nitrogen	0.35	0.30	1.46	1.17
Total Carbon	58.09	59.04	59.64	49.62
Sulphur	UT	UT	0.87	1.37
Oxygen	20.93	25.37	4.68	2.28
CV: (MJ/kg)	31.23	22.4	21.72	16.73
South Africa General Waste: **54.2 Mt** Proportion of total waste (%)	3.3	4.7	-	-

Ar: As received; db: dry basis; CV: Calorific value; O: Oxygen by difference [100-(Ash+C+H+N+S)]; UT: untraceable.

4.1.1 PROXIMATE ANALYSIS

The discard coal possesses the lowest volatile matter content of 20.59%, as seen in Table 4.1, and all samples had low moisture contents, ranging from 1.23 to 3.19% (inherent moisture). It was observed from the same table that the RDF samples contained a very large volatile matter content of 82.68% for sample PL and 83.82% for PB. The RDFs were also seen with a low percentage of fixed carbon of 6.07% and 9.30% and ash content of 11.25% and 6.66%, for PL and PB respectively. The sample PL, which contained a large amount of plastic had a higher ash content compared to PB, at 11.25%. The large content of volatile matter in the RDF samples are expected release a lot of heat when combusted which will aid the combustion of the fixed carbon in the sample (Hu, et al., (2015); Muthuraman, et al., (2010)). This will result in decreased fixed carbon initiation temperatures, as well as decreased burnout temperatures. The proximate analysis results from these RDFs are similar to those found in the literature. It can be observed that the RDFs used in this study are of higher grade compared to that used by Akdag et al. (2016), where the author reported a volatile matter within the range of 68.5 - 81.8%, ash content (12.9 - 14.9%) and fixed carbon content in the range of 5.2 - 16.6%.

The literature has shown that most of the coals utilized in the South African power plants are slightly higher grade than the coal utilized in this study. The proximate analysis of coals sampled from three South African coal fired plants reported by Rautenbach et al. (2018) was found with moisture contents in the range of 2 - 4.5%, ash content 25 - 35.9%, volatile matter 20.6 - 21.9% and fixed carbon 40.3 - 46.8%. Results from the sampling test conducted by Kalenga et al. (2011) on coal utilized by six different South African power plants, showed that the moisture content in these coals is less than 4%, ash content about 31.6% and fixed carbon content at around 43.6%. It can be seen from Table 4.1 that the coals used in this research are of lower quality, especially the discard coal (C2), which was found to have a very high ash content (42.83%) in comparison to the coal used in the South African coal fired plants. With this coal, more ash is expected to be generated at the power plant after its combustion, due to its high content of non-combustive inorganic minerals. The ROM coal (C1), with an ash content of 30.09% is similar to the quality used in the present South African coal power plants, but this coal may need to be washed in order to upgrade its volatile matter content to above 30%. With a volatile matter content of 23.40%, this coal is expected to have a higher ignition temperature and less stable flame stability compared to the two RDFs. The two coals can be categorized as a high-ash coal according to the ash yield classification of SANS 11760:2007.

4.1.2 CALORIFIC VALUE

The calorific value is the amount of energy produced by the fuel during complete combustion and is measured as the units of energy produced per unit mass of the fuel. In Table 4.1 it is evident that the sample PL has the highest calorific value at an average of 31.23 MJ/kg, this is followed by PB at 22.40 MJ/kg. Both coal samples have lower calorific values than the two RDF samples with the run-of-mine coal (C1) at 21.72 MJ/kg and the discard coal (C2) at 16.73 MJ/kg. In terms of the coal grade, according to the South African coal standard classification for calorific value, the ROM coal barely made the Grade D2, while the discard is below the Grade D3 of < 21.5 MJ/kg. The blending of a higher calorific value RDF with a low calorific value (CV) coal might increase the energy content of the blend and allow lower CV coal blend to be utilised for energy production. With the proper blending ratio of the PL (31.23 MJ/kg) and the discard coal (16.73 MJ/kg), a more reactive fuel with high energy density, lower burnout temperature and ignition temperature can be produced. In addition, the presence of RDF in a coal blend might lead to a stable flame formation and further combustion of the discard coal in the blend.

4.1.3 ULTIMATE ANALYSIS

The main elemental composition of a solid fuel is its total carbon, hydrogen and oxygen content. The nitrogen and sulphur content of the fuels contribute to the formation of NO_x and SO_x during their combustion. It can be seen from the results in Table 4.1 that the total carbon of the RDF samples (59.04% for PB and 59.04% for PL) is similar to that of the coal (C1) utilized in this study (59.64%). Both RDFs are seen with a similar total carbon obtained by Rotheut and Quicker (2017) where carbon was in the range of 27.8 - 61.8%. The total carbon in the discard coal was 49.62%, which is expected as it also has the lowest fixed carbon content of all the fuels. The hydrogen content of all the fuels was found to be below 10%, however, the hydrogen content of the RDF is much higher in comparison to the coal samples, which is consistent with the higher volatile matter content of these samples. It must likewise be mentioned that the nitrogen content is much lower in the RDF samples (0.30% for PB and 0.35% for PL) when compared to the coal samples (1.46% for C1 and 1.17% for C2). The co-combustion of these RDFs with these coals might lead to a reduction in the NO_x and SO_2 emission compared to when the coals are combusted solely.

The sulphur contents of the RDFs, according to Table 4.1, are found to be undetectable which is in agreement with the findings of other authors (Kaiser, 1968; Vekemans & Chaouki, 2016). This is similar to the result from Bai et al. (2007) and Zhao et al. (2012), in which both authors obtained a total sulphur of 0% (Table 4.2). The coals utilized in this study are found to have sulphur contents of 0.87% for C1 and 1.37% for C2 which are within the range of global coal reported by Wagner et al. (2018) as 0.5 – 5% total sulfur. This result is also in agreement with the average sulphur content (1.11%) found by Kalenga et al. (2011) from the coals utilized in six South African power stations. The range of the physicochemical characteristics of other RDF components found in the literature can be seen in Table 4.2, with the result obtained from this study included.

Table 4. 2: Ultimate analysis of various RDF components

	C	H	N	S	O	Reference
Newspaper	49.86	6.34	0.15	0.26	43.24	Hu et al. 2011
Cardboard	47.09	6.00	0.18	0.11	46.63	Dai 2007
Magazine	46.44	6.54	0.16	0.30	46.33	Hu et al. 2011
Cotton	44.92	9.00	0.19	0.03	45.86	Yan et al. 2009
PE	84.97	14.30	0.70	0.02	0	Chi et al. 2008
PP	85.41	12.51	0.23	0	1.85	Bai et al. 2007
PS	89.20	9.00	0	0	1.8	Zhao et al. 2012
Plastic RDF	57.38	9.26	0.34	UT	20.68	This study
Paper blend RDF	57.16	8.35	0.29	UT	24.35	This study

C – total carbon, H – hydrogen, N – nitrogen, S – total sulfur, PE – polyethylene, PP – polypropylene, PS – polystyrene, UT – untraceable

4.1.4 PARTICLE SIZE DISTRIBUTION

The particle size distributions (PSD) of the coal and RDF fuels can be seen in Figure 4.1. The percentage passing 250 μm was 71% for the ROM coal, 77% for the discard coal, 64% for the paper blend and 54% for the plastic sample. It is difficult to obtain a similar PSD for both RDFs and coals due to the difference in the friability and hardness of all the fuels utilized, as well as the low bulk-density and differences in particle shape between the various materials making up the RDF (Iacovidou, et al., 2018). From the PSD profile, the discard coal (C2), was seen to be the softest of the fuels, with about 70% of the coal milled under 200 μm, and the plastic at 48%. A similar difference in particle size distribution between coal and waste was found by other authors. In the co-combustion study by Wu et al. (2011), the coal PSD was found to have

50% passing 19 µm, while the solid recovered fuel had a PSD with 50% passing164 µm (Wu, et al., 2011). This difference can result in the delay in the burning of the larger particles, however due to the elasticity of the polypropylene and polyethylene plastics in the RDF a further reduction in size is difficult to achieve without pre-treatment of the material.

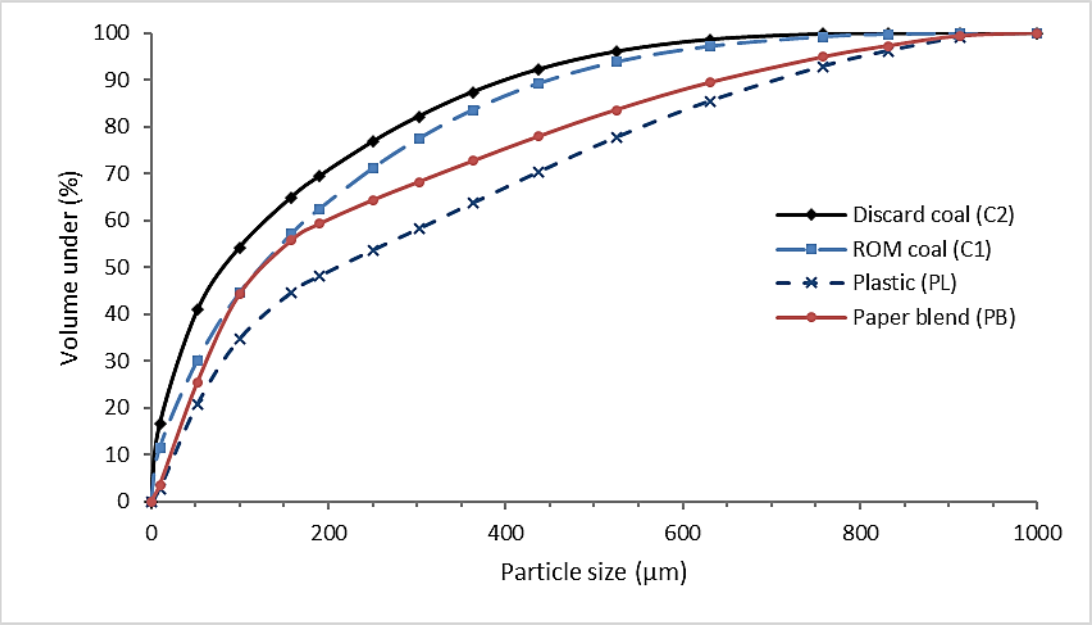

Figure 4. 1: Particle size distribution of the coal and RDF samples

4.1.5 ESTIMATED POTENTIAL ENERGY CONTENT FROM RDF

The evaluation of the total energy content that can be recovered from the RDF generated in South Africa for 2017 was based on the calorific value depicted in Table 4.1, with the assumption that the energy characteristic for the RDFs reported by DEA (2018) are similar to the plastic and paper utilized in this study. The lower heating value (LHV) of the plastic and the paper blend RDFs utilized in this study were determined using Equation (4.1). The LHV_i, is noted as the lower heating value of component i, HHV_i is the higher heating value of component i, W_e is the heat of evaporation of water (2.441 MJ/kg), H_i and M_i are the hydrogen and moisture contents of component i, respectively (Nam–Chol, et al., 2018). The total LHV from the two RDF resources were then estimated using Equation (4.2), where m_{total} is the total mass of waste produced per year, as seen in Table 4.1. For this evaluation, the σ known as the efficiency of RDF production, was assumed to be 80% and P_i is the proportion of the waste component i. The LHV_i of the individual paper waste and plastic waste components

determined through Equation (4.1) were found to be 20.3 MJ/kg and 29.2 MJ/kg, respectively. This resulted in a total LHV for the proportion of RDF resource reported for 2017 in South Africa to be estimated as 83 629 702 GJ/year, which is equivalent to 2673 MW per year.

$$LHV_i = HHV_i - W_e(9H_i + M_i) \qquad \text{Equation 4.1}$$

$$LHV_{total} = m_{total}\sigma \sum P_i LHV_i \qquad \text{Equation 4.2}$$

4.2 COMBUSTION PERFORMANCE OF COAL AND RDF

The combustion profiles of the raw materials used were obtained by conducting a thermogravimetric analysis on the samples as detailed in Section 3.3.5 above. The combustion profiles (DTG curves) for each of the samples in Figure 4.2 shows the sample's weight loss rate as representative mass (150 mg) of each sample which was heated from 25°C to 850°C at a heating rate of 10°C/min. The weight loss percentage of a sample is calculated according to the Equation 4.3, where m_I is the initial mass of the sample and m_L is the mass of sample lost (in mg). The weight loss rate is the change in the mass of the sample with time (ΔTG), as seen in Equation 4.4 where m is the mass in mg and t is the time in minutes, the subscript i denotes the point under consideration.

$$\frac{m_I - m_L}{m_I} \times 100 \qquad \text{Equation 4.3}$$

$$\Delta TG = \frac{m_i - m_{i-1}}{t_i - t_{i-1}} \qquad \text{Equation 4.4}$$

It can be seen that the raw paper samples, P1 and P2, have very similar combustion profiles with P1 having a higher reactivity, and the samples reaching their peak temperatures at 323°C and 325°C, respectively. On the same figure, the blended papers (P1 and P2), now denoted as PB, which is made up of 50% P1 and 50% P2, has a combustion profile similar to both paper samples, with the same initiation temperature for fixed carbon and peak temperature (PT) at 321°C. Therefore, for this study, the blend of two papers (PB) was utilized as the second RDF co-fired with coal. These combustion tests were repeated and the standard deviation (σ) of P1

ranged from 0 to a maximum of 1.9 at 350°C, P2 ranged from 0 to 1.03 at 296 °C and PB from 0 to 1.26 at 349°C.

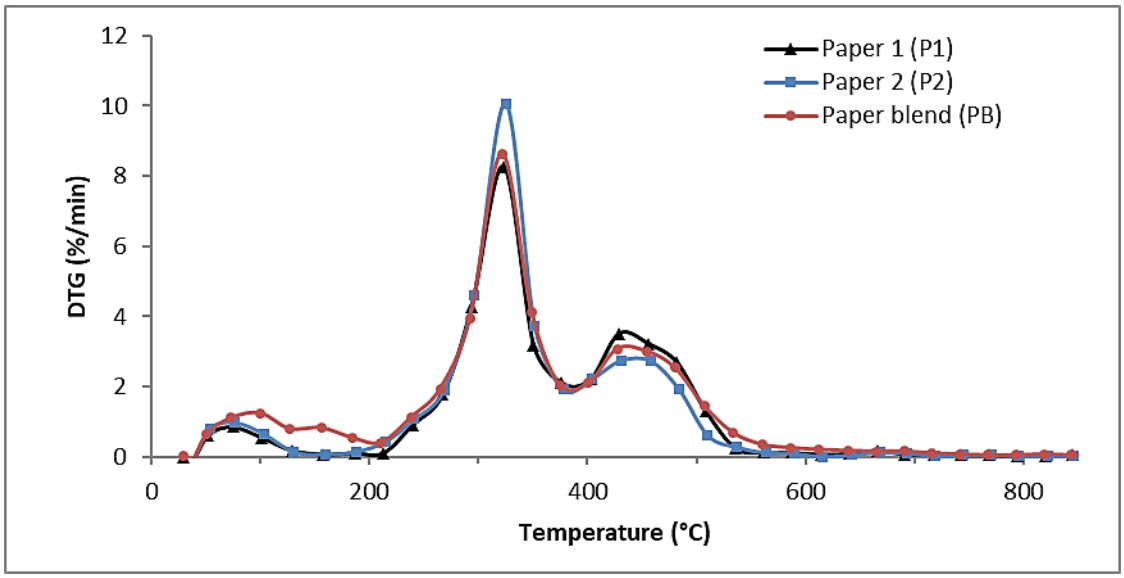

Figure 4. 2: DTG plots for paper 1, paper 2 and paper blend (PB)

The combustion tests were repeatable to within around 5°C of the peak temperature, and the repeat figures can be found in Appendix A (Norton, 1993). The standard deviations are presented in Table 4.3. The thermographs for the combustion of the raw RDF samples, PL (plastic blend) and PB (paper blend), as well as the coal samples C1 (ROM), and C2 (discard) can be seen in Figure 4.3. The combustion profile of the ROM coal (C1) was divided into three stages, the first stage which began at ambient temperature and continues to 155°C indicates the release of the inherent moisture. From the same figure, both coal samples (C1 and C2) show a deflection as the curve crosses the x-axis, which denotes an increase in sample weight. This occurs after the initial loss of moisture and it is due to the solid-state oxidation of the organic matter in the sample (Cumming & McLaughlin, 1982). The second stage of combustion begins immediately after the DTG curve crosses the x-axis and becomes positive again, signifying the release and combustion of the volatile matter. This occurs at a temperature around 320°C for the ROM coal and it is known as the initiation temperature of the volatiles IT_{VM}. The RDF samples were seen with a DTG curve above the x-axis, and a steep gradient, which might be responsible for their high reactivity and ignition at a lower temperature region (Iordanidis, et al., 2018). In addition, the volatile matter content of both RDFs is more than triple that of the

coals, and this might also be responsible for the lower ignition temperature noted for both samples (Hu, et al., 2015).

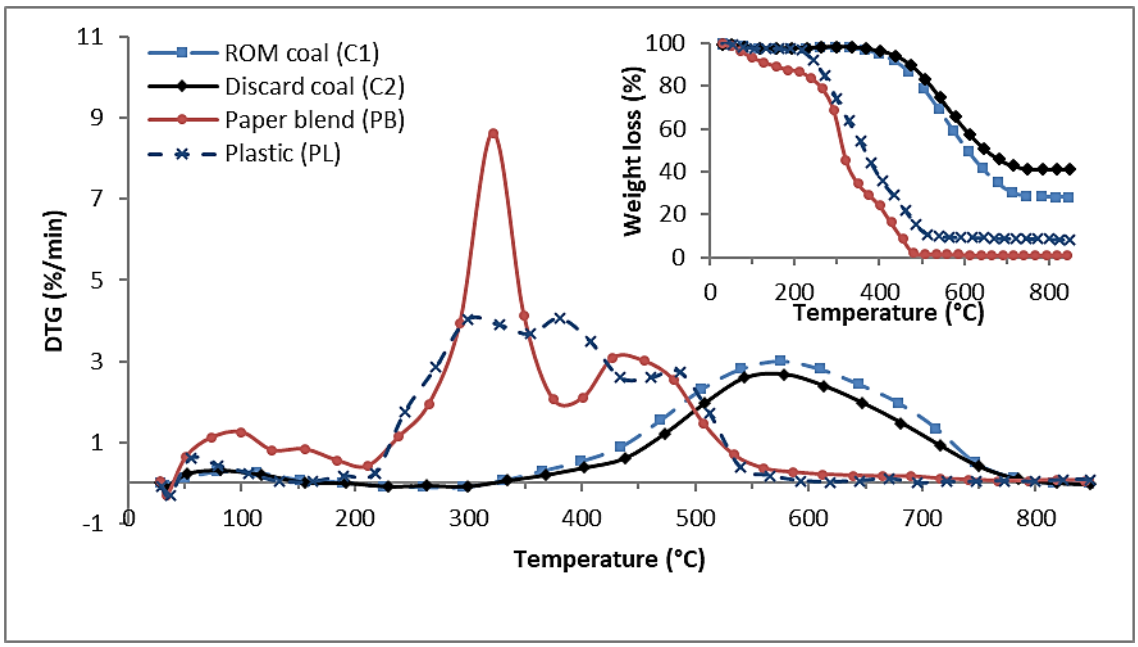

Figure 4. 3: The combustion profiles of the RDF samples PL and PB, and the coal samples C1 and C2

The third stage of the combustion can be seen as the gradient of the curve increases and this indicates the combustion of the fixed carbon and other residues. This is known as the initiation temperature of the fixed carbon (IT_{FC}), and this occurred at a temperature of 434°C for the ROM coal (C1), 472°C for the discard coal (C2) and about 250°C for the paper blend (Figure 4.3). With the aid of an intersection method, the ignition temperature (T_i) and the burnout temperature (T_b) for the ROM coal was found to be 440°C and 740°C, respectively. The discard coal reaches its peak temperature at 578°C with a weight loss rate of 2.68 %/min, while the ROM coal has a weight loss rate of 3 %/min and burnout temperature of 741°C.

The combustion of the RDF sample PB was also divided into three stages (Figure 4.3). The loss of inherent moisture occurred from ambient temperature and showed a peak at 100°C followed by the release and combustion of the volatile matter within 211°C - 375°C. The combustion of fixed carbon and other residuals occurred in the third stage of the reaction from 375°C to 651°C. The ignition temperature, initiation temperature of fixed carbon and burnout temperature were found to be 265°C, 375°C and 651°C, respectively. The paper blend was

seen with two distinctive peaks, which is expected as a result of the hemicellulose, cellulose and lignin functional groups in paper (Porshnov, et al., 2018). The first peak on the combustion profile could be attributed to the degradation of hemicellulose and the partial decomposition of cellulose (250 – 350°C). Whilst the second peak observed at a temperature of 430°C, could be attributed to the decomposition of lignin, which has been found to degrade over a wide range of temperatures, up to 900°C (Yang, et al., 2007). With the inclusion of some plastics in this blend, the second peak might also be attributed to the decomposition of plastic materials in the sample which occurred at a higher temperature compared to biomass. From Figure 4.3, the paper blend sample possesses the highest reactivity (8.64 %/min), followed by the plastic, ROM coal and the discard coal. The low ash content in the paper blend might be responsible for the easy diffusion of oxygen to the surface of the char, rather than hindering the diffusion and limiting the sample's reactivity (Cardozo, et al., 2014).

The plastic sample (PL) showed four combustion stages. The loss of inherent moisture which occurred from ambient temperature to 133°C, followed by the release and combustion of the light volatile components which occurred from 218°C to 355°C. The third stage occurred as a result of the combustion of the heavier volatile components which took place from 355°C to 460°C. The multiple weight loss peaks seen in this profile indicate the heterogeneous nature of the fuel as different components exhibit different reactivities (Vamvuka, et al., 2011). The first peak from the DTG plot is in the range of the decomposition of hemicellulose and cellulose. Porshnov et al. (2018) found that polyethylene decomposes in the temperature range of 397 to 519°C, while polypropylene (PP) decomposes in the temperature range of 267 to 498°C. The second peak seen in this profile might be as result of the decomposition of polypropylene present in the sample, while the third peak of the DTG plot could be due to the decomposition of polyethylene. The fourth stage was the combustion of the char and residues which occurred from 460°C to 670°C and featured one smaller peak at 486°C at a weight loss rate of 2.75 %/min. The ignition temperature (T_i) determined by the intersection method for the PL sample was 250°C, which is similar to that reported for plastic (249°C) by Iordanidis et al. (2018) from MSW. The burnout temperature of this RDF sample was found to be the lowest, at 547°C, of all the fuels utilized.

The coals utilized in this study were found to be less reactive than the RDF samples. The RDF samples have a much higher volatile matter content and thus a lower ignition temperature and a lower initiation temperature for the volatile matter to be released and combusted. This is in

agreement with findings of other authors including Muthuraman et al. (2010). This, in turn, leads to a decrease in T_b which was also experienced by Iordanidis et al. (2018).

4.2.1 CO-COMBUSTION PERFORMANCE OF RUN-OF-MINE COAL AND RDF

The ROM coal (C1) was co-combusted with the RDF samples at different weight percentage ratios. For each test, 150 mg of each raw sample and their blends were combusted in an atmosphere of air to produce the combustion profiles seen in Figure 4.4 and Figure 4.5 below. Due to the lower ignition and volatile matter initiation temperatures seen in the RDF samples, the RDF is expected to enhance the performance of both the ROM coal and the discard coal.

It can be seen in the thermograph (Figure 4.4) the blend of 85% C1 + 15% PL, as well as in Figure 4.5 for the blend of 85% C1 + 15% PB that there exists a similarity in these profiles and that of the ROM coal. These blends reached their peak temperatures in the region of char combustion, showing that this is the dominant stage of their combustion. These blends might be suitable for co-combustion in an existing coal-fired power stations with little or no modification since the fuel showed a similar and compatible burning profile to the coal utilized. The lowest ignition temperature achieved for the plastic sample blends with ROM coal was found to be 246°C, and this was attained for the blend of 75% PL and 25% ROM coal.

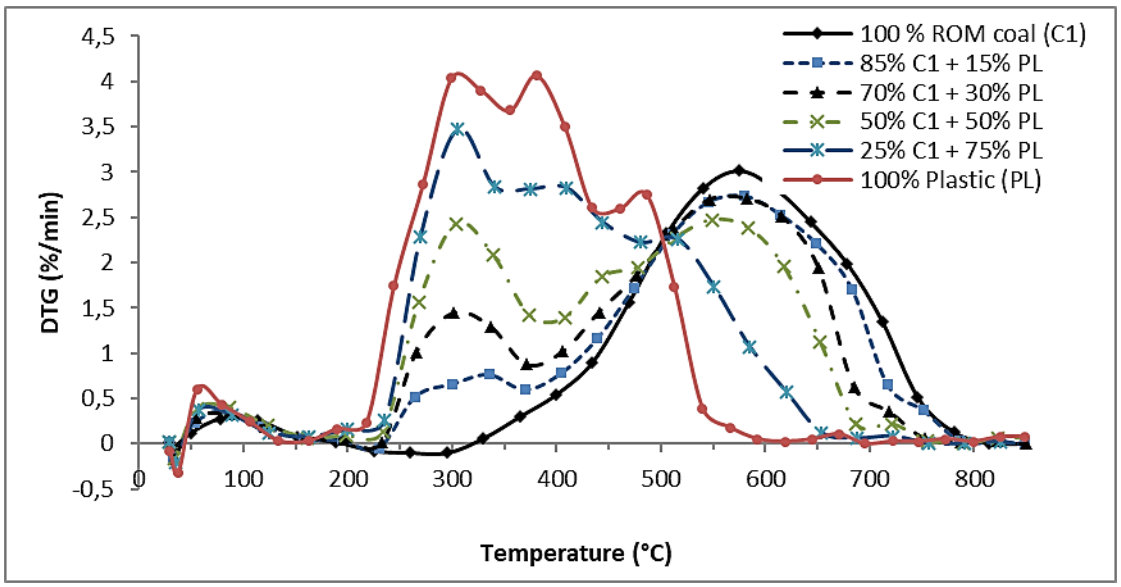

Figure 4. 4: The co-combustion profiles of the plastic (PL) and ROM coal (C1)

The initiation of volatile matter temperatures was found reduced to a lower temperature region for the blends of ROM coal with plastic (Figure 4.4) and same trend was seen for ROM coal with the paper blend (Figure 4.5). However, this did not decrease linearly with the increase of RDF in the blend. It is evident that for both types of RDF; PL and PB, the minimum temperature for IT_{VM} is achieved when 30% of RDF is present in the blend. A similar observation was made by Wang et al. (2012) during the co-pyrolysis of coal and biomass. The peak temperature increases as plastic RDF was added to the blend, up to the highest peak temperature for 70% C1 + 30% PL, and then begins to decrease as the plastic (PL) percentage in the blend is increased further. In the volatile combustion stage of the reaction the peak temperature decreases as the percentage of plastic in the blend decreases. At 25% C1 + 75% PL the peak temperature was reached in the lower temperature region and the combustion curve resembles that of raw PL. The profile also displays three peaks resembling a shoulder, with the first peak at 305°C, R_{max} value of 3.47 %/min, which is due to the reactivity of the RDF as the light volatiles are released and combusted.

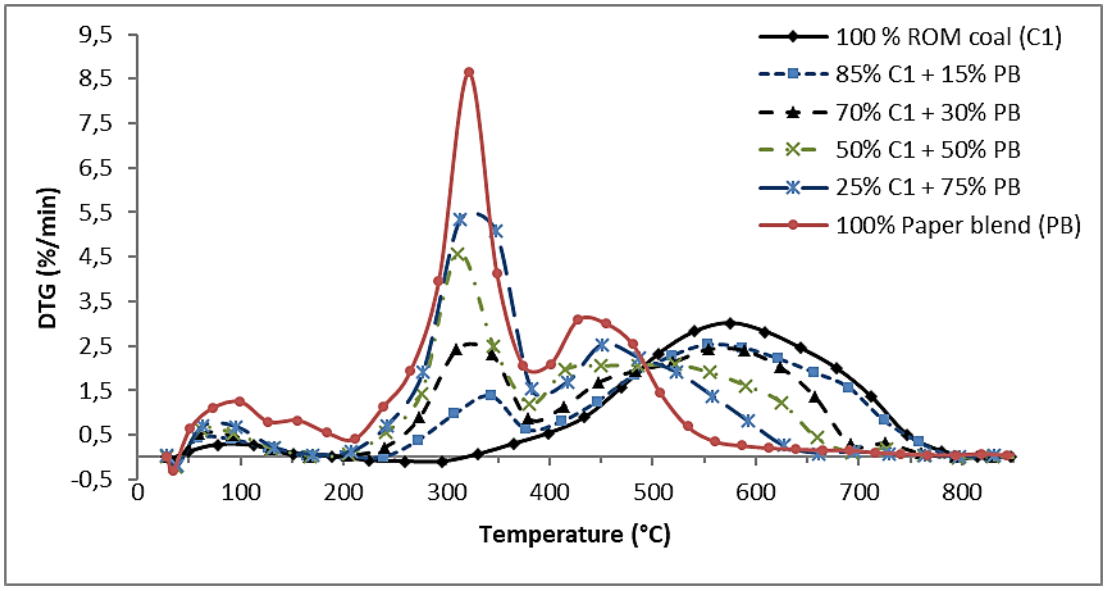

Figure 4. 5: The co-combustion profiles of the paper blend (PB) and ROM coal (C1)

The co-combustion of different blends of ROM coal with a paper blend (PB), also followed the same trend observed when ROM coal C1 was blended with plastic PL. The raw PB has the highest reactivity, and the reactivity of the coal was seen increasing as the percentage of the paper in the blend increases (Figure 4.5), with its peak temperature shifting from the fixed

carbon combustion region to volatile release and combustion region. The same trend was noted in Figure 4.4 for plastic and coal blend where the coal R_{max} increases drastically as it shifts to the lower temperature zone. The blends of C1 with PB show an overall decrease in the IT_{FC} with the lowest temperature observed for the blend of 50% C1 + 50% PB at 380°C.

The burnout temperature of the ROM coal used in this study was reduced with the addition of both PL and PB. The lowest T_b was achieved for the blend of 25% C1 + 75% PL at 619°C. The same percentage blend with PB gives a T_b of 673°C. The reduction in burnout temperature was also reported by Iordanidis et al. (2018) when co-firing waste components with coal. The same observation in the reduction of coal T_b was also made by Arias et al. (2008), Vamvuka et al. (2011) and Bada et al. (2015) in the studies of co-combustion of biomass with coal. The RDF samples are more reactive than the coal samples, they ignite at lower temperatures and therefore they burnout at a lower temperature (Iordanidis, et al., 2018).

4.2.2 CO-COMBUSTION PERFORMANCE OF DISCARD COAL AND RDF

The co-combustion potential of discard coal (C2) with PL and PB are depicted in Figure 4.6 and 4.7, respectively. As seen from both figures, the combustion profiles of discard (C2) with RDF are very similar to those of ROM (C1) with RDF. From Figure 4.6, it can be seen that as the RDF percentage in the blend increases, the DTG curves are seen with a dissimilar combustion profiles to that of the discard coal.

The ignition temperature for the discard coal show a downward trend with increasing amounts of plastic in the blend, up to 50%, thereafter no further decrease is achieved. The lowest ignition temperature (T_i) of 248°C was observed for the blend of 50% C2 + 50% PL (Figure 4.6), whilst the lowest T_i achieved for the same percentage blend with the RDF paper blend was 271°C, seen in Figure 4.7. In comparison with the blends of ROM coal (C1) and plastic (PL), the lowest ignition temperature with C1 was very similar (246°C), however, this was achieved with a greater proportion of PL in the blend 25% C1 + 75% PL. This shows that more discard coal (50%) can be blended with plastic to achieve a similar ignition temperature to that of 25% ROM coal with plastic.

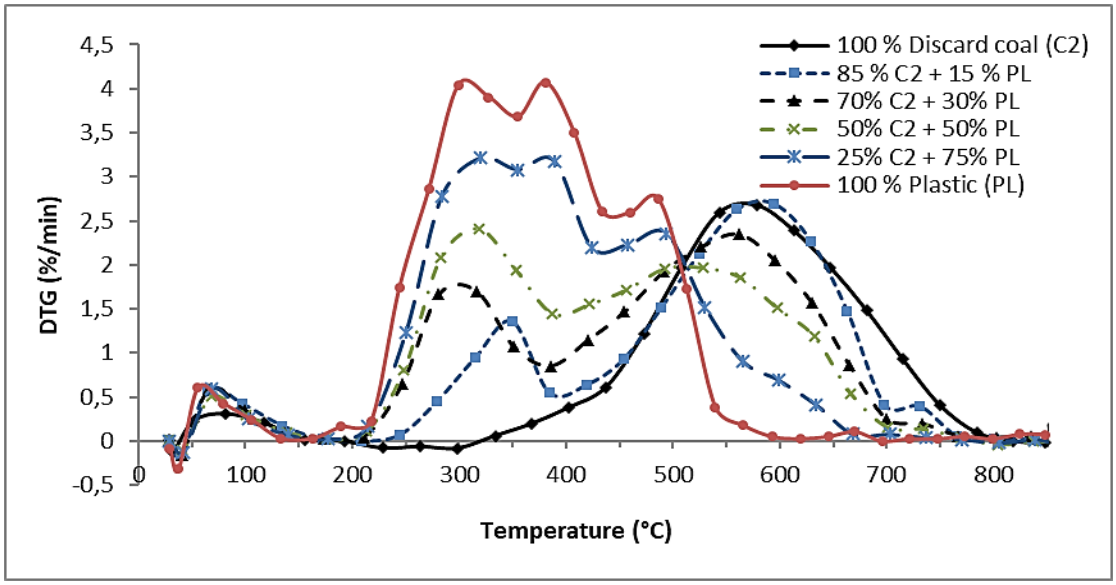

Figure 4. 6: The co-combustion profiles of the plastic (PL) and the discard coal (C2).

Both the discard and the ROM coal blends with PL and PB show roughly the same trend in initiation temperature of volatile matter, with an initial drop in the IT_{VM} which then becomes constant regardless of the increase in the RDF content in the blend. Figure 4.6 shows that the blend of 70% C2 + 30% PL achieved a lower IT_{VM} of 211°C than the corresponding blend with C1. The lowest IT_{VM} of 218°C was also achieved for the same percentage blend of C2 with PB (Figure 4.7). The blend with the lowest IT_{FC} was found to be the blend of 85% C2 + 15% PL at 454°C, thereafter as PL is increased in the blend, the IT_{FC} increases (Figure 4.6).

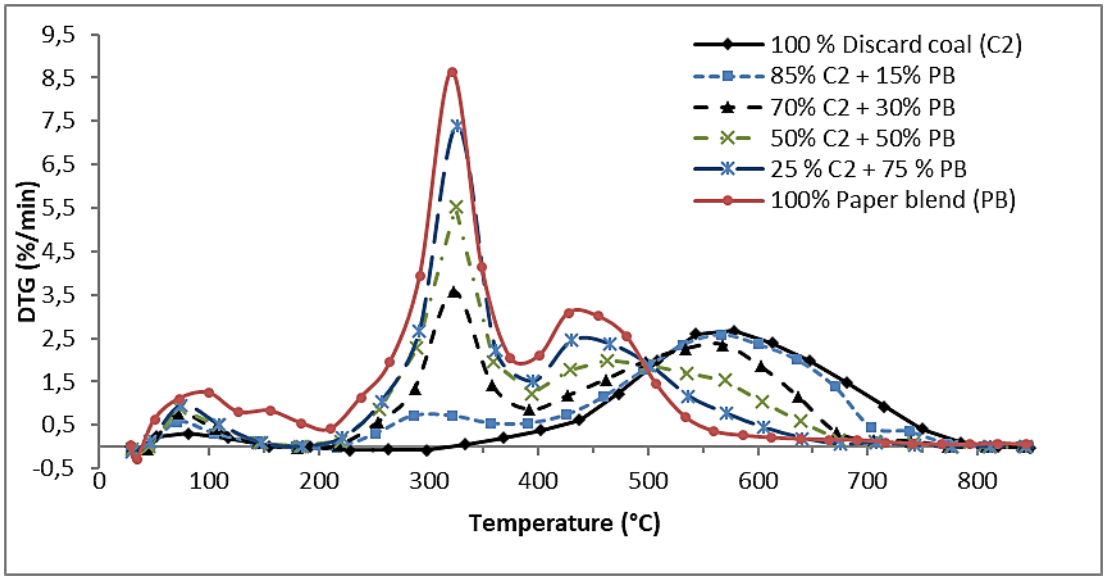

Figure 4. 7: The co-combustion profiles of the paper blend (PB) and the discard coal (C2)

From Figure 4.7, the paper blend with the lowest IT_{FC} was 70% C2 + 30% PB, and this was achieved at a temperature of 392°C. For the ROM coal (C1), the blends with the lowest overall IT_{FC} was the blend of 50% C1 + 50% PL, and the initiation of fixed carbon for this blend was achieved at a temperature of 439°C. The thermograph also shows that the R_{max} values which occur when the peak temperature is in the higher temperature regions, during the combustion of fixed carbon, are much lower than those that occur when the peak temperature occurs in the lower temperature region, during the volatile combustion. Figure 4.7 shows that the most reactive blend with the highest combustion rate was 25% C2 + 75% PB at 7.39 %/min.

It is evident from this study that as the plastic (PL) and paper blend (PB) is added to the blend with ROM coal (C1) and discard coal (C2) in greater amounts the burnout temperature T_b decreases. The lowest T_b is observed for the blend of 25% PL + 75% C2 at 630°C which is a significant improvement on the T_b of C2 which is 741°C. The addition of paper blend PB lowered the T_b even further, to 624°C. When comparing the burnout temperatures of C1 and C2 with both RDFs, and their blends, it can be seen that both RDF samples have a very low burnout temperatures, and as the RDF in the blends increases, the T_b for the blends decreases. From this study, the burnout temperature for the blend of ROM coal with PB was seen to be slightly higher than that of discard coal C2 with PB (Table 4.3). The same trend was seen with ROM coal C1 and blends of plastic blend, where the burnout temperature was found to be higher than when blended with discard coal.

Table 4. 3: Combustion performance parameters of the coal and RDF samples

Sample ID	T_i	IT_{VM}	IT_{FC}	PT	R_{max}	T_b	σ
100% C1	440	320	434	575	3.02	740	0 – 0.1
100% C2	455	324	438	578	2.68	741	0 – 0.1
100% PL	250	218	460	299	4.04	547	0 – 0.6
100% PB	265	211	375	321	8.64	651	0 – 1.2
85% C1 + 15% PL	388	235	439	580	2.73	734	0 – 0.2
70% C1 + 30% PL	366	233	441	582	2.7	710	0 – 0.2
50% C1 + 50% PL	300	234	479	549	2.47	706	0 – 0.3
25% C1 + 75% PL	246	236	480	305	3.47	619	0 – 0.2
85% C1 + 15% PB	390	238	411	552	2.54	740	0 – 0.2
70% C1 + 30% PB	340	203	413	554	2.43	710	0 – 0.4
50% C1 + 50% PB	258	205	380	314	1.92	679	0 – 0.3
25% C1 + 75% PB	260	207	382	313	5.33	673	0 – 0.9
85% C2 + 15% PL	400	245	454	594	2.69	722	0 – 0.4
70% C2 + 30% PL	335	211	455	561	2.35	720	0 – 0.3
50% C2 + 50% PL	248	213	456	318	2.41	681	0 – 0.1
25% C2 + 75% PL	249	215	458	320	3.21	630	0 – 0.2
85% C2 + 15% PB	415	220	426	567	2.58	730	0 – 0.2
70% C2 + 30% PB	272	218	392	323	3.57	690	0 – 0.2
50% C2 + 50% PB	271	220	394	325	5.52	667	0 – 0.2
25% C2 + 75% PB	272	222	396	327	7.39	624	0 – 0.4

σ – standard deviation of repeat tests

In conclusion, this section has shown that the combustion profiles of RDF and coal are dissimilar as the RDF samples displayed two or more peaks on the DTG plots, while the discard and ROM coal samples displayed only one weight loss peak. It was seen that the combustion performance of low-quality coal can be improved with the addition of RDF, as the ignition temperatures of the ROM coal and the discard coal shift to a lower temperature region as the RDF increases in the blend. This is in agreement with the findings of Iordanidis et al. (2018) who found that increasing MSW content when co-firing with lignite decreased the ignition temperature. Muthuraman et al. (2010) also found that increasing MSW content in the fuel blend with coal decreased the ignition temperature. This is favourable for a high-ash coal as the energy required for the combustion of the carbon is provided by the early release of the volatile matter. The RDF sample containing a bulk of plastic reduced the ignition and IT_{VM} parameters further than the RDF sample containing a majority of paper when blended with

discard coal. As a result, the burnout temperatures were also reduced with the addition of both PL and PB.

4.2.3 COMPARISON OF ROM COAL AND PLASTIC TO THE WEIGHTED AVERAGE

The interactions between the ROM coal and the RDF PL blends were investigated by comparing the experimental DTG plot with the weighted average DTG plot, calculated from Equation (4.3). The W_{total} is denoted as the total weight loss rate, x is the mass fraction of the fuel in the blend, and W is the individual weight loss rate for each fuel. It is evident from the difference in the combustion profiles (Figure 4.8) that there are some interactions between the RDF and coal which results in a combustion behaviour which is not linear additive. Experimentally, the ignition temperatures and the initiation of the volatile matter for the DTG curves takes place at a slightly higher temperature zone than the theoretical DTG. The volatile release showed two distinct peaks on the theoretical curve however, only one distinct peak was seen during this stage experimentally. The burnout of the co-combustion blends takes place sooner than theoretically expected. This deviation in the theoretical and experimental DTG, shows there is a synergistic reaction between the RDF and coal ROM coal C1, and this effect is in agreement with the findings of Hu et al. (2015) and Vamvuka et al. (2015). The synergistic effect on volatile release temperature was also found by Muthuraman et al. (2010). Up to 199°C, the theoretical and experimental curves show little to no deviation as this was below the ignition temperature and the decomposition had not occurred at this stage.

$$W_{total} = x_{ROM}W_{ROM} + x_{PL}W_{PL} \qquad \text{Equation 4.3}$$

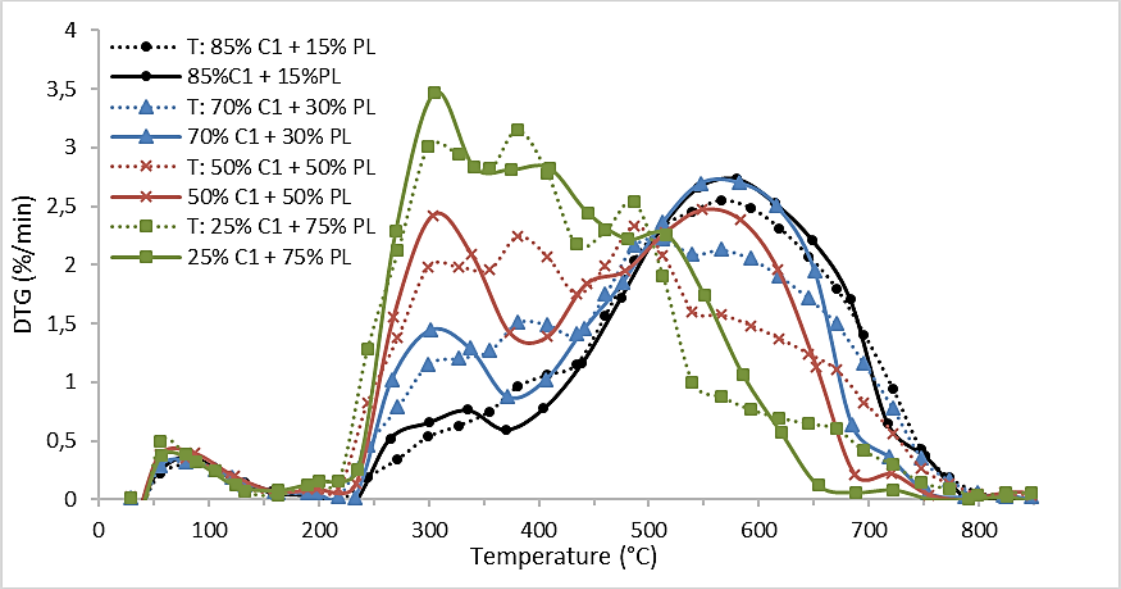

Figure 4. 8: The theoretical and experimental DTG plots of ROM coal and RDF PL

Figure 4.9, shows the weighted average DTG curves of the blends of C1 and PB with the experimental curves. It can be seen that the initiation temperatures of volatile matter and the burnout temperatures of these blends occurred at a slightly lower temperature than theoretically expected. This highlights the synergistic effect between the coal and RDF. The findings for the blends of discard coal with PL and PB were similar to those of the respective blends with ROM coal. These figures can be found in Appendix B.

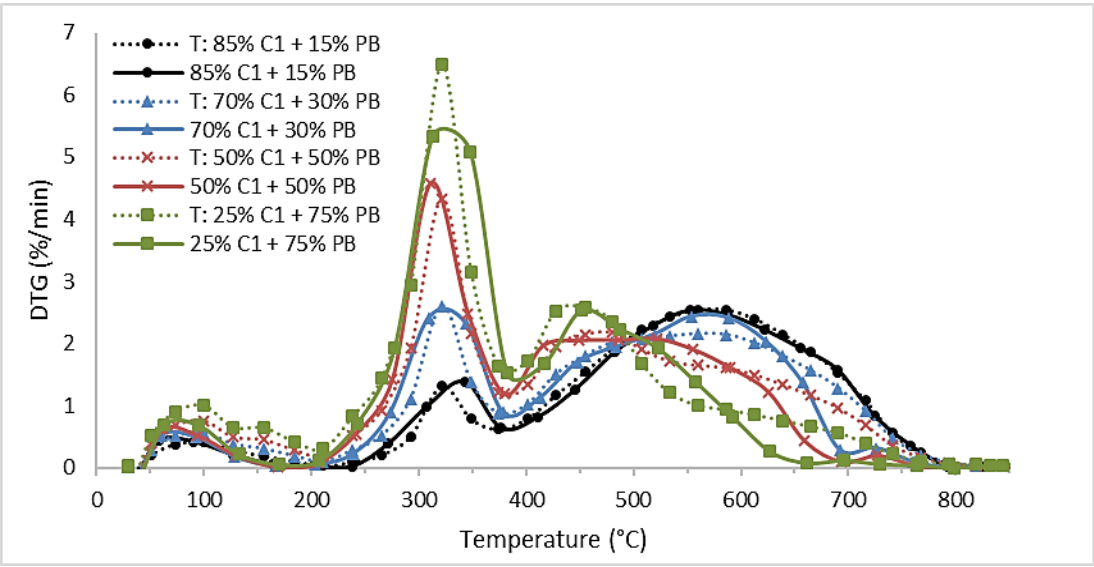

Figure 4. 9: The theoretical and experimental DTG plots of ROM coal and RDF PB

4.2.4 THE EFFECT OF HEATING RATE ON THE COMBUSTION PROFILE

In order to determine the effect of heating rate on the combustion profile, the samples were combusted at four different heating rates: 5°C/min, 7°C/min, 10°C/min and 14°C/min. The comparison of the combustion profiles of the discard coal and the RDF PL can be seen in Figure 4.10 and Figure 4.11, respectively (those for C1 and PB can be seen in Appendix B). There is a clear trend of increasing reactivity and weight loss rate as the heating rate increases for both sample C2 and sample PL in Figure 4.10 and Figure 4.11. It is also evident that the peak temperature corresponding to the maximum weight loss rate occurs at a higher temperature when the heating rate is increased. This shows that there is an overall shift of the combustion profile into the higher temperature zone when there is an increase in the heating rate. The shift of the DTG plot to the right results in delayed ignition and burnout temperatures, but increased weight loss rates. For the discard coal the R_{max} increased from 1.93 %/min (5°C/min) to 2.94 %/min (14°C/min). The increased reactivity and shift of the profile to the higher temperature zone is expected for all blends, when combusted at higher heating rates. The addition of RDF to the blend with coal would, however, reduce the burnout temperature and allow for the complete combustion of the sample.

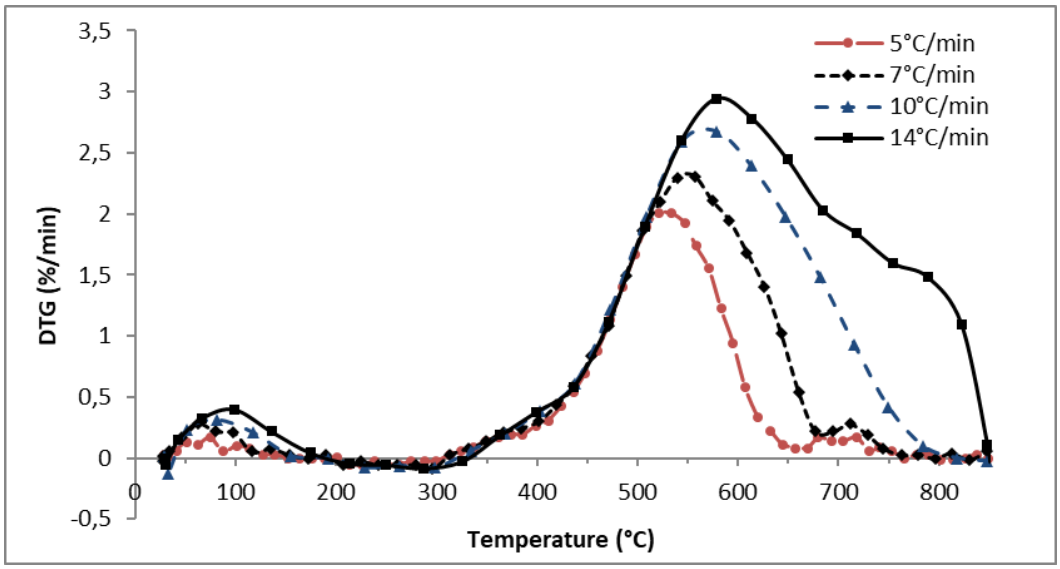

Figure 4. 10: Discard Coal C2 combustion profile at different heating rates

A larger increase was seen for the RDF sample PL (Figure 4.11), the R_{max} of PL increased from 2.24 %/min (5°C/min) to 6.41%/min (14°C/min). This is due to the fast increase in temperature, which rapidly releases the volatiles and combusts the large volatile matter content in the sample. The shift in the combustion profile to the higher temperature zone and the increase in the reactivity is in agreement with the findings of Wang et al. (2016) for the co-combustion of rice husk, pine sawdust and coal. It is also evident from the combustion profiles of PL below, that the area covered by the second peak increases as the heating rate increases, and this is due to the incomplete combustion of the lighter volatile matter, which combines with the adjacent higher temperature reaction of the heavier volatile components (Wang, et al., 2016).

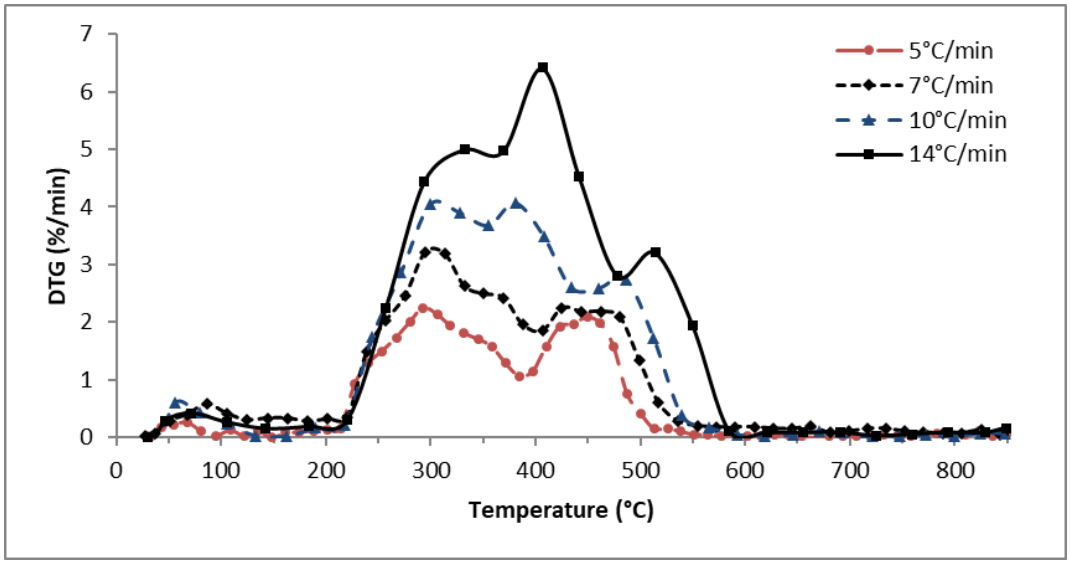

Figure 4. 11: PL combustion profile at different heating rates

4.3 REACTION KINETICS

The Coats-Redfern model-fitting method was utilised to determine the apparent activation energies for each raw sample and all the co-combustion samples. The samples were all combusted at a heating rate of 10°C/min and the conversion (α) of each sample was determined from Equation (2.13), this was then plotted against temperature to obtain the conversion plot presented in Figure 4.12. The combustion reactions which take place are considered in various different ways by different authors when determining the reaction kinetics using a suitable model-free or model-fitted method. Gil et al. (2010) and Alvarez et al. (2016) use a two-stage reaction in which oxidative degradation occurs in the first step, followed by the combustion of

char in the second step. Fang et al. (2013) and Gangavati et al. (2005) consider one reaction which is then divided into the stages of moisture loss, pyrolysis and char combustion. In this study one reaction is considered which is divided into three and also four stages for the loss of moisture, the release and combustion of volatiles - which can occur in two stages, and the combustion of char.

In order to determine the solid-state reaction model which best fitted the reaction achieved in this study, the data obtained were fitted to several solid-state reactions mechanisms and the linear regression was determined. The solid-state reaction model with the linear regression closest to 1 was deemed to be the reaction model which best fitted the data obtained from this study. The Jander's diffusion model (D3), $g(\alpha) = \left[1 - (1 - \mathrm{x})^{\frac{1}{3}}\right]^2$, was found to fit the data from each stage of combustion very well. This equation for three-dimensional diffusion was developed for spherical solid particles, it describes a reaction where the rate-controlling step is the diffusion of the reactant through the product layer. That is, the product layer which was developed replaces the reactant consumed in a one to one ratio. Gil et al. (2010) also found that the Jander's diffusion model described the combustion kinetics of coal co-fired with biomass very well, with a linear regression constant between 0.98 and 0.99 for stage B and close to 1 for stage C. Table 4.4 shows the stages of each combustion and co-combustion profile along with the calculated apparent activation energy for that stage.

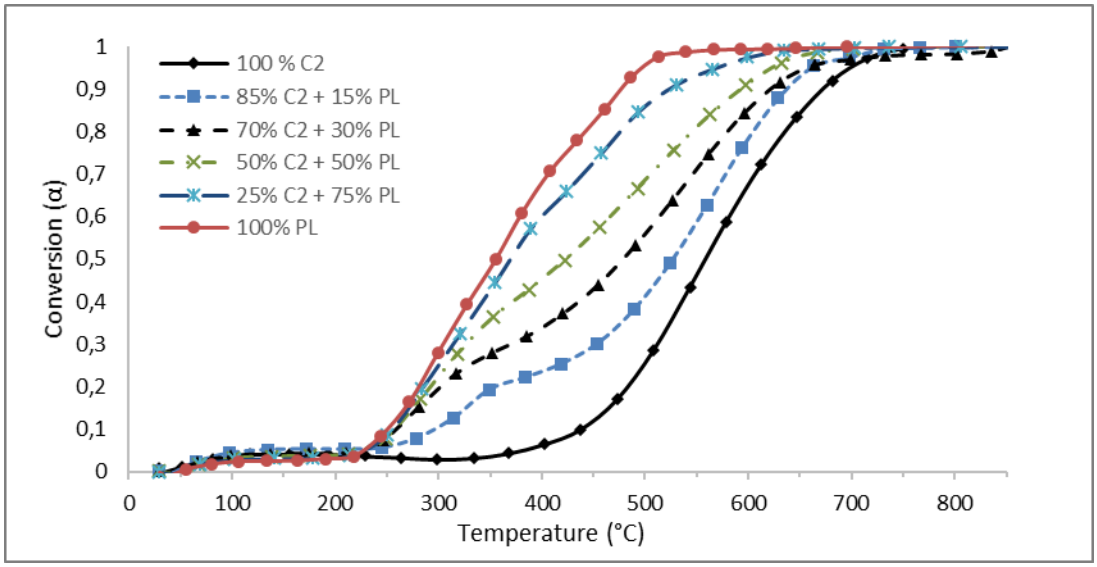

Figure 4. 12: Conversion plot of discard coal C2 and plastic PL

The combustion profile for all the raw samples were divided into different stages (3 or 4), as seen in Figure 4.13. For example; in the sample PL stage 1 occurred within the temperature range of 25 - 218°C. The next stage is denoted as stage 2 and corresponds to the release and combustion of the light volatiles in the sample and this occurred in the range of 218 - 355°C for sample PL. At higher temperatures, volatile components with higher molecular weight, diffuse through the pores of the samples and are released and combusted in stage 3, and this occurred within the temperature range of 355 - 434°C for the plastic blend RDF sample. The fourth stage signifies the char combustion, which occurred in the range of 460 – 547°C for PL. For the coal samples, the third stage occurred within the temperature of 320 - 438°C, while the 4th stage occurred in the range of 434 – 741°C. During the char combustion stage diffusion is generally the rate controlling step as the high temperature allows the chemical reaction to proceed faster than the diffusion of oxygen to the particle (Smith, et al., 1981).

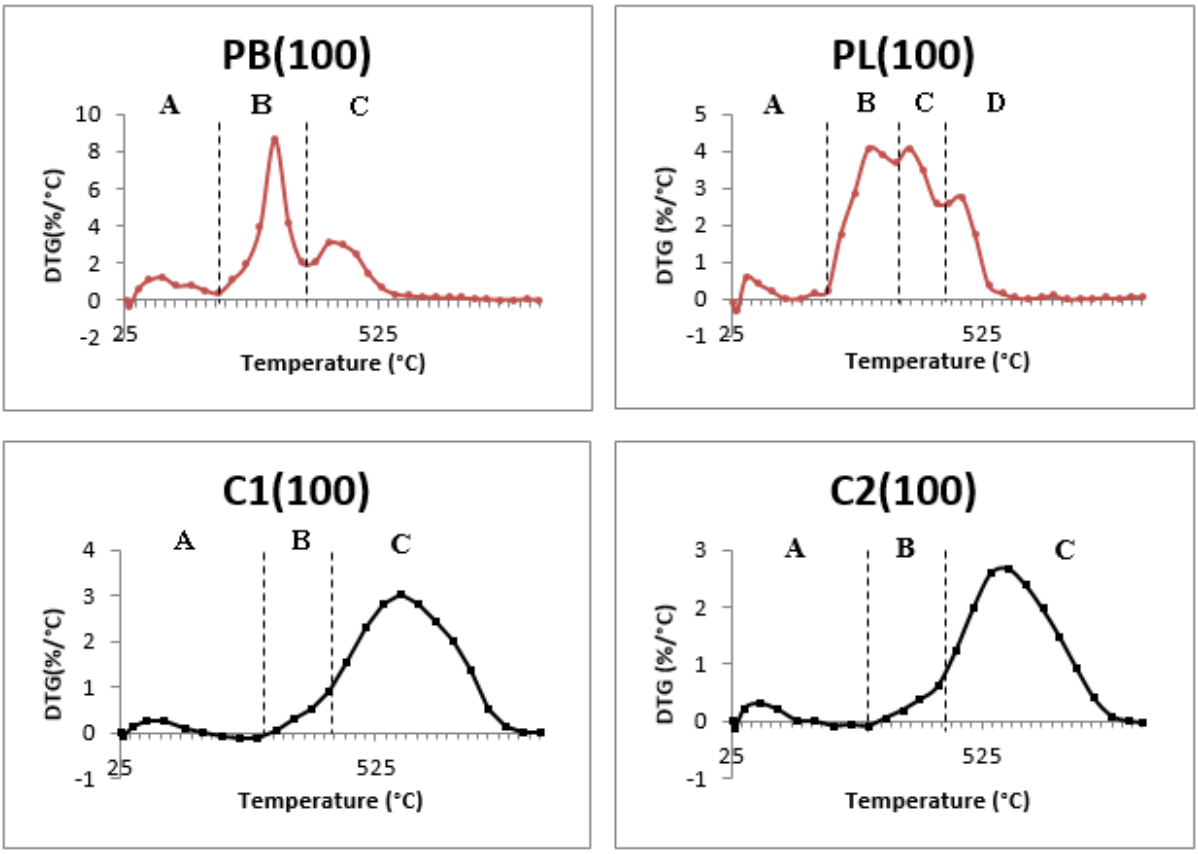

Figure 4. 13: Stages of combustion of the raw materials

The release and combustion of the volatile matter for the coal samples used in this study showed an apparent activation energy in the range of 68.7 - 83.7 kJ/mol. These values are within the range (53 and 290 kJ/mol) reported by Smith et al. (1981), for the apparent activation energies for various ranks of coals for the release and combustion of the volatiles. The activation energy for the combustion of the fixed carbon in the low-quality ROM and discard coals were found to be 104.4 kJ/mol and 109.9 kJ/mol, respectively. These values are similar to that found for the high ash coal used in the study by Muthuraman, et al. (2010), of 119.3 kJ/mol.

The activation energy for the release and combustion of the volatile matter in the raw plastic sample, was obtained by dividing this stage into 2. Stage 2, noted as combustion of volatiles had an E_a of 96.3 kJ/mol, with stage 3 having an E_a of 49.6 kJ/mol for initiating the combustion of fixed carbon and 37.3 kJ/mol for the combustion of the remaining char in stage 4. For the paper blend (PB) sample, the E_a obtained was 71.1 kJ/mol for the release and combustion of volatiles, which was lower than that from the plastic sample, i.e. less energy is needed for the combustion of paper compared to the plastic sample. The higher oxygen content in the paper might be responsible for the lower activation energy attained by the sample. This can also be supported by the higher IT_{VM} seen in Table 4.3 for the paper sample compared to the plastic sample.

From Table 4.4, it can be seen that adding the plastic (PL) to the blend with ROM coal increases the apparent activation energy of the pyrolysis process. In the blend with 85% ROM the E_a was 47.8 kJ/mol, and this increases to 83.8 kJ/mol in the blend with only 25% ROM + 75% PL for the volatile combustion. The same trend is seen with discard coal, where the E_a of the blend with 85% discard coal has an E_a of 52.4 kJ/mol, and then increases to 88.5 kJ/mol for the blend with 75% PL. This was in agreement with the study conducted by Wang et al. (2016) on the co-combustion of coal and biomass. The author found that the E_a of the volatile combustion was higher than that of the char combustion as a result of the lower temperature environment of the volatile combustion which resulted in a higher energy requirement for the reaction (Wang, et al., 2016). In addition, after the volatiles are released a porous char remains which results in easier diffusion of oxygen to the surface and lower the required activation energy for the char combustion stage (Wang, et al., 2016). This is also in agreement with the findings of the study by Alvarez et al. (2016) in which 12 of the 28 tested biomass samples showed a higher activation energy in the first stage from 210 to 400°C, due to the decomposition of cellulose in this temperature range (Alvarez, et al., 2016). The increase in activation energy in this

temperature range was also found by Jayaraman et al. (2017) for the co-combustion of coal with both poplar wood and hazelnut shells.

The release of the heavier volatiles showed a nonlinear decrease in the E_a for stage 3 when plastic was added to the blend with both ROM coal and discard coal (Table 4.4). The combustion of the fixed carbon showed a much smaller peak on the combustion profile for plastic PL and an E_a for Stage 4 of 37.3 kJ/mol, due to the smaller fixed carbon content of the sample when compared to coal. This reduced the E_a of Stage 4 during co-combustion when PL was added to the blend, from 78.7 kJ/mol for the blend with 85% ROM to 35 kJ/mol for the blend with 25% ROM + 75% PL. When PL was co-combusted with the discard coal, the E_a was reduced from 77.8 kJ/mol for the blend of 85% discard to 33.5 kJ/mol for the blend with 25% discard. The same trend of decreasing activation energy was observed by Muthuraman et al. (2010) when co-firing coal with MSW, as the E_a decreased from 119.3 - 151.7 kJ/mol for the two coals tested to 83.2 kJ/mol for char combustion of the 50-50 blend of coal with MSW. This is also in agreement with the findings of Wang et al. (2016) for the fixed carbon reaction kinetics of the co-pyrolysis of biomass and coal.

In summary, for the RDF tested in this study, the calculated apparent activation energies for the combustion of the volatile matter was seen to be increasing as the RDF was added to the blend with coal, which could be due to the low temperature environment of the pyrolysis. This result was found to be in contrast to the E_a obtained from the combustion of the char. The reduction in the E_a for the combustion of the char showed that the addition of RDF to low-quality coal results in a fuel which requires less energy and time to combust. The coal blend with RDF PL ($\leq$ 30%) shows a similar combustion profile to 100% coal making these blends the most suitable for co-firing in an existing coal power station infrastructure. Of these blends, the blend of discard coal (70%) and PL (30%) showed the lowest apparent activation energies of 55.8 kJ/mol and 54.2 kJ/mol for the volatile and char combustion, respectively, making this the most favourable blend for co-combustion.

Table 4. 4: The reaction kinetics of the combustion and co-combustion of coal, RDF and their blends

Sample ID	Stage 1 (°C)	Stage 2 (°C)	E_a (kJ/mol)	R^2	Stage 3 (°C)	E_a (kJ/mol)	R^2	Stage 4 (°C)	E_a (kJ/mol)	R^2
100% C1	25-320				320-434	83.7	0.99	434-740	104.4	0.99
100% C2	25-324				324-438	68.7	0.98	438-741	109.9	0.99
85% C1 + 15% PL	25-235	235-370	47.8	0.99	370-439	42.9	0.99	439-734	78.7	1
70% C1 + 30% PL	25-233	233-372	64.8	0.96	372-441	34.9	0.99	441-710	68.3	0.99
50% C1 + 50% PL	25-234	234-374	72	0.96	374-479	33.8	0.99	479-706	56	0.99
25% C1 + 75% PL	25-236	236-341	83.8	0.97	341-480	41.1	1	480-619	35	0.96
85% C1 + 15% PB	25-238	238-377	53.2	0.98	377-411	28.1	1	411-740	68	1
70% C1 + 30% PB	25-203	203-379	57.3	0.97	379-413	22.2	1	413-710	53.8	0.99
50% C1 + 50% PB	25-205	205-380	67.6	0.95				380-679	42	1
25% C1 + 75% PB	25-207	207-382	73.7	0.96				382-673	31.4	0.97
85% C2 + 15% PL	25-245	245-384	52.4	0.98	384-454	27.2	0.98	454-722	77.8	0.99
70% C2 + 30% PL	25-211	211-386	55.8	0.96	386-455	33.9	0.99	455-728	54.2	0.99
50% C2 + 50% PL	25-213	213-387	70.1	0.97	387-456	32.6	1	456-681	48.1	1
25% C2 + 75% PL	25-215	215-355	88.5	0.99	355-458	44.6	0.98	458-630	33.5	0.99
85% C2 + 15% PB	25-220	220-390	40.2	0.98	390-426	33.3	1	426-730	78.7	1
70% C2 + 30% PB	25-218	218-392	65.3	0.95				392-690	54.1	0.99
50% C2 + 50% PB	25-220	220-394	73.2	0.95				394-667	35.5	0.99
25% C2 + 75% PB	25-222	222-396	78.9	0.95				396-624	30.9	0.99
100% PL	25-218	218-355	96.3	0.98	355-460	49.6	0.99	460-547	37.3	0.91
100% PB	25-211	211-375	71.1	0.95				375-651	31.1	0.95

C1 - ROM coal, C2 - Discard coal, PL- Plastic RDF, PB - Paper blend RDF, E_a - apparent activation energy, R^2 - linear regression

4.4 ASH ANALYSIS

This section details the results of the ash analysis which was conducted on selected samples. The 100% RDF samples and 100% discard sample were chosen, as well as the blends of discard coal with RDF at 30% and 75% RDF. The discard coal was chosen as this research focuses on the utilisation of high ash and low-quality South African coal co-fired with RDF. This is aimed at improving the combustion performance of the coal and reducing its emission. One of the main concerns of combusting RDF in a conventional coal-fired boiler is the detrimental effect the ash produced will have on the boiler surfaces. RDF contains alkali and alkali-earth metals which form low-melting point deposits. These deposits hinder heat transfer and decrease the efficiency of the boiler, they can also accumulate and result in costly mechanical breakdowns (Teixeira, et al., 2012). It is expected that the composition of ash can be improved upon by co-firing the RDF with a high ash South African coal.

4.4.1 ASH SURFACE MORPHOLOGY

The surface morphology of the ash samples was determined using scanning electron microscopy (SEM). The image as well as the semi-quantitative elemental analysis can be seen in Figure 4.14 – Figure 4.20. The depressions seen in the SEM image of some of the samples is due to the carbon tape used in the analysis. Spectrum 1 gives the overall composition of the sample, while spectrum 2 and 3 are localised compositions of the chosen spots. The ash of 100% paper blend PB (Figure 4.14) is heterogenous in nature and is comprised of very large irregular agglomerated deposits as well as fine particles. The ash of the 100% plastic PL sample (Figure 4.15) contained much more fine particles in comparison to the 100% PB sample. The large particles seen in Figure 4.14 are made up of aluminium (88.92%), which could be from the packaging components and paper containing aluminium foil. This indicates that the materials in the RDF did contain a number of elements, including alkali and alkali-earth metals known to form low melting point deposits, as well as chlorine known to cause corrosion to boiler surfaces.

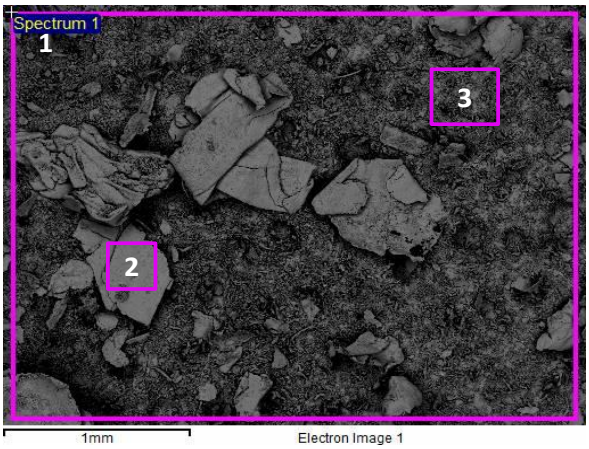

Element	Spectrum		
	1	2	3
Al	33.72	88.92	13.51
Ca	12.42	1.92	15.66
Cl	2.41	-	-
Mg	0.94	-	1.58
Na	3.77	-	5.92
Si	8.47	-	12.13
Ti	3.75	-	5.31

Figure 4. 14: SEM image of 100% paper blend (PB) ash

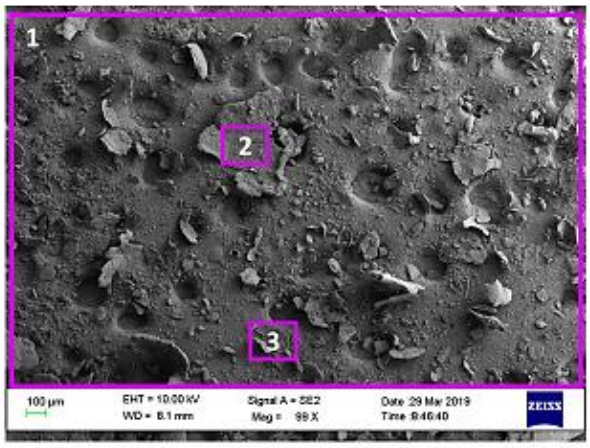

Element	Spectrum		
	1	2	3
Al	24.96	70.27	22.27
Ca	9.77	-	12.42
Cl	-	2.52	3.35
Mg	-	-	-
Na	4.02	2.21	3.74
Si	8.11	-	9.02
Ti	11.01	-	17.43

Figure 4. 15: SEM image of 100% plastic (PL) ash

The SEM image of 100% discard coal (Figure 4. 16) shows that the ash contained mostly fine particles. The larger particles which were seen in the micrograph are made up of Al and Si, which are the most common elements found in South African coals. This is in agreement with the findings of Fuller et al. (2018) on the co-firing of coal and biomass where the SEM analysis also revealed that the coarse particles were composed of alumina silicates. The angular shapes of the particles indicate that they are crystalline in nature (Fuller, et al., 2018). There was no presence of alkali metals or chlorides, however there were small amounts of Ca and Ti. The images in Figure 4.17 and Figure 4.18 show that as the discard coal (C2) content in the fuel is increased there are fewer large irregular particles and more fine particles, which is in agreement with the findings of Fuller et al. (2018). The semi-quantitative analysis also shows that the

content of Ca, Mg, Na, Cl and Ti decreased as discard coal is added to the fuel blend. The Si content increases as discard coal is increased.

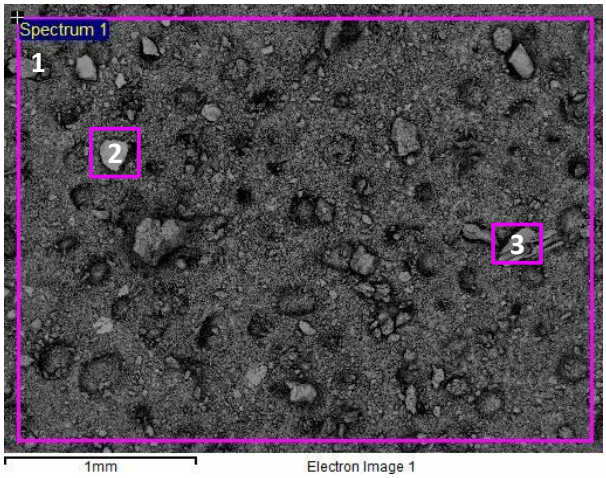

Element	Spectrum		
	1	2	3
Al	19.29	28.32	24.66
Ca	4.63	-	-
Cl	-	-	-
Mg	-	-	-
Na	-	-	-
Si	28.86	36.07	29.03
Ti	-	-	2.51

Figure 4. 16: SEM image of 100% discard coal C2 ash

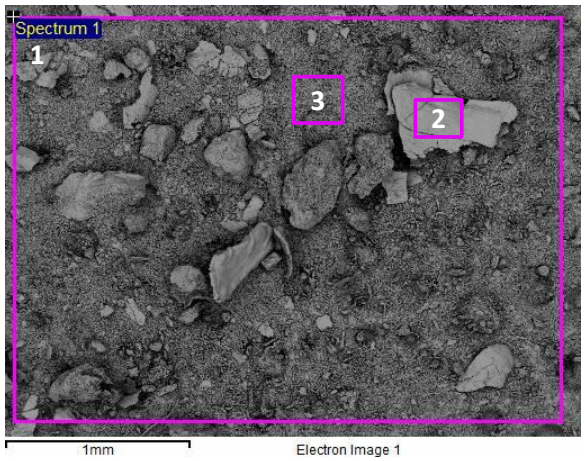

Element	Spectrum		
	1	2	3
Al	27.04	89.50	13.83
Ca	8.00	-	13.36
Cl	-	-	-
Mg	-	-	0.91
Na	1.69	-	2.35
Si	17.53	1.27	19.81
Ti	3.41	-	4.34

Figure 4. 17: SEM image of 25% C2 + 75% PB ash

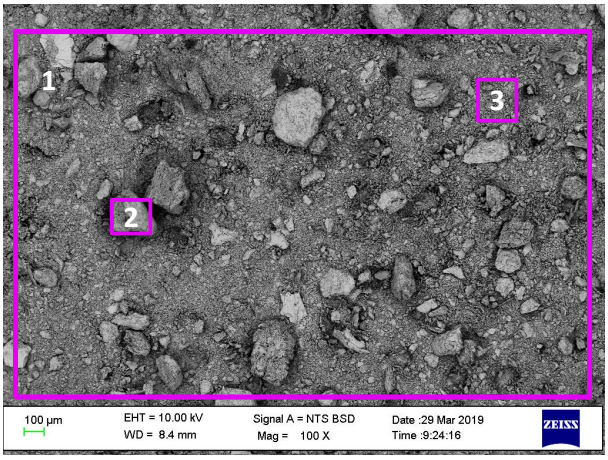

Element	Spectrum		
	1	2	3
Al	19.81	23.08	20.57
Ca	6.43	-	4.80
Cl	-	-	-
Mg	-	-	-
Na	-	-	0.86
Si	25.74	29.81	26.78
Ti	2.94	-	3.42

Figure 4. 18: SEM image of 70% C2 + 30% PB ash

Figure 4.19 and Figure 4.20 show the SEM images of the ash from the co-combustion of discard coal C2 with plastic PL. These images show a larger quantity of agglomerates and irregular shaped particle deposits in comparison to the co-combustion ash from paper blend PB. The 100% PL ash sample (Figure 4.15) did not show as many large deposits which shows that there were some interactions between the elements within this fuel. Fuller et al. (2018) found that the presence of alkalis metal such as Na, Mg in biomass causes low melting point deposits which stick and cause particles to cluster and agglomerate. These findings are also in agreement with those of Wu et al. (2011), who found a combination of spherical particles and agglomerated nucleates in the ash from the co-combustion of coal and SRF. The agglomerates were formed from the vaporization of the inorganic species and were irregular in shape (Wu, et al., 2011).The large particle deposits in the ashes of co-combustion of C2 and PL are made up of mostly Si and Al, with smaller amounts of alkali/alkali-earth metals and Ti. Overall, the content of Ca, Na and Ti decreased as the discard coal was increased in the fuel (Figure 4.19 and 4.20).

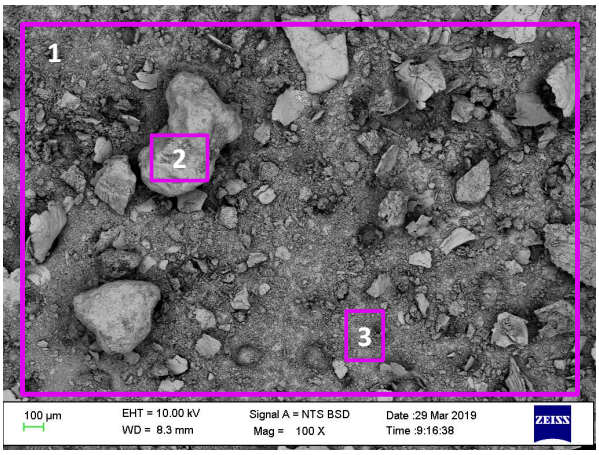

Element	Spectrum		
	1	2	3
Al	23.00	17.48	12.57
Ca	10.09	7.00	10.90
Cl	-	-	-
Mg	-	-	-
Na	1.91	2.44	2.54
Si	15.79	34.91	15.77
Ti	7.61	-	8.85

Figure 4. 19: SEM image of 25% C2 + 75% PL ash

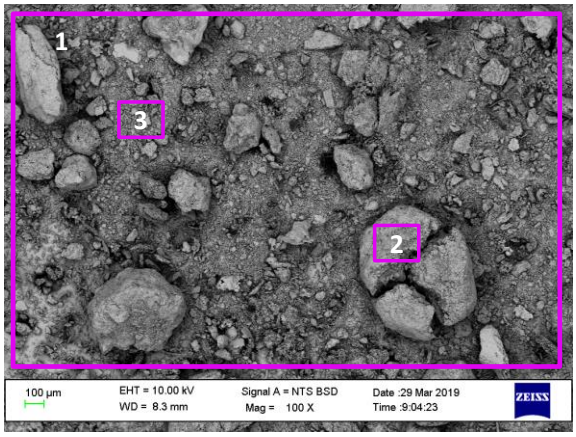

Element	Spectrum		
	1	2	3
Al	19.10	21.26	17.78
Ca	5.90	2.33	9.46
Cl	-	-	-
Mg	-	-	-
Na	-	-	-
Si	24.08	26.73	22.56
Ti	3.78	5.28	3.89

Figure 4. 20: SEM image of 70% C2 + 30% PL ash

Taylor et al. (1982) identified four basic morphologies for ash from the combustion of RDF, these include the ‘shredded sponge’, ‘rolled paper’, ‘paint chip’ and ‘spheres’ morphologies. The RDF samples in this study mostly resembles the ‘shredded sponge’ morphology (Figure 4.21 A, taken from 100% PL) which is in agreement with the findings of Taylor et al. (1982). Figure 4. 21 B shows the less common ‘paint chip’ morphology taken from the 100% PB ash sample.

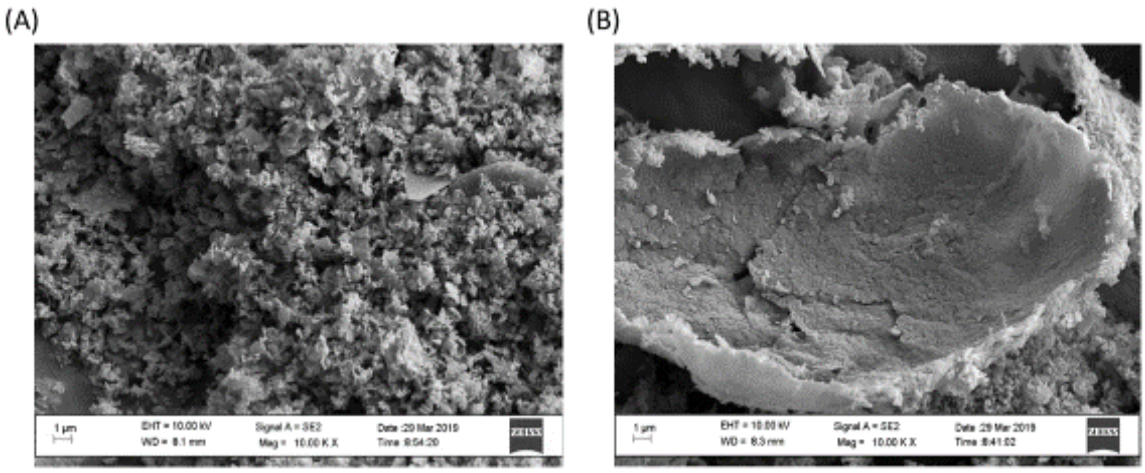

Figure 4. 21: 'Shredded sponge' and 'paint chip' morphologies of RDF samples

From the analysis conducted in this study, the RDF sample PB was seen to be made up of large irregular shaped particles as well as fine particles, while the discard coal sample contained mostly fine particles. The co-firing of RDF and coal worked to improve the composition of the ash samples by reducing the alkali metals, alkali-earth metals, and chlorides in the RDF ash, which is in agreement with the findings of Wu et al. (2011). Co-firing also reduced the amount of agglomerated deposits from the RDF. Section 4.4.2 below explores the quantitative analysis of the above ash samples, through X-ray fluorescence (XRF) analysis.

4.4.2 ELEMENTAL ANALYSIS OF THE ASH

The results of the XRF analysis conducted on the coal ash obtained from the seven selected samples utilized in this study are depicted in Table 4.5. The major elemental composition of the ash from the discard coal (C2) (Table 4.5), was compared with that of coal ash from different South African coals from literature as seen in Table 4.6.

Table 4. 5: Major elemental composition of the ash samples

	Major elemental composition (wt%)								
Sample ID	Fe_2O_3	CaO	MgO	K_2O	Na_2O	SiO_2	TiO_2	Al_2O_3	SO_3
100% C2	9.42	6.47	1.01	1.09	1.38	50.87	2.51	34.49	3.26
100% PB	1.44	29.66	3.35	1.08	13.65	32.15	9.04	73.55	8.62
100% PL	1.10	18.83	1.55	1.01	8.24	21.22	16.71	45.19	4.29
70% C2 + 30% PL	8.49	7.76	1.00	1.14	1.91	46.04	3.98	34.57	5.22
25% C2 + 75% PL	5.75	12.51	1.17	1.05	4.41	35.67	9.18	43.11	9.57
70% C2 + 30% PB	8.47	7.29	1.06	1.16	2.16	47.77	2.83	34.33	4.49
25% C2 + 75% PB	6.55	13.88	1.42	1.01	4.27	40.47	4.82	41.41	11.68

wt% - weight percentage average of three results

The predominant oxides found in the 100% coal ash are SiO_2, Al_2O_3, Fe_2O_3 and CaO. This result is in agreement with the findings of other authors with regard to South African coal ash. Akinyeye et al. (2016) analysed ash from the electrostatic precipitator of a South African coal-fired power station and found the same major oxides as what was found in this study. Similar results were also found by Maledi (2017) from the analysis of South African discard coal and Waanders et al. (2003) from the analysis of ash from Lethabo coal Power Station which receives coal from the New Vaal mine in the Free State province. The results from these authors are depicted in Table 4.6. It is evident that SiO_2 and Al_2O_3 make up the majority of the discard coal ash at 50.87% and 34.49%, respectively. Although the XRF analysis does not indicate the percentage composition of other minerals present in the ash analysed in this study, the literature had shown that the South African coal ash also consists of other minerals such as clay minerals, kaolinite ($Al_2Si_2O_5(OH)_4$), illite ($K_{0.75}(Al_2)Al_{0.75}Si_{3.25}O_{10}(OH)_2$) and montmorillonite ($Na_{0.7}Mg_{0.7}Al_{3.3}Si_8O_{20}(OH)_2$) which contain both Si and Al (Maledi et al., 2017). Therefore,

the ash obtained from this discard coal, with concentrations of K_2O, Na_2O and MgO, is also expected to contain some of these minerals.

The discard coal ash was found to contain a relatively high Fe_2O_3 content of 9.42%, which was higher than those reported by other authors, however, it was close to the 7.7% reported by Hattingh (2013) on the coal ash from Inyanda colliery in Mpumalanga. Most of the reported values given are for bituminous to sub-bituminous coals, however, the discard coal used in this study is likely to contain many more unwanted minerals, leading to an increase in Fe_2O_3 content. This high Fe_2O_3 content indicates the presence of pyrite (Fe_2S) minerals, which is further supported by the relatively high sulfur content of this coal. Other sources of Fe could include the minerals siderite ($FeCO_3$), chlorite ($Fe_5Al_2Si_3O_{10}(OH)_8$) and jarosite ($(Na,K)Fe_3(SO_4)_2(OH)_6$) (Maledi, 2017). The presence of CaO indicates that the ash could contain calcite ($CaCO_3$) and dolomite ($CaMg(CO_3)_2$) minerals (Maledi, 2017). The presence of TiO_2 indicates that the ash contains rutile or anatase minerals. Rutile is the most common titanium dioxide found in South African coals, while anatase appears in minor amounts from 1 to 2 wt.% (Maledi, 2017).

Table 4. 6: Major elemental composition of South African coal ash from literature

Major elemental composition (wt.%)	Maledi (2017)	Akinyeye et al. (2016)	Waanders et al. (2003)
SiO_2	45.10	52.30	49.05
Al_2O_3	23.80	23.80	31.79
Fe_2O_3	5.61	5.62	6.83
CaO	7.53	5.07	6.64
TiO_2	1.89	1.41	1.92
K_2O	0.77	0.71	0.67
MgO	2.35	1.41	1.54
Na_2O	0.66	-	-

wt.% - weight percentage

Table 4.5 shows that the most abundant oxide in the RDF (PB and PL) ash composition was found to be Al_2O_3, followed by SiO_2. The Al_2O_3 content could be due to the presence of aluminium foil from the various packaging materials contained in the RDF, such as the multi-component soup and spice packaging, as well as the ice cream packaging and the foil backed paper. The reaction of Al with oxygen is rapid and Al_2O_3 is formed according to the reaction in Equation (4.5). The alkali, Na_2O and K_2O, and alkali-earth metal oxides, CaO and MgO, present in the RDF ash indicate that these elements were present in the RDF in their ionic or organic forms (Iacovidou, et al., 2018). These forms of the elements are more volatile than their mineral forms found in coal (Iacovidou, et al., 2018).

$$4Al + 3O_2 \rightarrow 2Al_2O_3 \qquad \text{Equation 4.5}$$

From Table 4.5, it can be seen that the SiO_2 content in the ash decreased with increasing RDF content in the fuel, which is in agreement with the findings of Zhang et al. (2018) on the ash obtained from the co-combustion of coal and MSW. Zhang et al. (2018) also found a decrease in the content of Al_2O_3 with the addition of MSW to the fuel blend. According to Table 4.5 the Al_2O_3 content in coal ash was seen to increase from 34.49% to 43.11% and 41.41% for the blends with 75% PL and 75% PB, respectively. This increase is due to the high Al_2O_3 content of the 100% RDF samples. The content of Fe_2O_3 can also be seen to decrease in the discard coal ash as RDF is increased in the fuel blend. The same trend was observed by Wu et al. (2011) where Fe_2O_3 decreased from approximately 6.4% in 100% coal combustion to 4.3% in the ash from the blend with 25% SRF. There was no significant change in the concentrations of MgO and K_2O from the co-combustion of coal with RDF. Wu et al. (2011) also found only slight variation in the MgO concentrations in the ash during co-combustion of coal and SRF. An increase in the CaO content of the ash can be observed as the proportion of RDF in the fuel was increased, the increase is similar for the addition of both PL and PB. An increase in CaO was also found by Wu et al. (2011) where the weight percentage of CaO in the cyclone ash was found to be around 3.5% when SRF was 25% in the fuel blend. This is in line with the findings of this study where the CaO from the coal ash increases from 6.47% to 7.76% for the 30% PB +70% coal discard ash (Table 4.5).

Table 4.5 also shows that the Na_2O content in the ash increased as the RDF in the fuel was increased, this was also found by Wu et al. (2011) as the Na_2O increased from approximately 0.9% to 1.2% in the ash with 25% SRF co-combustion. The SO_3 content in the ash was seen to increase as the RDF content in the fuel increased, especially for the paper blend co-fired with discard coal. This higher sulfur content was not in line with the ultimate analysis which found the sulfur content of the RDF samples to be negligible. It was also found by other authors that the sulfur content of the ash was not in line with the properties of the fuel and an increase in SO_3 was seen as the waste proportion in the fuel was increased. The investigation conducted by Wu et al. (2011) had shown that sulfur content in ash is related to the sulfur retention capability of the ash, rather than the sulfur content of the fuel. The author also concluded that the sulfur retention capability of the ash is influenced by the CaO content, which increased the retention of sulfur. Prior to this, Kaiser (1968) also noted that MSW had low fuel sulfur content, and the major portion of the sulfur is retained as SO_3 in the ash due to the presence of alkaline oxides, while in coal most of the sulfur is emitted as SO_2, with minor amounts retained as SO_3 in the ash. Figure 4.22 below verifies this, as it shows the relationship between the CaO and SO_3 in the ash of the blended fuels to be linear ($R^2 = 0.99$).

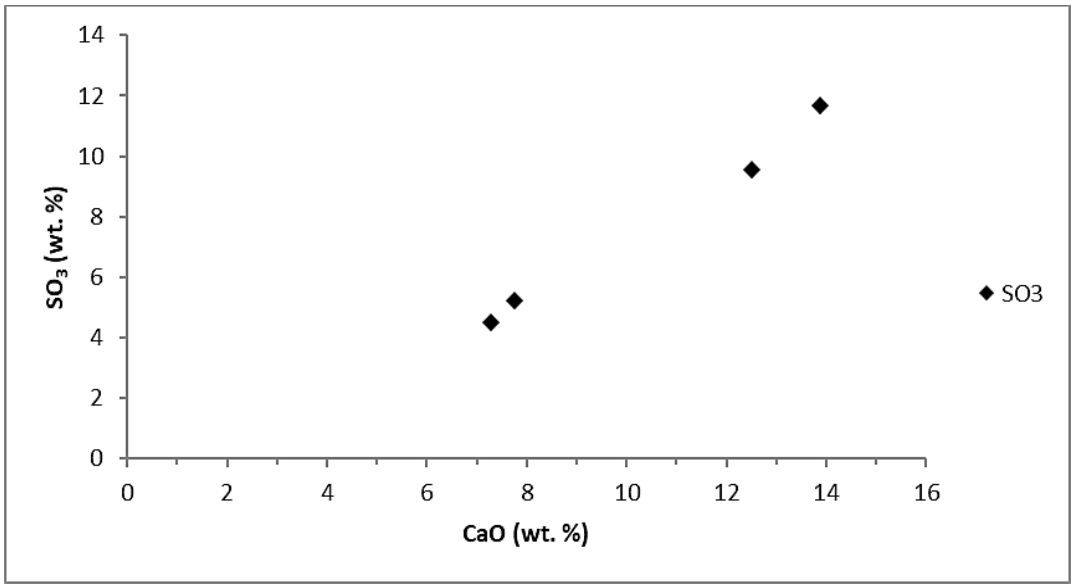

Figure 4. 22: The relationship between CaO and SO_3 in the co-combustion ash

For the seven selected ash samples, the base-to-acid ratio theoretical equation (Equation 2.10) and the fouling index (Equation 2.11) was used to predict the fouling and slagging propensity of the coal, RDF and their blends. The formation of slag is known to reduce the efficiency of a boiler, since it reduces the radiant heat generated on the boiler surfaces, while fouling occurs in the lower temperature regions on the convective heating surfaces (Miller, 2011). The fouling and slagging indices developed for coal applications are also useful in predicting the behaviour of biomass and even waste ash. However, there are some limitations to the indices as they do not take into account the reactivity of the elements in the ash and they assume that the alkali and alkali-earth metal oxides have an equal effect on the slagging propensity (Teixeira, et al., 2012).

Table 4. 7: Slagging and fouling indices of the ash samples

Sample ID	$R_{B/A}$	F_u
100% C2	0.22	0.55
100% PB	0.43	6.31
100% PL	0.37	3.42
70% C2 + 30% PL	0.24	0.73
25% C2 + 75% PL	0.28	1.55
70% C2 + 30% PB	0.24	0.79
25% C2 + 75% PB	0.31	1.65

$R_{B/A}$ - base-to-acid ratio, F_u - fouling index

The acid oxides (SiO_2, TiO_2 and Al_2O_3) are known to increase the melting temperature of the ash and thereby reduce its slagging potential, while the basic oxides (Fe_2O_3, CaO, MgO, K_2O and Na_2O) reduce the melting temperature and increase the likelihood of slagging. It can be seen in Table 4.7 that only the 100% PB sample had a high slagging propensity (index value between 0.4 and 0.7), with a value of 0.43. This could be attributed to the high content of CaO and Na_2O in its ash (Table 4.5) at 29.65% and 13.65%, respectively. In addition, the presence of alkali metal salts, Na and K, and alkali-earth metals, Ca and Mg, also form low viscosity deposits with low melting points. From the indices presented in Table 4.7, all the other ash samples showed a low propensity to slag, from the base-to-acid ratio. For the fouling index (F_u), an ash with an index value between 1.6 and 40 indicates a high propensity to foul, that is, such fuel has the potential to reduce the convective heat on the surface of a boiler, which was the case for the 100% PB and PL samples with an index of 6.31 and 3.42, respectively.

From Table 4.7, it can be seen that 25% C2 + 75% PB is also within the high range, due to the large quantity of PB in this sample. This is expected of samples containing large amounts of RDF. With an increase in the blending ratio of coal in the blend, the fouling and slagging potential of the fuel sample is expected to reduce significantly, and this was achieved as the discard coal is added to the fuel blend (Table 4.7). Sample 25% C2 + 75% PL was reduced to 1.55 which is in the range for medium fouling propensity. The samples containing 30% RDF + 70% discard coal were both in the lower to medium fouling propensity range at 0.73 and 0.79 for PL and PB, respectively.

In this study, the concentration of the potentially toxic elements (PTE), such as As, Co, Cr, Cu, Mn, Ni, Sb and V were also investigated, and these are expected to be higher in RDF wastes in comparison to coal (Iacovidou, et al., 2018). It is important to determine the concentrations of the elements in the ash generated from the co-combustion of different fuels, as the volatile fractions of these PTEs can be emitted, while the non-volatile fractions are contained in the coarse ash leading to environmental issues (Iacovidou, et al., 2018). The concentration of the trace elements in the ashes obtained from this study are reported in Table 4.8. It can be seen that the concentrations of As, Co, Cr, Nd, Rb, Sr, Th, V, Y and Zr increase as the quantity of discard coal is increased in the blend. As the RDF content in the blend is increased the concentrations of Cu, Ga and Zn are increased in the ash for both PL and PB. The paper blend (PB) specifically increases the concentrations of Mn, Pb and Ni in the ash, while the plastic RDF increases the concentrations of Ba, Sn and Sb. This is in agreement with the study conducted by Taylor et al. (1982) on the ash from the co-combustion of RDF and coal in a small power plant, where the coal was noted to increase the content of As, V and the rare earth metals such as Nd and Y, among other elements. Taylor et al. (1982) also found an increase in the concentrations of Ba, Mn, Sb, and Pb with the addition of RDF to the fuel blend. The results of the study by Norton et al. (1988) also found that co-firing coal with RDF increased the concentrations of Cu, Ga, Ni, Sn, Pb and Zn. There was little to no change in the concentrations of Mo, Se, Hg, Nb and Br when the fuel blend was altered in the present research.

Table 4. 8: Trace elements in co-combustion ash

	Trace element concentration (ppm)						
	100% C2	100% PB	100% PL	70% C2 + 30% PL	25% C2 + 75% PL	70% C2 + 30% PB	25% C2 + 75% PB
As	13	3	-	11	5	10	7
Ba	713	895	2695	958	1522	912	682
Br	1	34	11	1	4	1	6
Ce	71	-	17	34	42	25	-
Co	14	19	-	53	30	31	21
Cr	254	221	164	254	230	248	244
Cu	67	353	746	135	375	79	170
Ga	52	75	79	53	65	51	62
Hg	2	1	4	2	4	2	3
Mn	437	930	188	439	340	442	620
Mo	10	12	12	11	11	11	10
Nb	39	13	37	39	39	37	28
Ni	95	111	90	84	85	86	93
Nd	200	74	124	222	215	205	181
Pb	57	104	51	56	57	62	74
Rb	50	17	13	46	36	48	39
Sb	4	79	155	22	69	49	37
Se	1	1	1	1	2	1	4
Sn	18	46	205	47	105	56	34
Sr	50	17	13	46	36	48	39
Th	47	10	10	43	34	43	35
V	192	-	-	163	34	184	127
Y	65	9	8	61	44	61	47
Zn	48	2424	3910	427	1788	182	848
Zr	476	79	145	451	331	447	322

C2 – discard coal, PB – paper blend RDF, PL- plastic RDF, ppm – parts per million

The concentration limits of some heavy metals reported for Lithuania, Sweden and Finland are depicted in Table 4.9. The ash obtained from the co-combustion of RDF and coal utilized in this study meets the concentration limit required for most of the elements, however, the Hg concentration, seen in Table 4.8, in the 100% PL and blend of 25% C2 + 75% PL (4 ppm) was found to be above the limit for Hg. Therefore, the other ashes from the combustion and co-combustion of the fuels and their blends could be used as a soil conditioner in forests and agriculture in some countries.

Table 4. 9: Ash elemental concentration limits for utilisation in forests and agriculture (Lanzerstorfer, 2015)

Trace element	Concentration (ppm)
As	30 - 40
Cr	100 - 300
Cu	400 - 700
Hg	1 - 3
Ni	70 - 150
Pb	150 - 300
Zn	700 - 7000

4.4.3 INFLUENCE OF CHLORIDE CONTENT IN THE FUELS

The chloride content in the 100% RDFs, coal discard ash, and their blends were determined using ion chromatography, and the results from this analysis are depicted in Table 4.10. It can be seen that the water-soluble chloride concentration of the ash from the combustion of 100% RDF was much higher than that of the coal ash. The plastic sample (PL), was seen with the highest chloride concentration of 28 440 mg/kg, followed by the 100% paper blend with a high concentration of chlorides at 8982 mg/kg. The chloride content in the coal discard sample was found to be undetectable (Table 4.10), it is therefore expected that the co-combustion of this coal discard with RDF utilized in this study would help to reduce the chloride content of the RDF. This was seen experimentally as the coal content in the blend increases, the ash produced was seen to have a decreasing chloride content. This was in agreement with the findings of Wan et al. (2008) for the ashes obtained from the co-combustion of coal and RDF-5 (densified RDF in the form of pellets).

According to the standard EN 450-1 (2012) for the chemical requirements for fly ash use in the construction industry (concrete), the chloride concentration in the ash is required to be less or equal to 0.1%. From the results obtained in this study, both ashes produced from 100% RDFs are found to be unsuitable for use in concrete application. The required chloride limit of 0.1% was set to avoid the corrosion of steel reinforcements used in concrete (Fuller, et al., 2015). Of the ash samples tested for chlorides, samples 100% C2, 85% C2 + 15% PL, 70% C2 + 30% PL, 85% C2 + 15% PB, 70% C2 + 30% PB and 50% C2 + 50% PB were within this limit for concrete utilisation. Due to the very high chloride concentration in the PL sample, all the blends

of PL and discard coal still contained chlorides, although the concentration decreased as the coal ratio in the blend increases. For the PB sample, due to its lower chloride concentration, all the blends from 70% or more coal discard proportion were found to be undetected for chloride content. In the study conducted by Wu et al. (2011), the water-soluble chloride concentration of the ash from the co-combustion of coal with 25% SRF was found to be below 0.1%. This is in line with the findings from this study as all the blends containing up to 30% RDF had a chloride concentration less than 0.1%. The pH of the ash shows that all the samples are alkaline in nature, with the discard coal having the most alkaline pH of 12.2. It was found by other authors that the alkaline nature of ash was due to the presence of soluble basic oxides such as MgO and CaO (Akinyeye, et al., 2016).

Table 4. 10: Chloride concentration, pH and electrical conductivity of ash samples

Sample ID	pH	EC (µS/cm)	Cl^- concentration (mg/kg)	Cl^- concentration (%)
100% PL	10.8	5710	28440	2.840
100% PB	10.6	3600	8982	0.898
100% C2	12.2	4350	UT	UT
85% C2 + 15% PL	11.5	2610	70.80	0.007
70% C2 + 30% PL	11.8	2480	495.4	0.050
50% C2 + 50% PL	10.3	2350	2808	0.281
25% C2 + 75% PL	10.3	2720	7308	0.731
85% C2 + 15% PB	12.1	4220	UT	UT
70% C2 + 30% PB	11.8	2420	UT	UT
50% C2 + 50% PB	10.0	2200	158.6	0.016
25% C2 + 75% PB	9.91	2240	1629	0.163

Cl^- - chlorides, EC – electrical conductivity, UT – untraceable

4.5 GASEOUS EMISSIONS FROM THE COMBUSTION OF THE COAL AND RDF SAMPLES

The gaseous emissions from the batch combustion tests, conducted at 850°C under an air atmosphere for both the RDFs and coal samples can be seen in Figure 4.23. The plot shows the concentration of individual gases (SO_2, NO_x, CO and CO_2) emitted from the samples utilized and labelled as Figure 4.23 A, B, C and D, respectively. These tests were repeated twice and the graphs can be seen under Appendix C. The RDFs and the coal samples fed into the reactor, underwent a drying process before the volatile matter was released and combusted, along with the char. According to SO_2 emissions in Figure 4.23 (A), the paper blend (PB) was seen with an initial sharp peak which corresponds to the combustion of the volatile matter. This was detected by the gas analyser as the formation of SO_2, and this occurs at 16 seconds with a peak concentration of 143 ppm, thereafter a shoulder was observed which coincides with the char combustion. For the plastic sample (PL) the initial peak for the SO_2 occurs at 26 seconds with a concentration of 107 ppm. There was no shoulder noted in this curve, but rather a reduction in the gradient of the curve, which indicates that there was less SO_2 emitted during the volatile matter combustion stage for this sample. The char combustion stage occurred up to 340 seconds for both the RDF samples. The low concentration of SO_2 emitted (Figure 4.23 A) by the RDF samples as recorded by the gas analyser was expected, as the total sulfur content of these fuels was so low that it was undetected during the ultimate analysis test.

The discard coal (C2), was seen with the highest SO_2 concentration, with a peak of 387 ppm at 61 seconds. This high emission was expected as the discard coal showed a total sulfur content more than 1.5 times that found in the ROM coal (C1), in Table 4.1. The ROM coal also reaches its peak concentration value at the same time as the discard coal, 61 seconds, showing that for both coals the volatile combustion stage was the dominant stage for the SO_2 emission. The emission of SO_2 for both coals continued till 315 seconds for C2 and 450 seconds for C1, showing that there was still an on-going emission of SO_2 during the char combustion, but at a much lower concentration. Based on the emission standard require for new coal-fired power plants in South Africa with SO_2 of 500 mg/m^3 or 191 ppm, the discard coal tested in this study was found to be above the current legislated maximum limit (IEA, 2015).

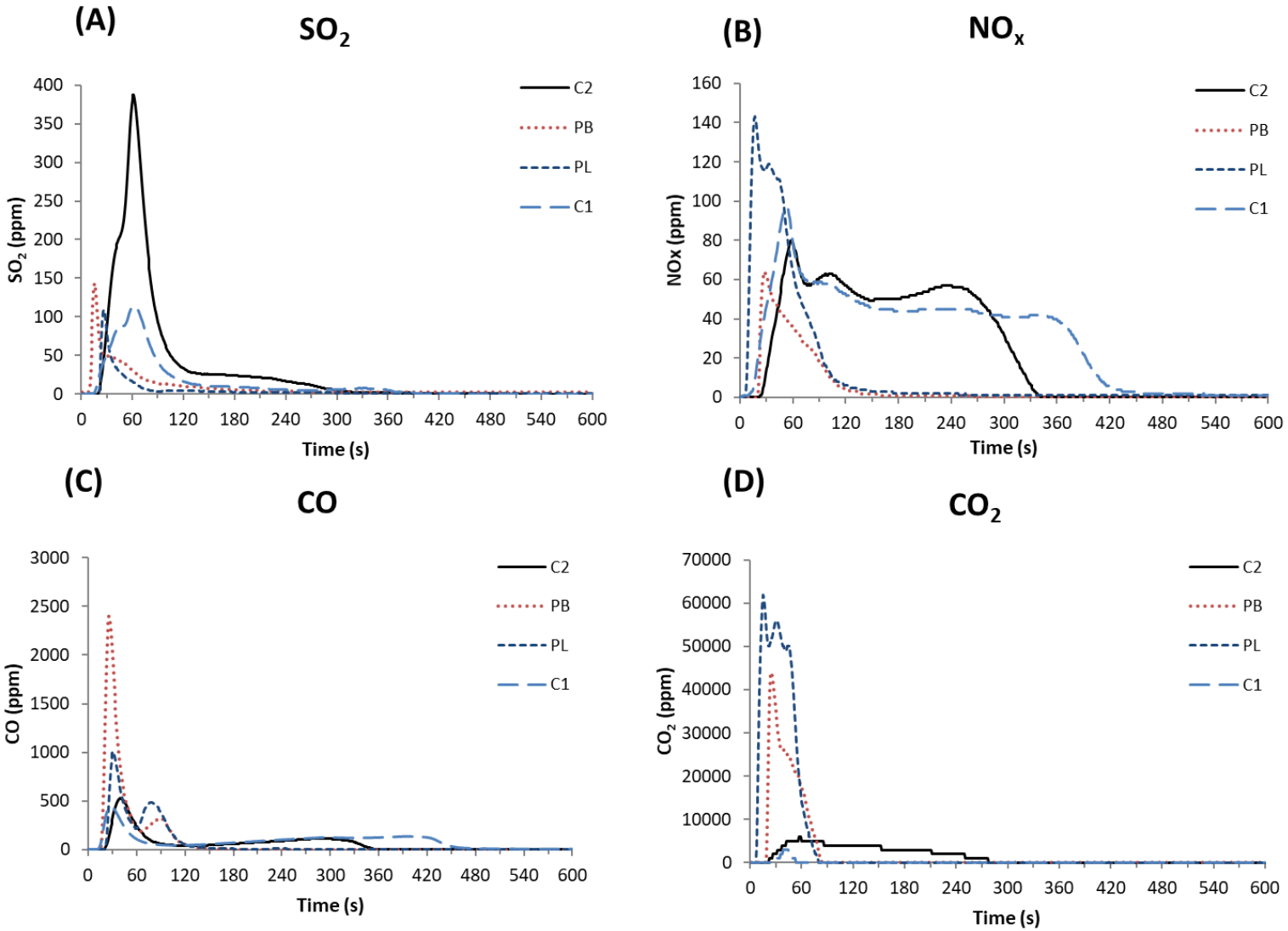

Figure 4. 23 A, B, C and D: The emission profiles of the 100% coal and 100% RDF samples

From Figure 4.23 B above, the NO_x emission of the plastic sample PL was found to be the highest, and its emission profile was similar to its weight loss profile, with two peaks displayed, at 17 seconds (143 ppm) and 32 seconds (119 ppm). The two peaks displayed by this sample (PL) might indicate the combustion of different fractions of volatiles associated with the fuel nitrogen and char nitrogen. The NO_x emission curve during the char combustion stage was seen with a shoulder at $t > 36\ s$. This shows that the dominant stage for NO_x release was the combustion of the volatile matter and the NO_x formation was governed by the reaction in Equation (2.6), thereafter the concentration fell drastically and the release was completed around 270 seconds for both plastic and paper blend samples. This is in agreement with the findings from the ultimate analysis which showed that PB had a smaller fuel nitrogen content of 0.30% in comparison to the 0.35% of PL (Table 4.1).

The NO_x emissions reach their peaks for discard coal (C2) at 58 seconds (80 ppm) and ROM coal (C1) at 43 seconds (99 ppm) which corresponds to the volatile combustion stage. NO_x continued to form in both coal samples, throughout the char combustion, which is in agreement with the findings of Chen et al. (2018) during the combustion of anthracite. It is evident, from Figure 4.23 (B), that sample C1 had a higher peak concentration of NO_x and that the gas evolved over a greater period of time, when compared to C2. This is in agreement with the ultimate analysis result in Table 4.1, which shows that C1 contained a higher nitrogen content of 1.46% in comparison to C2 (1.17%). All of the samples were in compliance with the South African emission standard of 750 mg/m^3 (399 ppm) for NO_x in new coal-fired power plants (IEA, 2015).

The emissions of CO, seen in Figure 4.23 (C), show that there are two stages of release for the RDF samples (PB and PL). The volatile release occurs at $t < 60\ s$ and the char combustion from $60 < t\ (s) < 130$ for sample PB, and from $60 < t\ (s) < 160$ for sample PL. During the first stage of volatile combustion the CO formed rapidly which can be seen from the sharp and narrow peak at 26 seconds for PB and 31 seconds for PL. The concentration of CO emitted is high during this stage, reaching a maximum of 2404 ppm for PB and 1006 ppm for PL, showing that the majority of CO is released from the volatile combustion. The peak concentrations during the char combustion stage can be seen at 78 seconds at a value of 485 ppm for PL and at 89 seconds at 320 ppm for sample PB. This shows that the char combustion stage is not the dominate stage in the release of CO. This is in agreement with the observations

made by Chen et al. (2018). According to the Figure 4.23 (C), both the ROM and discard coal also show two stages CO release, the first occurs up to approximately $t < 105\ s$ for both coals and corresponds to the volatile combustion. The peak during this stage is higher than that of the char combustion, at 527 ppm and 451 ppm for discard coal (C2) and ROM coal (C1), respectively, showing that the volatile combustion is once again the dominant stage for CO release. The emission of CO for the char combustion of the coals takes place over a longer period in comparison to the RDF from around $120 < t\ (s) < 360$ and $120 < t\ (s) < 566$ for C2 and C1, respectively. The two stages observed for CO release in coal is in agreement with the findings of Chen et al. (2018). The extended release of CO for the ROM coal can be attributed to the higher carbon content of this coal in comparison to the discard coal.

The CO_2 emissions of PL, seen in Figure 4.23 (D), show that CO_2 was evolved up to $t < 80\ s$, during the volatile combustion stage. The two distinct peaks of volatile combustion, as observed in the DTG plot for the 100% plastic (PL) can be seen at 15 seconds and 32 seconds. A small shoulder seen on the curves of PL and PB, corresponds to the release of CO_2 during the char combustion. On the other hand, the CO_2 emissions for the coal samples shows much lower concentrations in comparison to the RDF samples (Figure 4.23 D).

4.6 GASEOUS EMISSIONS FROM THE CO-COMBUSTION OF DISCARD COAL WITH RDF SAMPLES

Figure 2.24 and Figure 2.25, show the SO_2 emissions from the co-combustion of discard coal (C2) with plastic (PL) and paper blend (PB), respectively. It is evident that co-firing C2 with RDF reduces the concentration of the SO_2 and alters the profile of the gaseous emissions. This observation is in agreement with the findings of Wan et al. (2008), Akdag et al. (2016) and Chen et al. (2018). Figure 4.24 shows that the two blends containing a majority of C2 exhibit an emission profile similar to that of the discard coal, however at a much lower concentration. The peak SO_2 emission for 85% C2 + 15% PL occurs at 57 seconds with a concentration of 191 ppm, which is equal to the maximum SO_2 emission limit for a new South African coal-fired power plant. This is already a significant reduction from the 387-ppm peak of C2 combustion alone. The blend with 70% C2 shows a further reduction to 161 ppm at 54 seconds, with another small peak at 16 seconds (88 ppm) which is due to the volatile combustion of the PL. It is also noted that the peak concentration occurs earlier on as the PL content is increased in the fuel. The blend 50% C2 + 50% PL shows a SO_2 emission profile with three stages, the

first coincides with the SO_2 release during the volatile combustion of PL, the second coincides with the SO_2 release during the volatile combustion of C2 and the third coincides with the release of SO_2 from the char combustion of C2. The blend 25% C2 + 75% PL shows the lowest emissions of SO_2, with a peak value of 50 ppm at 22 seconds, this is lower than even the 100% PL emission which shows a synergistic effect for this blend. The RDF samples (plastic and paper blend) used in this study contained higher amounts of alkali and alkali-earth metal oxides in comparison to the discard coal utilized. These oxides, that are found in the RDF samples might be responsible for the reduction in the emissions of SO_2, noted in Figure 4.24, by combining with SO_2 to form sulfates (Guo & Zhong, 2018). CaO is one of such oxides which is known to reduce SO_2 emissions, the reaction mechanism can be seen in Equation (2.7).

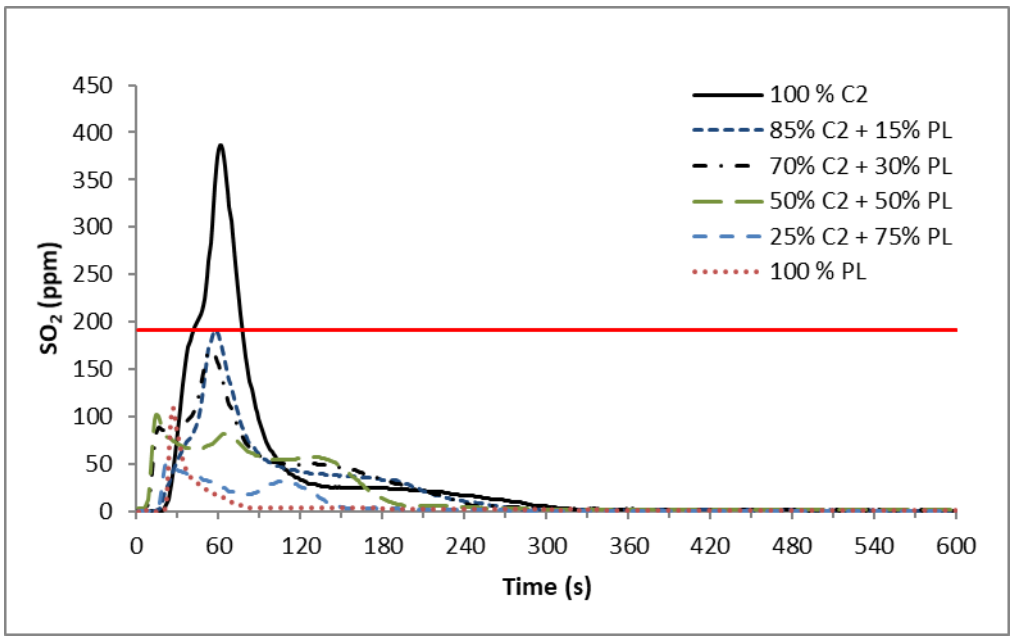

Figure 4. 24: SO_2 emissions from the co-combustion of discard coal C2 and PL

The SO_2 emission profiles of 85% C2 + 15% PB and 70% C2 + 30% PB depicted in Figure 4.25 are very similar to that of discard coal with plastic RDF, however, in these blends with PB the emission is greater than the South African standard for new coal-fired power stations. This is due to the paper blend sample PB displaying a higher SO_2 emission in comparison to sample PL. The samples containing 50% and more of the RDF PB are, however, well below the emission standard. Sample 50% C2 + 50% PB displays two emission peaks, at 20 seconds (110 ppm) and 49 seconds (102 ppm), which corresponds to the SO_2 release from the

combustion of the volatile matter of PB and C2, respectively. The peak emission of sample 25% C2 + 75% PB occurs at 26 seconds at a concentration of 146 ppm, this is higher than the peaks observed in sample 50% C2 + 50% PB, however the concentration quickly decreases as it follows the profile of 100% PB closely.

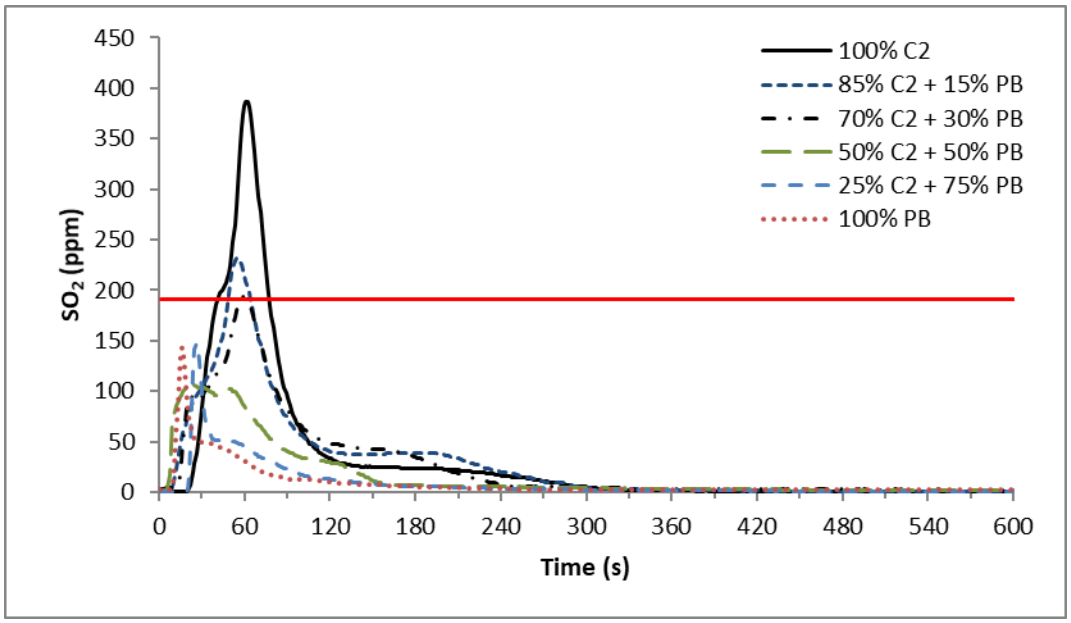

Figure 4. 25: SO_2 emissions from the co-combustion of discard coal C2 and PB

The NO_x emissions from the co-combustion of discard coal with RDF PL and PB are presented in Figure 4. 26 and Figure 4. 27, respectively. The 85% C2 + 15% PL sample in Figure 4.26 has a similar emission profile to C2, but the emission of NO_x in this sample occurred at an earlier time zone, with a peak at 42 seconds at a concentration of 88 ppm, which is slightly higher than the emission from 100% discard coal (C2). It is evident that the addition of PL to C2 results in a higher concentration of NO_x during the volatile combustion stage, however the duration of the emission is decreased by adding PL as the profile shifts to an earlier time zone of the plot. The samples containing 30%, 50% and 75% of PL all show two clear stages of NO_x emissions. The first stage is due to the volatile combustion from the PL fraction in the fuel and the concentration in this stage is similar for all three blends at 102 ppm, 106 ppm and 96 ppm for 30%, 50% and 75% PL, respectively. The second stage is the release of the NO_x from the char combustion, the duration of the emission in this stage is seen to decrease as PL is added to the blend. The increase in NO_x concentration seen in the first stage of combustion (volatile

combustion), with increasing PL content could be due to the lower proportion of coal char component in the fuel (Chyang, et al., 2010). The fixed carbon content of PL is only 6.07%, which indicates that there is less char produced in this fuel. It is expected that the char from coal would react with NO to reduce the NO_x formed, according to the reactions presented in Equations (2.3), (2.4) and (2.5), thus the reduced char content will result in an increase in NO_x for samples with higher PL ratio. This trend of increasing NO_x concentration due to the reduction of char from coal was also observed by Chyang et al. (2010) and Wan et al. (2008).

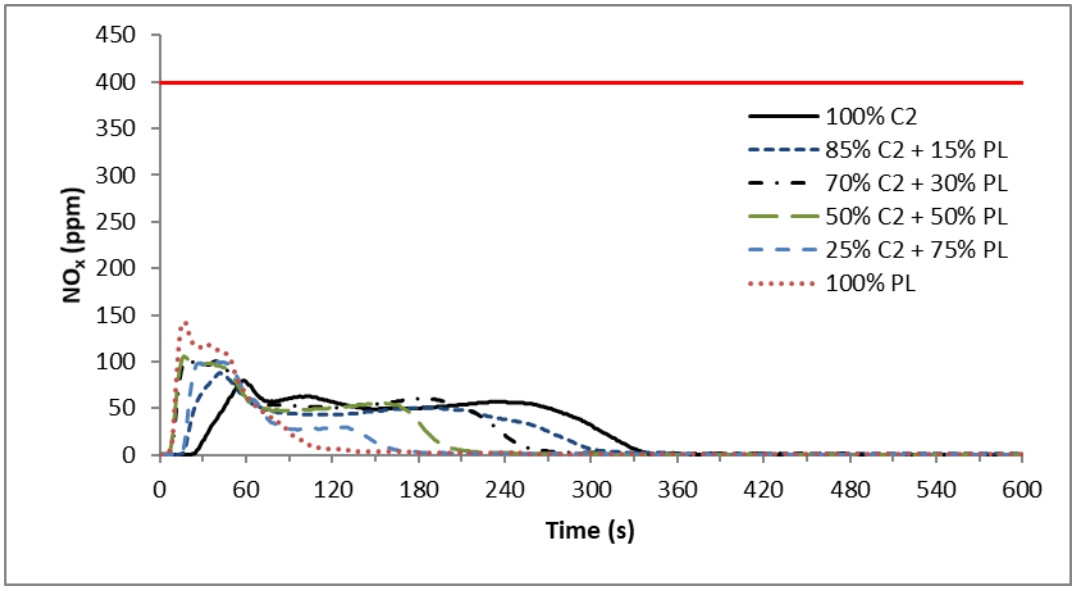

Figure 4. 26: NO_x emissions from the co-combustion of discard coal C2 and PL

Figure 4.27 shows the NO_x emissions from the co-combustion of discard coal (C2) and paper blend (PB). The 85% C2 + 15% PB sample was seen with a similar profile to that of 100% discard coal, however, its emission duration was shorter, due to the addition of PB. The samples containing 30% and 50% PB display an emission profile with two stages, the first is the release of NO_x due to the volatile combustion of PB. Both samples show a peak concentration which exceeded that of 100% PB, denoting that there might be an interaction between the two fuels. The peak concentration of 70% C2 + 30% PL reached 101 ppm at 16 seconds while 50% C2 + 50% PB reached a concentration of 120 ppm at 17 seconds. The second stage, which was due to the combustion of the char occurred from $114 < t\,(\mathrm{s}) < 240$ in sample 70% C2 + 30% PB, and $75 < t\,(\mathrm{s}) < 210$ in sample 50% C2 + 50% PB. The sample containing the most PB

(75%) displayed an emission profile very similar to 100% PB with a peak concentration just slightly higher, at 70 ppm. The release of NO_x due to the char combustion is seen as a slight increase of only a few ppm at 112 s. The concentrations of NO_x for the majority of the blends co-fired in this study are in agreement with those from Wan et al. (2008), who found that the emissions during co-firing of coal and RDF-5 remained below 100 ppm. The increase in NO_x emissions was also noticed by Zhang et al. (2018) in the co-firing of MSW with coal when the MSW content was increased above 15%.

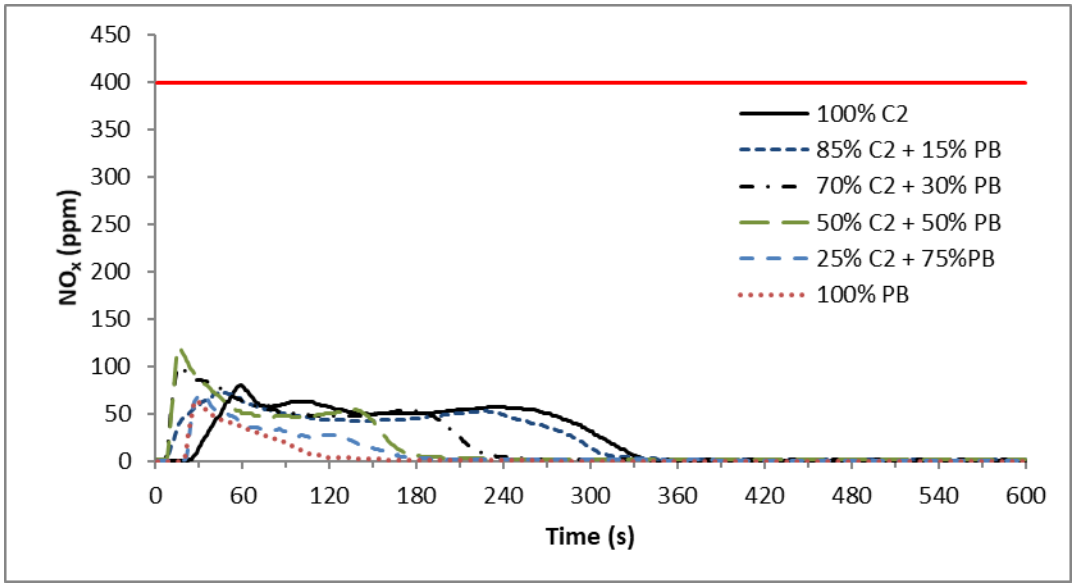

Figure 4. 27: NO_x emissions from the co-combustion of discard coal C2 and PB

The CO emission profiles from the co-combustion of discard coal (C2) and plastic sample (PL) are depicted in Figure 4.28, with each sample profile showing two clear stages for the release of carbon -monoxide. It can be seen from this Figure 4.28 that 85% C2 + 15% PL and 70% C2 + 30% PL samples have a similar profile to 100% discard coal and display a peak at 26 seconds (217 ppm) and 17 seconds (127 ppm), respectively. This peak corresponds to the combustion of the volatile matter and the concentration of CO emitted in this stage is below that of both 100% C2 and 100% PL, showing there might be a synergistic effect between these two fuels at this blending ratio. The shift in the peak to the earlier time zone noted for the two samples can be attributed to the light volatile component of the PL in the blend. For 50% C2 + 50% PL and 25% C2 + 75% PL samples, both have a first stage which corresponds to the release of the

light volatile components of the RDF PL. Thereafter, there is a second stage which coincides with the release of the heavier volatile components of PL and the char combustion of the discard coal C2. This takes place during $53 < t\ (\mathrm{s}) < 270$ for sample 50% C2 + 50% PL and during $68 < t\ (\mathrm{s}) < 240$ for sample 25% C2 + 75% PL.

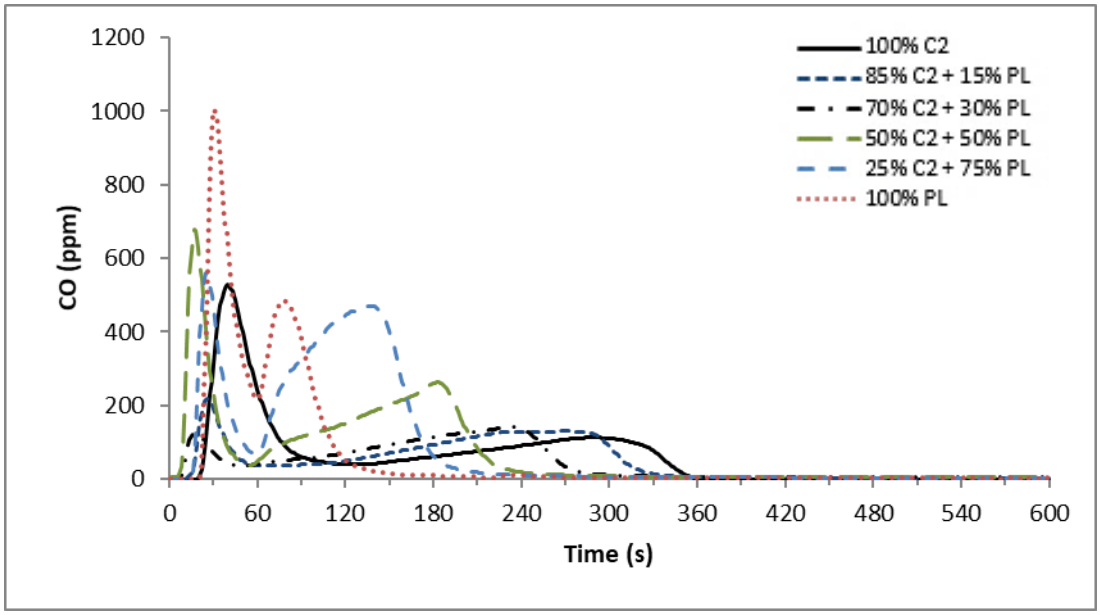

Figure 4. 28: The CO emissions from the co-combustion of discard coal C2 and PL

Figure 4.29 shows the CO emissions from the co-combustion of C2 and PB. In this Figure 4.29, the peak concentration of the 85% C2 + 15% PB blend was seen to be lower than the corresponding blend with 85% C2 + 15% PL in Figure 4.28 above, at 17 seconds and 151 ppm. On the other hand, the concentrations of CO from the samples containing 30%, 50% and 75% paper blend (PB) seen in Figure 4.29 all exceed the concentrations of CO from the same blend ratios with the RDF PL in Figure 4.28 above. This is due to the high concentration of CO from the 100% RDF PB, which is more than double that of the RDF PL. The high CO emission from the RDF PB could be influenced by the higher moisture content in this sample seen in Table 4.1 (3.19%), which can delay the combustion of the sample, resulting in high CO emissions, which is in line with the findings by Iacovidou et al. (2018). These blends all showed a dominant first stage of the emission profile, which was attributed to the release of CO due to the volatile combustion of the RDF PB. The peak concentration of 25% C2 + 75% PB sample was higher than that of 100% PB, at 18 seconds and 3159 ppm, which showed that there might be some interactions between the two fuels in the blend. A great reduction in the peak

concentration to 705 ppm was seen in sample 70% C2 + 30% PB. The second stage in Figure 4. 29 showed an emission which was relatively low in concentration and occurred over a longer period.

The period over which the CO was emitted became shorter as the RDF was increased in the blend. Overall, there was an increase in the CO concentration when RDF was added to the blend with discard coal, Wan et al. (2008) also experienced an increase in the CO emissions when the RDF-5 content was increased when co-firing with coal. Guo and Zhong (2018) and Akdag et al. (2016) attributed the increasing concentration of CO from RDF co-firing to the increased volatile matter content of the RDF, which when released causes a depletion in the available oxygen and results in the production of carbon monoxide. Wu et al. (2011) attributed the increase in CO emissions, with the increase in solid recovered fuel (SRF) in the fuel blend with coal, to the larger particle size of the SRF which requires a longer time to combust completely.

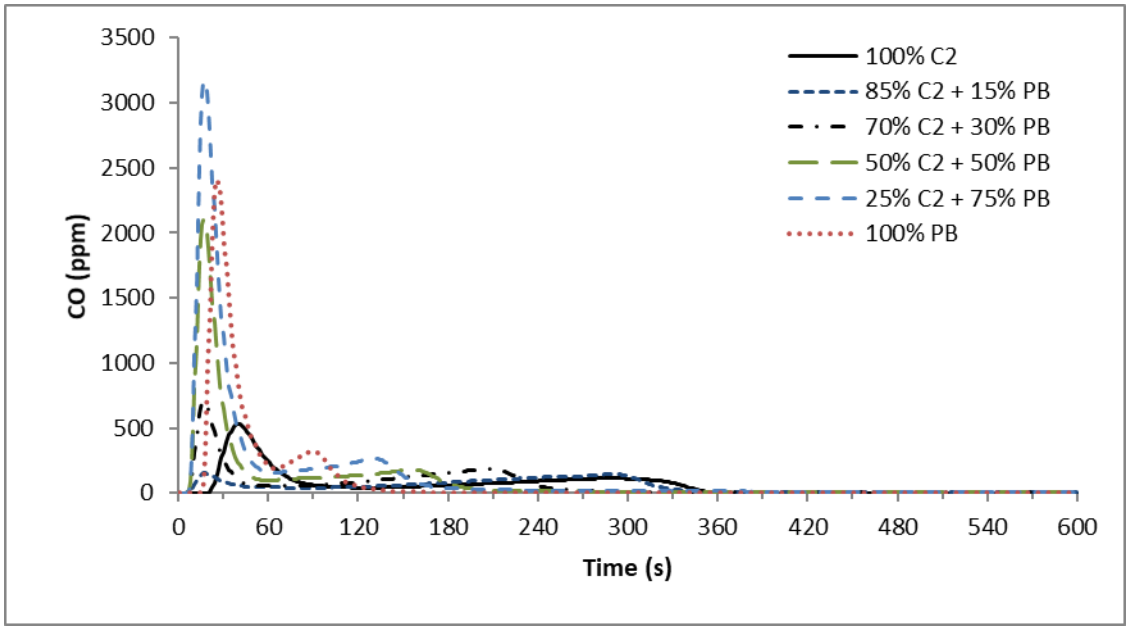

Figure 4. 29: The CO emissions from the co-combustion of discard coal C2 and PB

The emissions of CO_2 in Figure 4.30 show an increasing trend, as the content of PL is increased in the blend. The samples containing 75%, 50% and 30% PL show a two-stage profile, where

the first peak is due to the combustion of the volatile matter in the sample. This is a combination of the two initial peaks seen in the 100% PL sample for the combustion of the light and heavy volatile components. The second stage is due to the combustion of the char, which was seen as the third peak in the 100% PL sample. The sample 85% C2 + 15% PL displays a single stage profile with a peak in the range of the char combustion for sample PL (the third peak) and the volatile combustion for the sample C2, at 39 seconds and 16 000 ppm. The emission profile of this sample has a much shorter duration than that of 100% C2 which shows that the increase in the volatile matter has a great effect on the CO_2 emission of the fuel. The samples containing ≥ 50% of PL show the highest peak to be due to the volatile matter combustion at 25 seconds and 55 000 ppm, and 14 seconds and 41 000 ppm for 75% and 50% PL respectively. It can be seen that as PL is added to the blend, the first peak of the emission profile increases and the second peak decreases.

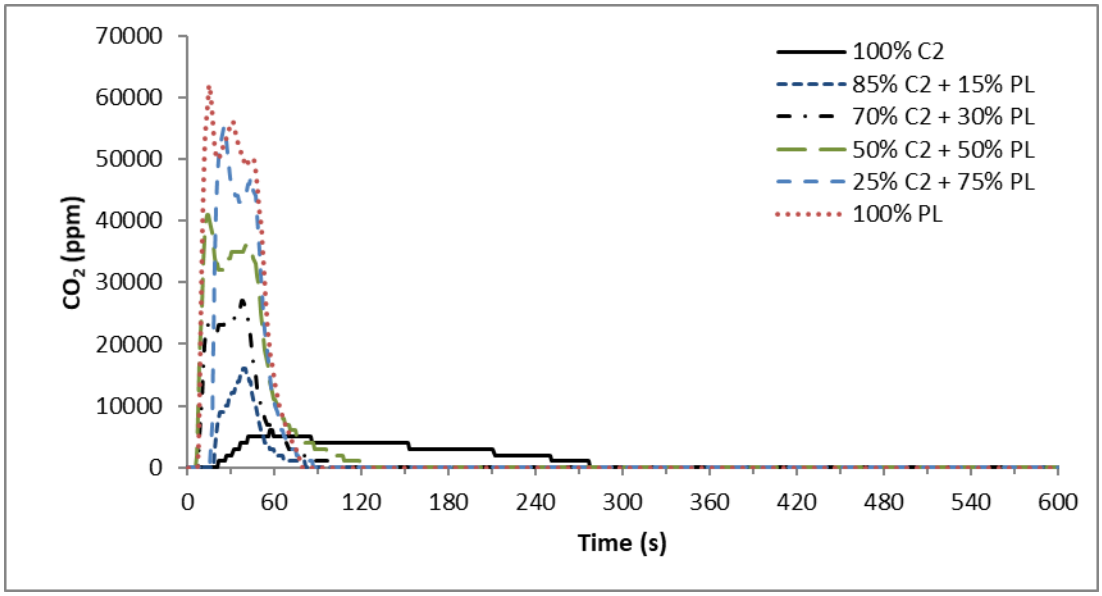

Figure 4. 30: The CO_2 emissions from the co-combustion of discard coal C2 and PL

Figure 4.31 shows that the CO_2 emission profiles from the co-combustion of discard coal C2 and paper blend PB are below those of the co-combustion with PL for all blends (Figure 4.30). This is probably due to the higher amount of CO being formed from the blends with PB, showing that there was incomplete combustion. The CO_2 emissions increased as the ratio of PB in the blend was increased. The blends with paper blend (PB) all appear to release CO_2 in

a single stage, which shows a peak corresponding to the combustion of the volatile matter, which occurred $t < 60\ s$ for all the blends. The sample 85% C2 + 15% PB emitted the lowest concentration of CO_2, at 25 seconds and 6000 ppm, which is due to the large amount of discard coal in this sample. As discussed previously, the discard coal showed very low CO_2 emissions which indicates that might be an incomplete combustion of the fuel, possibly due to the air flow within the reactor and the nature of the coal.

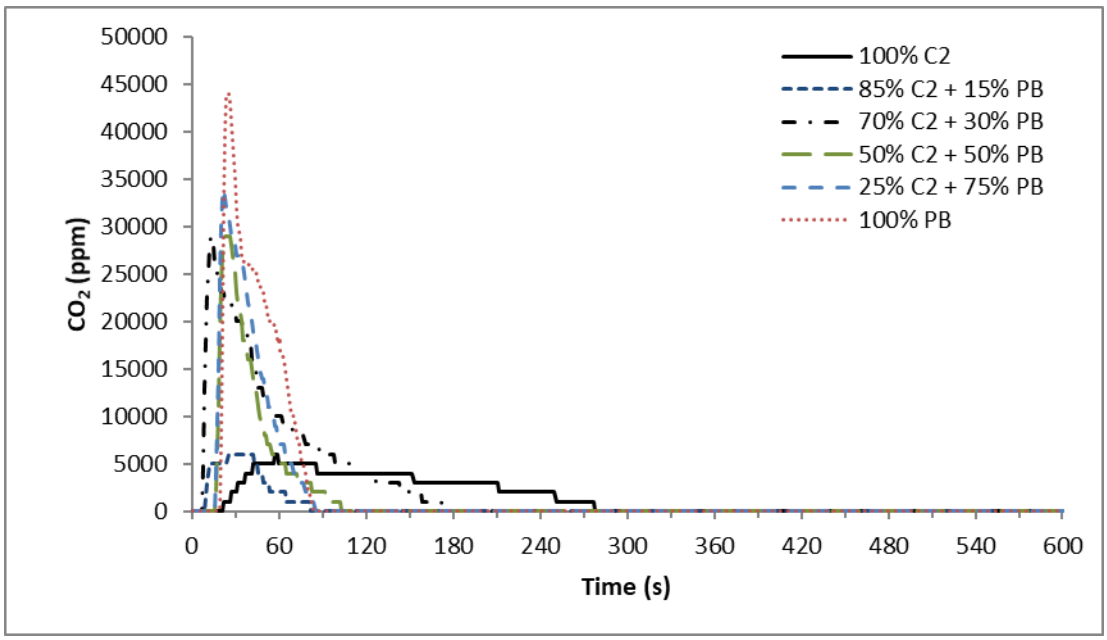

Figure 4. 31: The CO_2 emissions from the co-combustion of discard coal C2 and PB

To conclude the above discussions and determine which blend is the most favourable for co-combustion in existing coal-fired power stations, the burnout temperature, apparent activation energy, SO_2, NO_x and CO_2 emissions was considered. The combustion profiles showed that blends containing less than 70% of discard coal were not suitable for combustion in existing coal-fired power stations due to their dissimilarity to the conventional coal combustion profile. Of the remaining blends of 85% and 70% discard coal with RDF, the blend with 30% PB showed the lowest burnout temperature of 690°C, followed by the blend with 30% PL which has a burnout temperature of 720°C. The lower T_b of the 70% C2 + 30% PB blend was offset by the higher activation energy of 65.3 kJ/mol in the volatile combustion stage, as well as the higher SO_2 and CO_2 emissions, when compared to the blend of 70% C2 + 30% PL. The 70% C2 + 30% PL blend is the most favourable for co-combustion as it shows the lowest SO_2

emissions of 161 ppm and the lowest apparent activation energy. In addition, the combustion profile is similar to that of coal and the burnout temperature is relatively low.

4.7 THE EFFECT OF TEMPERATURE ON EMISSIONS

In order to determine the effect of temperature on the emissions of NO_x and SO_2 from the discard coal, 100 mg of the discard coal sample C2 was combusted in the horizontal tube reactor at 850°C and 950°C, in an atmosphere of air, and the gaseous emissions were measured, as seen in Figure 4.32. The plot shows that at 950°C, the devolatilization and combustion of volatiles occurred first with a NO_x concentration of about 99 ppm, and this might be due to the availability of more heat for the devolatilization process. The high concentration of NO_x released and heat available in the first stage might have been responsible for the low NO_x shoulder seen at the tail end of the curve. In addition, the rate at which the char combustion was seen to be completed might be due to the higher furnace temperature at 950°C. The lower NO_x seen at 850°C is expected, as the conversion of nitrogen bound in solid fuel to NO_x is dependent on combustion temperature (Chen, et al., 2017). The peak concentration of the SO_2 emission was also seen to occur at a slightly earlier time for the plot of 950°C, and this is expected because as the reaction rate increases, the sample devolatilization and combustion occurs more rapidly (Chen, et al., 2018). The peak concentration was found to be lower in the volatile combustion region at 950°C, however, the concentration during the char combustion is higher than at 850°C (Figure 4.32). This is in agreement with the findings of de las Obras-Loscertales et al. (2013) who found that the emissions of SO_2 from coal combustion decrease with increasing temperature up to 925°C.

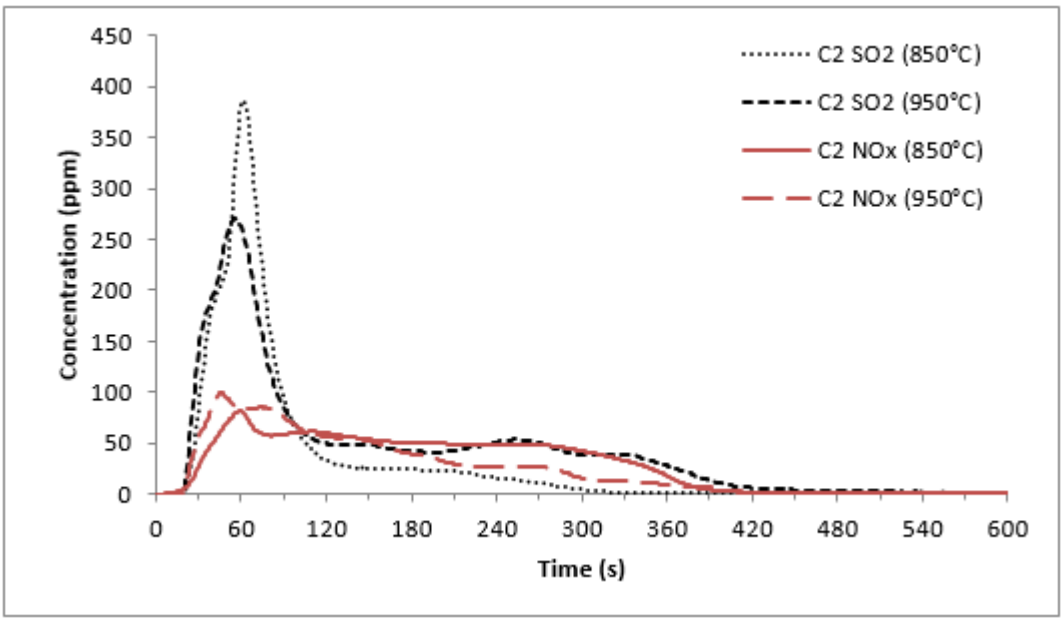

Figure 4. 32: SO_2 and NO_x emissions of discard coal C2 at 850°C and 950°C

Figure 4.33 shows the CO and CO_2 emissions from discard coal C2 under different temperature environments. It is evident that the CO_2 emission of the sample is lower at 950°C, while the peak concentration is emitted at an earlier time. The emission of CO is also much higher at 850°C than at 950°C, which is in agreement with Chen et al (2018), who found CO to be up to 20 times higher at 800°C compared to 900°C. The decrease in CO emissions at 950°C can be attributed to a more efficient combustion process which is achieved at higher temperatures (de las Obras-Loscertales, et al., 2013). The repeats of the emission tests at 950°C can be found in Appendix C.

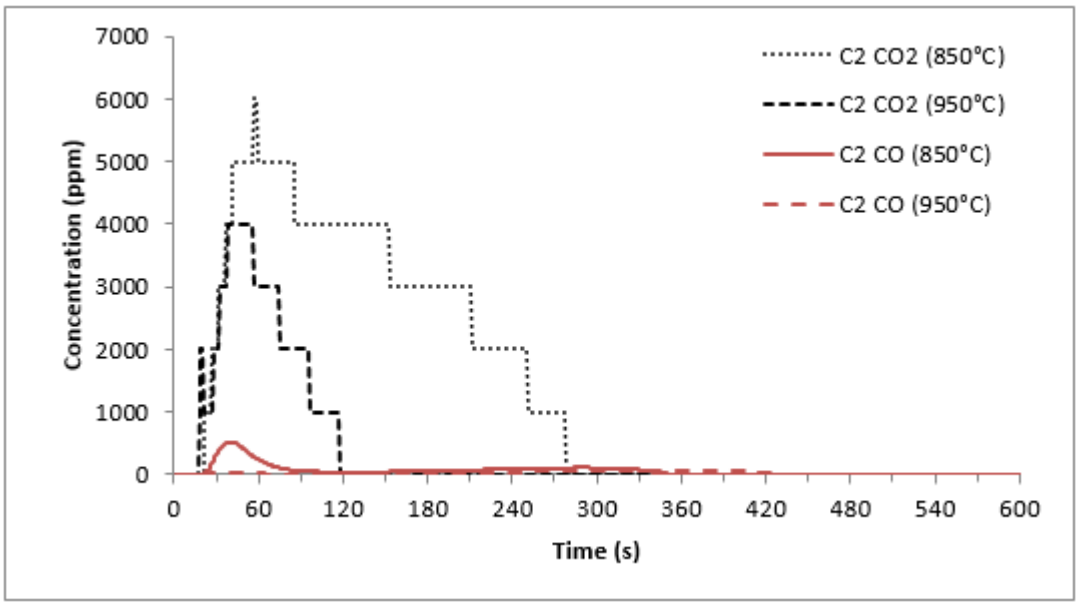

Figure 4. 33: CO_2 and CO emissions of discard coal C2 at 850°C and 950°C

To conclude this section, it was found that the discard coal emitted the highest concentration of SO_2, while the RDF samples emitted less SO_2 than both coals. The RDF sample PL showed the highest peak concentration of NO_x during the volatile combustion, however, NO_x was emitted and sustained throughout the combustion of the coal. The co-combustion experiments showed that the concentration of SO_2 reduced as RDF was increased in the fuel blend. The blends of ≥ 30% PL and ≥ 50% PB were within the maximum South African SO_2 emission standard for new coal fired power plants. The peak concentration of NO_x increases with the addition of RDF to the blend which could be due to the decrease in the char (carbon) from coal which is known to react with NO and thus reduce the NO_x emission. The duration of the NO_x emission does, however, reduce as the content of RDF increased. The addition of RDF to the co-combustion blends was found to increase the CO and CO_2 emissions concentration which could be due to the large volatile matter content of the RDF.

CHAPTER 5: CONCLUSION AND RECOMMENDATIONS

5.1 CONCLUSION

The aim of this research was to determine the co-combustion performance of coal and RDF blends with the most favourable combustion characteristics, as well as to minimise the concentration of harmful gases and ash emissions. The aim and objectives outlined in this research were all achieved, and through the course of the research the following conclusions were made.

1. The physicochemical analysis revealed that the calorific value of the RDF samples was higher (PL: 31.23 MJ/kg and PB: 22.4 MJ/kg) than those of the ROM (21.72 MJ/kg) and discard coal (16.73 MJ/kg) utilized. The RDF contained a higher volatile matter content and a lower ash content when compared to the coal samples. For the ultimate analysis result, the RDF samples contained less nitrogen and total sulfur than the coals. The energy potential of the RDF resource in South Africa was estimated to be 83 629 702 GJ/year.

2. The TGA profiles for the RDF combustion were found to be dissimilar to those from the ROM and discard coals. The co-combustion of samples containing up to 30% RDF were most similar to the combustion profiles of 100% coal. The DTG curves obtained from the blending of RDFs with the low-quality coals utilized in this study, shows that the energy and thermal characteristic (ignition, peak and burnout temperatures) of these coals can be improved.

3. The calculated apparent activation energies (E_a), showed that the E_a for the volatile combustion stage increased as RDF was added to the blend due to the low temperature environment of the pyrolysis, while the E_a of the char combustion stage decreased as the content of RDF in the fuel was increased.

4. The reduction in the E_a for the combustion of the char (stage 4) showed that the addition of RDF to low quality coal results in a fuel which requires less energy and time to combust. The blend of discard coal (70%) and PL (30%) showed the lowest apparent

activation energies of 55.8 kJ/mol and 54.2 kJ/mol for the volatile and char combustion, respectively, making this the most favourable blend for co-combustion.

5. The analysis of the ash from the co-combustion of discard coal and RDF showed a decrease in the chloride, alkali and alkali-earth metal content of the ash as the ratio of coal was increased in the blend. It was also found that the water-soluble chloride content of the ash decreases with the addition of coal to the fuel blend.

6. The calculated slagging and fouling indices showed that as the coal proportion in the blend increases, the propensity of the blend or fuel to slag and foul decreases.

7. The discard coal was found to have the highest SO_2 emission, and with an increased RDF content in the blend a decrease in SO_2 emissions to the required maximum emission standard for South African coal fired plant was attained.

8. The peak concentration of NO_x emitted was found to increase with the addition of RDF, however, the duration of the emission was greatly reduced. There was also an increase in the emissions of CO and CO_2 which could be due to the high volatile matter content of the RDF.

5.2 RECOMMENDATIONS

Due to the successful outcomes of this research which showed that the co-firing of coal with RDF improves the combustion characteristics and reduces the activation energy for char combustion, as well as reduces the SO_2 emissions, the following recommendations are made for further research.

1. In this study the RDF utilised was milled to 250 μm. The form of the RDF, be it fine powder, fluff, pellets or briquettes, used in co-combustion can have an effect on the combustion performance. Further research can be conducted into the sample preparation of RDF that would be most suitable for co-firing in existing coal-fired power stations.

2. The ash slagging and fouling indices in this research were calculated using the oxide concentrations from the XRF analysis. It is recommended that further ash fusibility analysis be conducted to verify these results. In addition, the mineral phases present in the ash could be researched through XRD to give further insight into the ash characterisation.

3. This research investigated the gaseous emissions of SO_2, NO_x, CO and CO_2. It is recommended that further research be conducted into the particulate emissions produced from co-firing of RDF and coal. $PM_{2.5}$ can contain chemicals, acids and metals which have a negative effect on the environment and human health, as such there are standard limits which need to be adhered to in the emission of $PM_{2.5}$ (Iacovidou, et al., 2018). The South African standard for $PM_{2.5}$ is 50 mg/m^3 in new installations and 100 mg/m^3 in existing combustion plants (IEA, 2015). The flue gas emitted from the co-combustion may also be analysed for HCl, PCDD, PCDF, and other trace elements which could be harmful to the environment and human health.

4. Finally, it is recommended that a feasibility study be conducted into the cost implications, as well as the operational changes required to accommodate co-firing coal with refuse derived fuel in existing coal-fired power plants.

6 REFERENCE LIST

Abdul, A., Rozainee, M., Johari, A. & Alwi, R., 2012. Combustion studies of fluff refuse derived fuel (RDF) in fluidised bed (FB) system. *International Journal of Renewable Energy Resources* , Volume 2, pp. 23-26.

Aderoju, O., Dias, G. & Echakraoui, Z., 2017. Assessment of Renewable Energy Sources & Municipal Solid Waste for Sustainable Power Generation in Nigeria. *IOP Conference Series: Earth and Environmental Science,* Volume 95, pp. 1-10.

Akdag, A., Atimtay, A. & Sanin, F., 2016. Comparison of fuel value and combustion characteristics of two different RDF samples. *Waste Management* , Volume 47, pp. 217-224.

Akinyeye, R., Pereao, O., Petrik, L. & Olaofe, O., 2016. Comparative Chemical and Trace Element Composition of Coal Samples from Nigeria and South Africa. *American Journal of Innovative Research and Applied Sciences,* pp. 391-404.

Alvarez, A. Pizarro, C., Garcia, R., Bueno, J., & Lavi, A., 2016. Determination of kinetic parameters for biomass combustion. *Bioresource Technology*, Volume 216, pp. 36-43.

Anca-Coucea, A., Bergerb, A. & Zobel, N., 2014. How to determine consistent biomass pyrolysis kinetics in a parallel reaction scheme. *Fuel*, Volume 123, pp. 230-240.

Arias, B., Pevida, C., Rubiera, F. & Pis, J., 2008. Effect of biomass blending on coal ignition and burnout during oxy-fuel combustion. *Fuel,* Volume 87, p. 2753–2759.

ASTM, 2009. *Standard Test Methods for Proximate Analysis of the Analysis Sample of Coal and Coke by Instrumental Procedures.* [Online] Available at: https://www.astm.org-/Standards/D5142.htm [Accessed 1 October 2018].

ASTM, 2019. *Standard Test Method for Gross Calorific Value of Coal and Coke.* [Online] Available at: https://www.astm.org/Standards/D5865.htm [Accessed 1 October 2019].

Bada, S., Falcon, R. & Falcon, L., 2015. Characterization and co-firing potential of a high ash coal with Bambusa balcooa. *Fuel,* Volume 151, pp. 130-138.

Bai, G., Wang, Y., Bai, Q. & Chu, X., 2007. Pyrolysis characteristics study ofsimulative medical waste on cannular electric furnace. *Chinese Journal of Environmental Engineering,* Volume 1, pp. 128-32.

Belaid, M., 2017. Behaviour of Selected South African Coals in Circulating Fluidised Bed in Comparison with Russian Coal. In: s.l.:Univerisity of the Witwatersrand, PhD thesis .

Belaid, M., Falcon, R., Vainikka, P, & Patsa, K., 2013. *Potential and Technical basis for Utilising Coal Beneficiation Discards in Power Generation by Applying Circulating Fluidised Bed Boilers.* London, UK, 2nd International Conference on Chemical, Ecology and Environmental Sciences.

Blaine, R. & Kissinger, H., 2012. Homer Kissinger and the Kissinger equation. *Thermochimica Acta,* Volume 540, pp. 1-6.

BSI, 2009. *BS EN 14775:2009: Solid biofuels. Determination of ash content.* [Online] Available at: https://shop.bsigroup.com/ProductDetail/?pid=000000000030198062 [Accessed 30 January 2019].

Cardozo, E., Erlich, C., Alejo, L. & Fransson, T., 2014. Combustion of agricultural residues: An experimental study for small-scale applications. *Fuel,* Volume 115, pp. 778-787.

Chatziaras, N., Psomopoulos, C. & Themelis, N., 2016. Use of waste derived fuels in cement industry: a review. *Management of Environmental Quality: An International Journal*, 27(2), pp. 178 - 193.

Chen, C., Chen, F., Cheng, Z. C., Kook, S., & Yeoh, G., 2017. Emissions characteristics of NOx and SO2 in the combustion of microalgae biomass using a tube furnace. *Journal of the Energy Institute* , Volume 90, pp. 806-812.

Chen, X., Xie, J., Mei, S. & He, F., 2018. NOx and SO2 Emissions during Co-Combustion of RDF and Anthracite in the Environment of a Precalciner. *Energies,* Volume 11, p. 337.

Chi, Y., Zheng, J., Jin, Y., Mi, H., Jiang, X., & Ni, M., 2008. Experimental study on fluidized-bed gasification of simulated MSW. *P. CSEE,* Volume 28, p. 59–63.

Chyang, C., Han, Y., Wu, L., Wan, H., Lee, H., & Chang, Y., 2010. An investigation on pollutant emissions from co-firing of RDF and coal. *Waste Management,* Volume 30, pp. 1334-1340.

CoM, 2018. *Coal Strategy 2018,* s.l.: Chamber of Mines of South Africa.

Cozzani, V., Petarca, L. & Tognotti, L., 1994. Devolatilization and pyrolysis of refuse derived fuels: characterization and kinetic modelling by a thermogravimetric and calorimetric approach. *Fuel,* 74(6), pp. 903-912.

Cumming, J. & McLaughlin, J., 1982. The Thermogravimetric Behaviour of Coal. *Thermochimica Acta,* Volume 57, pp. 253-272.

Dai, K., 2007. *Experimental study on compositions variation on waste combustion of a fixed bed,* Harbin, China: Harbin Institute of Technology.

Dalai, A., Batta, N., Eswaramoorthi, I. & Schoenau, G., 2009. Gasification of refuse derived fuel in a fixed bed reactor for syngas production. *Waste Management,* Volume 29, pp. 252-258.

de las Obras-Loscertales, M., M., Rufas, A., de Diego, L., García-Labiano, F., Gayán, P., Abad, A., & Adánez, J., 2013. Effects of temperature and flue gas recycle on the SO2 and NOx emissions in an oxy-fuel fluidized bed combustor. *Energy Procedia 37,* Volume 37, pp. 1275-1285.

DEA, 2010. *National Environmental Management: Air Quality Act, 2004 (ACT NO. 39 OF 2004).* s.l.:Department of Environmental Affairs .

DEA, 2012. *Municipal Solid Waste Tariff Strategy,* South Africa: Department of Environmental Affairs.

DEA, 2018. *South Africa State of Waste Report,* Pretoria: Department of Environmental Affairs.

DME, 2011. *National Inventory Discard and Duff Coal – Summary Report,* s.l.: Department of Minerals and Energy .

Elementar, n.d. *vario EL cube.* [Online] Available at: http://www.spektronika-.ru/sites/default/files/vario_el_cube.pdf [Accessed 21 May 2019].

Eskom, 2018. *Integrated Report.* [Online] Available at: http://www.eskom.co.za-/IR2018/Documents/Eskom2018IntegratedReport.pdf [Accessed 10 April 2019].

Falcon, R., 2013. *Coal Geology, Type, Ranks and Grades. Conference on Coal, Coke and Carbon* Johannesburg: www.fossilfuel.co.za.

Falcon, R. & Ham, A., 1988. The Characteristics of South African Coals. *Journal of the South African Institute of Mining and Metallurgy,* 88(5), pp. 145-161.

Fang, X., Jia, L. & Yin, L., 2013. A weighted average global process model based on two-stage kinetic scheme for biomass combustion. *Biomass Bioenergy,* Volume 48, p. 43–50.

Febrero, L., Granada, E., Regueiro, A. & Míguez, L., 2015. Influence of Combustion Parameters on Fouling Composition after Wood Pellet Burning in a Lab-Scale Low-Power Boiler. *Energies,* Volume 8, pp. 9794-9816.

FFF, 2017. *FFF Submission to the Department of Energy RE. IRP 2016,* s.l.: Fossil Fuel Foundation.

Fodisch, 2017. *MGA 11 - Product Information,* Germany: Dr Fodisch.

Fuller, A., Carbo, M., Savat, P., Kalivodova, J., Maier, J., & Scheffkncht, G., 2015. Results of fly ash quality for disposal options from high thermal shares up to pure biomass combustion in a pilot-scale and large scale pulverized fuel power plants. *Renewable Energy,* Volume 75, pp. 899-910.

Fuller, A., Maier, J., Karampinis, E., Kalivodova, J., Grammelis, P., Kakaras, E., & Scheffknecht, G., 2018. Fly Ash Formation and Characteristics from (co-)Combustion of an Herbaceous Biomass and a Greek Lignite (Low-Rank Coal) in a Pulverized Fuel Pilot-Scale Test Facility. *Energies* , 11(1581).

Gangavati, P., Safi, M., Singh, A., Prasad, B., & Mishra, I., 2005. Pyrolysis and thermal oxidation kinetics of sugar mill press mud. *Thermochimica Acta,* Volume 428, pp. 63-70.

Gasperetti, S., 2013. *ENEL experience on Refused Derived Fue lco-combustion in a coal fired Power Plant,* Milano: Enel.

Gendebien, A., Leavens, A., Blackmore, K., Godley, A., Lewin, K., & Whiting, K. J., 2003. *Refuse Derived Fuel, Current Practice and Perspectives Final Report,* s.l.: European Commission.

Gil, M., Casal, D., Pevida, C., Pis, C., & Rubiera, F., 2010. Thermal behaviour and kinetics of coal/biomass blends during co-combustion. *Bioresource Technology,* Volume 101, pp. 5601-5608.

Guo, F. & Zhong, Z., 2018. Co-combustion of anthracite coal and wood pellets: Thermodynamic analysis, combustion efficiency, pollutant emissions and ash slagging. *Environmental Pollution,* Volume 239, pp. 21-29.

Hattingh, B., 2013. *Coal characterisation: conventional coal analyses,* s.l.: s.n.

Hossain, F., 2018. *Sustainable Designa and Build.* New York: Elsevier.

Hu, G., Zhu, X. & Zhou, X., 2011. *Waste incineration power generation and secondary pollution control technology,* Chongqing, China: Chongqing University Press.

Hu, S., Ma, X., Lin, Y., Yu, Z., & Fang, S., 2015. Thermogravimetric analysis of the co-combustion of paper mill sludge and municipal solid waste. *Energy Conversion and Management,* Volume 99, pp. 112-118.

I&M, 2012. *Imaging & Microscopy.* [Online]
Available at: https://www.imaging-git.com/products/electron-and-ion-microscopy/carl-zeiss-reveals-high-definition-fe-sem-sigma-hd [Accessed 26 October 2019].

Iacovidou, E., Hahladakis, J., Deans, I., Velis, C., & Purnell, P., 2018. Technical properties of biomass and solid recovered fuel (SRF) co-fired with coal: Impact on multi-dimensional resource recovery value. *Waste Management,* Volume 73, pp. 535-545.

IEA, 2015. *Emission Standards: South Africa,* London: s.n.

Interwaste, 2018. *Intergrated Waste Management.* [Online] Available at: https://www.inter-waste.co.za/integrated-waste-management [Accessed September 2018].

Iordanidis, A., Asvesta, A. & Vasileiadou, A., 2018. Combustion behaviour of different types of solid wastes and their blends with lignite. *Thermal Science* , 22(2), pp. 1077-1088.

ISO, 2010. *ISO 1171:2010: Solid mineral fuels — Determination of ash.* [Online]
Available at: https://www.iso.org/standard/55944.html [Accessed 30 January 2019].

James, A., Thring, R., Helle, S. & Ghuman, H., 2012. Ash Management Review—Applications of Biomass Bottom Ash. *Energies,* Volume 5, pp. 3856-3873.

Jayanti, S., Maheswaran, K. & Saravanan, V., 2007. Assessment of the effect of high ash content in pulverized coal combustion. *Applied Mathermatical Modelling,* 31(5), pp. 934-953.

Jeffrey, L., 2005. Characterization of the coal resources of South Africa. *The Journal of The South African Institute of Mining and Metallurgy*, pp. 95-102.

Jeffrey, R., Falcon, R. & Kinghorn, A., 2014. The Benefits and Challenges Associated with Coal in South Africa. *Society and Culture* , pp. 66-70.

Ji, S., Li, F., Li, J. & Fang, Y., 2016. Adjustment behaviors of blending coal on the ash fusion characteristics of coal with a high ash fusion temperature. *Journal of Thermal Analysis Calorimetry,* Volume 125, pp. 45-52.

Kaiser, E., 1968. The Sulfur Balance of Incinerators. *Journal of the Air Pollution Control Association,* 18(3), pp. 171-174.

Kalenga, P., Cukrowska, E., Tutu, H. & Chimuka, L., 2011. Characterization of South African Coal for Metals, Inorganic and Organic Sulfur Compounds. *South African Journal of Chemistry,* Volume 64, p. 254–262.

Kara, M, Gunay, E., Tabak, Y., Yildiz, S., & Enc, V., 2008. *The Usage of Refuse Derived Fuel from Urban Solid Waste in Cement Industry as an Alternative Fuel.* Greece, 6th IASME/WSEAS International Conference on Heat Transfer, Thermal Engineering and Environment.

Lanzerstorfer, C., 2015. Chemical composition and physical properties of filter fly ashes from eight grate-fired biomass combustion plants. *Journal of Environmental Sciences,* Volume 30, pp. 191-197.

LECO, n.d. *AC500 Isoperibol Calorimeter.* [Online] Available at: https://www.leco.com-/product/ac500 [Accessed 25 October 2019].

Lilley, R., 2015. *The Fossil Fuel Foundation: What is the future for fossil fuels in South Africa?.* [Online] Available at: http://www.ee.co.za/article/future-fossil-fuels-south-africa.html [Accessed 10 June 2018].

Lu, J. & Chen, W., 2015. Investigation on the ignition and burnout temperatures of bamboo and sugarcane bagasse by thermogravimetric analysis. *Applied Energy* , Volume 160, pp. 49-57.

Malaťák, J., Velebil, J. & Bradna, J., 2018. Speciality types of waste paper as an energetic commodity. *Agronomy Research* , 16(2), p. 534–542.

MARC, n.d. *MARC Technologies.* [Online] Available at: https://www.marctech.com.au-/contact-us/ [Accessed 25 October 2019].

Maledi, N., 2017. *Characterisation of Mineral Matter in South African Coals Using Micro-Raman Spectroscopy and Other Techniques,* Johannesburg: University of the Witwatersrand (PhD thesis).

Manninen, H., Peltola, K. & Ruuskanen, J., 1997. Co-Combustion of Refuse-Dervied and Packaging-Derived Fuels (RDF and PDF) with Conventional Fuels. *Waste Management and Research,* 15(2), pp. 137-147.

Materazzi, M., Lettieri, P., Taylor, R. & Chapman, C., 2016. Performance analysis of RDF gasification in a two stage fluidized bed - plasma process. *Waste Management,* Volume 47, pp. 256-266.

Metrohm, n.d. *Metrohm Process Analysers.* [Online] Available at: https://www.metrohm.-com/en-gb/products-overview/process-analyzers/ [Accessed 26 October 2019].

Miller, B., 2011. *Clean Coal Engineering Technology.* 2 ed. United Kingdom: Butterworth-Heinemann.

Muthuraman, M., Namioka, T. & Yoshikawa, K., 2010. A comparative study on co-combustion performance of municipal solid waste and Indonesian coal with high ash Indian coal: A thermogravimetric analysis. *Fuel Processing Technology,* Volume 91, pp. 550-558.

Norton, G. A., Malaby, K. L. & DeKalb, E. L., 1988. Chemical Characterization of Ash Produced during Combustion of Refuse-Derived Fuel with Coal. *ES&T Research,* 22(11), pp. 1279-1283.

Norton, G. A., 1993. A review of the derivative thermogravimetric technique (burning profile) for fuel combustion studies. *Thermochimica Acta,* 214(2), 171–182.

Porshnov, D., Ozols, V., Ansone-Bertina, L., Berlakovs, J., & Klavins, M., 2018. Thermal decomposition study of major refuse derived fuel components. *Energy Procedia,* Volume 147, pp. 48-53.

Prevost, X., 2003. *SA coal resources and reserves, a present-day outlook.* s.l., South Aflican Institute of Mining and Metallurgy.

Provis, J., 2016. On the use of the Jander equation in cement hydration modelling. *RILEM Technical Letters,* Volume 1, p. 62 – 66.

PWC, 2017. *SA Mine 9th edition,* s.l.: PWC.

Ramani, R. & Evans, M., 1998. *Coal Mining.* [Online] Available at: https://www.britannica-.com/technology/coal-mining [Accessed 23 April 2019].

Rautenbach, R., Strydom, C., Bunt, J., Matjie, R., Campbell, Q., & van Alphen, C., 2018. Mineralogical, chemical, and petrographic properties of selected South African power stations' feed coals and their corresponding density separated fractions using float-sink and reflux

classification methods. *International Journal of Coal Preparation and Utilization,* Volume 87, pp. 1-26.

Rensburg, W., Bishopp, D. & Savage, W., 1969. *South Africa's Coal Resources*, s.l.: Coal Advisory Board.

Retsch, n.d. *Cutting Mill SM 200.* [Online] Available at: https://www.retsch.com/products-/milling/cutting-mills/sm-200/function-features/[Accessed 25 October 2019].

Rigamonti, L., Grosso, M. & Biganzoli, L., 2012. Environmental Assessment of Refuse-Derived Fuel Co-Combustion in a Coal-Fired Power Plant.

Rotheut, M. & Quicker, P., 2017. Energetic utilization of refuse derived fuels from landfill mining. *Waste Management* , Volume 62, pp. 101-117.

RTI, 2007. *Human and Ecological Risk Assessment of Coal Combustion Wastes,* North Carolina: RTI.

Schweinfurth, S., 2009. *Chapter C: An Introduction to Coal Quality,* Virginia: U.S. Geological Survey Professional Paper 1625–F.

Sharma, A., Saikia, A., Khare, P., Dutta, D., & Baruah, B., 2014. The chemical composition of tertiary Indian coal ash and its combustion behaviour – a statistical approach: Part 2. *Journal of Earth System Sciences,* 123(6), p. 1439–1449.

Shen, X., n.d. Coal Combustion and Combustion Products. In: *Coal, Oil Shale, Natural Bitumen, Heavy Oil and Peat.* s.l.:Encyclopedia of Life Support Systems.

Smith, S., Neavel, R., Hippo, E. & Miller, R., 1981. DTGA combustion of coals in the Exxon coal library. *Fuel,* Volume 60, pp. 458-462.

StatsSA, 2014. *The importance of coal.* [Online] Available at: http://www.statssa-.gov.za/?page_id=1854&PPN=P0441&SCH=5957 [Accessed 10 April 2019].

StatsSA, 2018. *Coal Remains South Africa's Dominant Source of Energy.* [Online] Available at: http://www.statssa.gov.za/?p=11292[Accessed 12 September 2018].

Tappi, 2007. *Ash in wood, pulp, paper and paperboard: Combustion at 525C.* s.l.:Tappi.

Taylor, D., Tompkins, M., Kirton, S., Mauney, T., & Natusch, D., 1982. Analysis of Fly Ash Produced from Combustion of Refuse-Derived Fuel and Coal Mixtures. *Environmental Science and Technology,* Volume 16, pp. 148-154.

Teixeira, P., Lopes, H., Gulyurtlu, I., Lapa, N., & Abelha, P., 2012. Evaluation of slagging and fouling tendency during biomass co-firing with coal in a fluidized bed. *Biomass and Bioenergy,* Volume 39, pp. 192-203.

Umraw, A., 2019. *Quality of Gupta-supplied coal to Eskom questioned at state capture inquiry.* [Online] Available at: https://www.timeslive.co.za/politics/2019-02-26-quality-of-

gupta-supplied-coal-to-eskom-questioned-at-state-capture-inquiry/[Accessed 25 October 2019].

Vamvuka, D., El Chatib, N. & Sfakiotakis, S., 2011. *Measurements of Ignition Point and Combustion Characteristics of Biomass Fuels and their Blends with Lignite.* [Online] Available at: https://www.researchgate.net/publication/232168026 [Accessed 4 December 2018].

Vamvuka, D., Sfakiotakis, S. & Saxioni, S., 2015. Evaluation of urban wastes as promising co-fuels for energy production – A TG/MS study. *Fuel,* Volume 147, pp. 170-183.

Vekemans, O. & Chaouki, J., 2016. Municipal Solid Waste Cofiring in Coal Power Plants: Combustion Performance . In: *Developments in Combustion Technology.* s.l.:s.n., pp. 118-142.

Waanders, F., Vinken, E., Mans, A. & Mulaba-Bafubiandi, A., 2003. Iron Minerals in Coal, Weathered Coal and Coal Ash - SEM and Mossbauer Results. *Hyperfine Interactions.*

Wagner, N., Malumbazo, N. & Falcon, R., 2018. *Southern African Coals and Carbons.* Cape Town: Stuik Nature .

Wan, H., Chang, Y., Chien, W., Lee, H., & Huang, C., 2008. Emissions during co-firing of RDF-5 with bituminous coal paper sludge and waste tires in a commercial circulating fluidized bed co-generation boiler. *Fuel,* Volume 87, p. 761–767.

Wang, J., Zhang, S., Guo, X., Dong, A., Chen, C., Xiong, S., Fang, Y., Yin, W., 2012. Thermal Behaviors and Kinetics of Pingshuo Coal/Biomass Blends during Copyrolysis and Cocombustion. *Energy and Fuels,* Volume 26, p. 7120−7126.

Wang, G., Zhang, J., Shao, J., Liu, Z., Zhang, G., Xu, T., Guo, J., Wang, H., Xu, R., Lin, H., 2016. Thermal behavior and kinetic analysis of co-combustion of waste biomass/low rank coal blends. *Energy Conversion and Management,* Volume 124, p. 414–426.

WorldBank, 2019. *Solid Waste Management.* [Online] Available at: http://www.worldbank-.org/en/topic/urbandevelopment/brief/solid-waste-management [Accessed 23 May 2019].

WRI, 2014. *Climate Analysis Indicators Tool (CAIT) Version 2.0.*. Washington, DC, World Resources Institute.

Wu, H., Glarborg, P., Frandsen, F., Dam-Johansen, K., Jensen, P., & Sander, B., 2011. Co-combustion of pulverized coal and solid recovered fuel in an entrained flow reactor – General combustion and ash behaviour. *Fuel,* Volume 90, pp. 1980-1991.

Yan, J., Zhu, H., Jiang, X., Chi, Y., & Cen, K., 2009. Analysis of volatile species kinetics during typical medical waste materials pyrolysis using a distributed activation energy model. *Journal of Hazardous Materials,* Volume 162, p. 646–651.

Yang, H. Yan, R., Chen, H., Lee, D., & Zheng, C., 2007. Characteristics of hemicellulose, cellulose and lignin pyrolysis. *Fuel,* Volume 86, p. 1781–1788.

Yelland, C., 2019. *Special report: New pressures on Eskom's plant performance as contract workers down tools.* [Online] Available at: https://www.fin24.com/Economy/Eskom/special-report-new-pressures-on-eskoms-plant-performance-as-contract-workers-down-tools-20190207 [Accessed 25 October 2019].

Zabetta, E., Barisic, V., Peltola, K. & Hotta, A., 2008. *Foster Wheeler Experience with Biomass and Waste in CFBs,* Finland: Foster Wheeler – R&D Department.

Zhang, S., Lin, X., Chen, Z., Li, X., Jiang, X., & Yan, J., 2018. Influence on gaseous pollutants emissions and fly ash characteristics from co-combustion of municipal solid waste and coal by a drop tube furnace. *Waste Management,* Volume 81, p. 33–40.

Zhao, L., Wang, Z., Chen, D., Ma, X., & Luan, J., 2012. Influence of impurities on waste plastics pyrolysis: products and emissions.. *Environmental Sciences,* Volume 33, p. 329–336.

APPENDIX A

Table A. 1: Repeat results of proximate analysis and calorific value tests

	Moisture (%)	Volatile Matter (%)	Ash (%)	Fixed Carbon (%)	Calorific Value
P1	4.41	83.28	4.98	7.33	24.93
P1 repeat	3.53	81.87	7.25	7.35	24.82
P2	3.58	82.36	5.75	8.31	22.51
P2 repeat	3.4	82.99	5.57	8.04	22.13
PL	1.02	81.69	11.42	5.87	31.15
PL repeat	1.44	81.64	10.79	6.13	31.31
PB	3.19	81.23	6.65	8.92	22.08
PB repeat	3.19	81.07	6.66	9.08	22.4
C1	2.21	22.87	29.74	45.19	21.74
C1 repeat	2.27	22.88	29.09	45.76	21.7
C2	2.08	20.26	41.92	35.74	16.75
C2 repeat	2.04	20.07	41.97	35.92	16.7

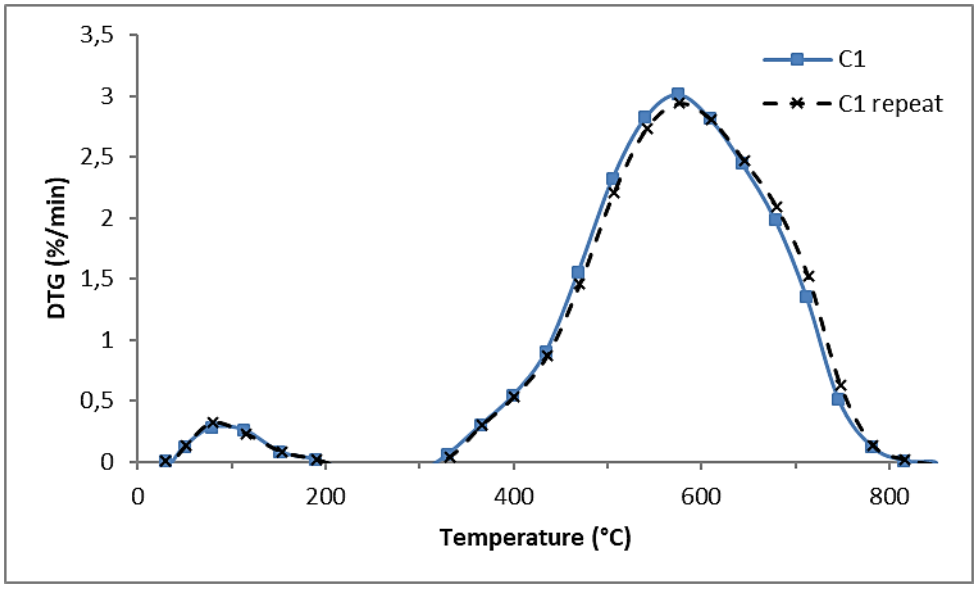

Figure A. 1: Repeat combustion tests of ROM coal

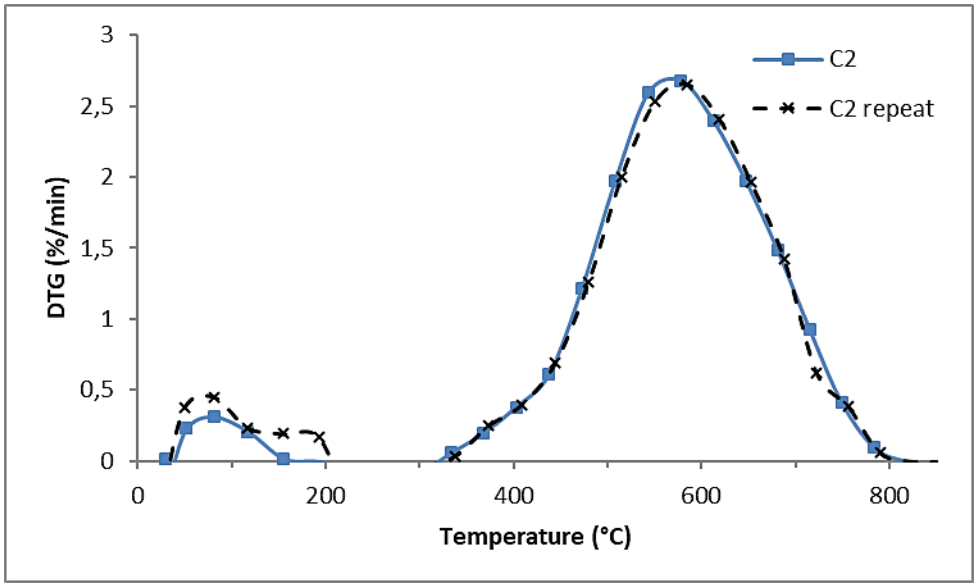

Figure A. 2: Repeat combustion tests of discard coal

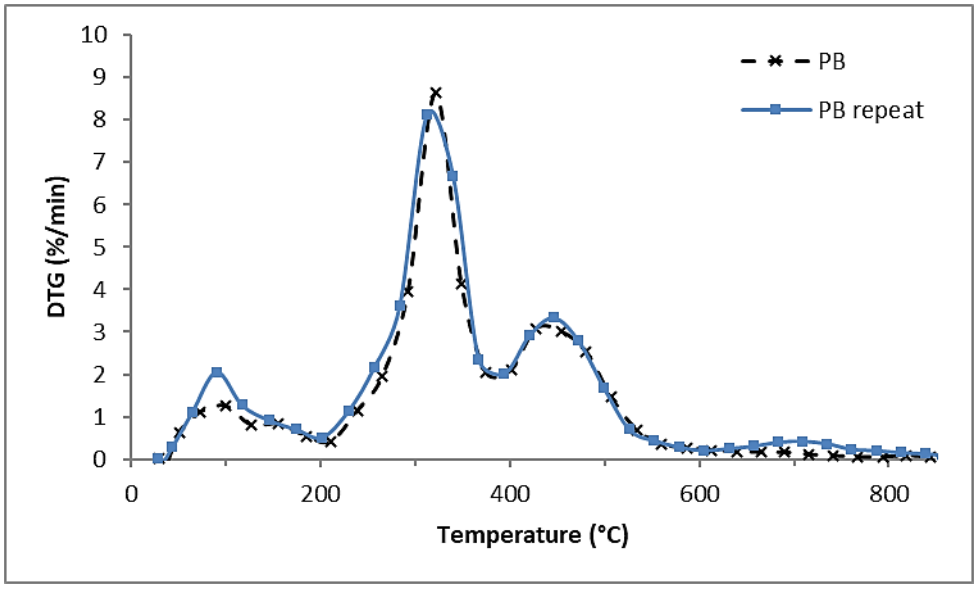

Figure A. 3: Repeat combustion tests of RDF PB

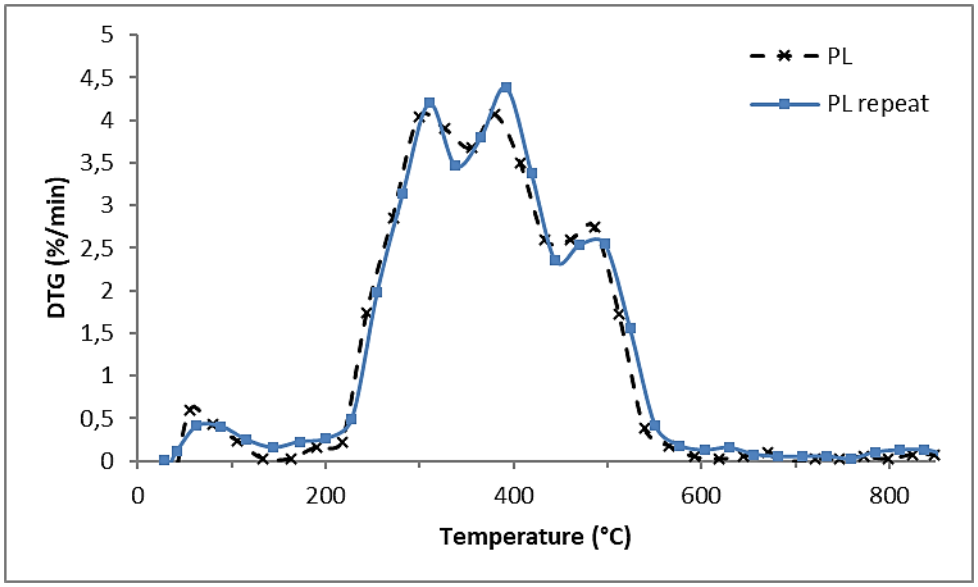

Figure A. 4: Repeat combustion tests of RDF PL

The intersection method for determining ignition temperature

The figure below shows how the intersection method was used to determine the ignition temperatures from the combustion profiles. Point A is the point at which the line through the peak temperature intersects with the TG plot. Point B is the point at which the horizontal line through the devolatilisation temperature intersects with the gradient line from point A. The vertical line from this point to the x-axis gives the ignition temperature.

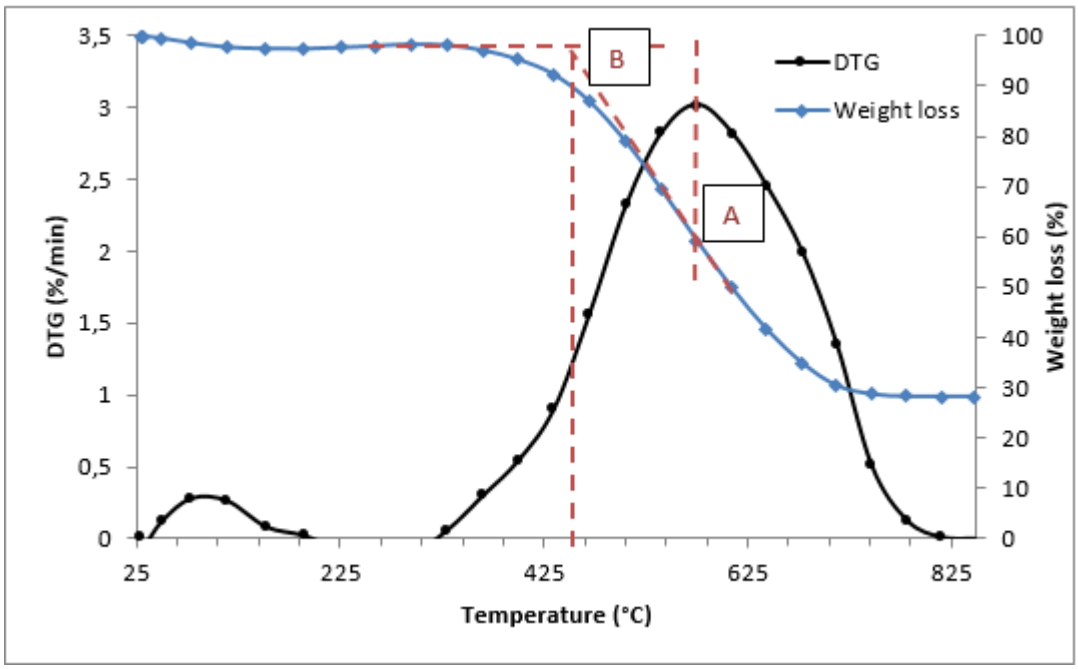

Figure A. 5: The intersection method for ignition temperature

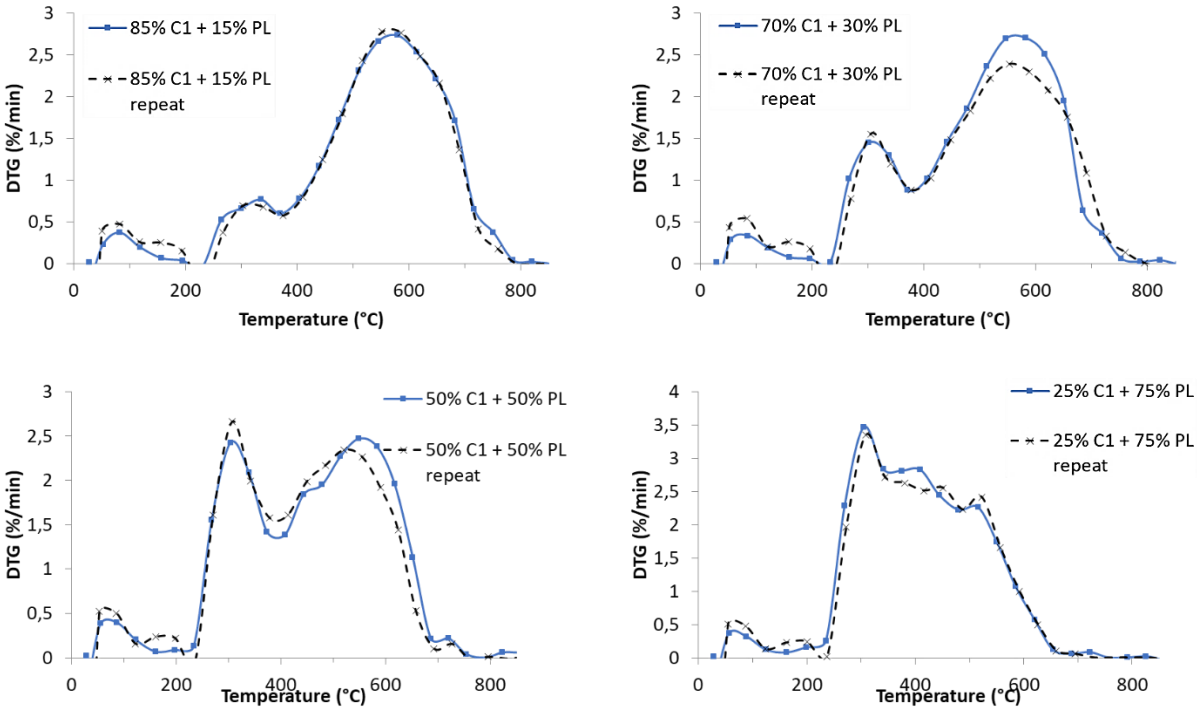

Figure A. 6: Repeat co-combustion tests of C1 and PL

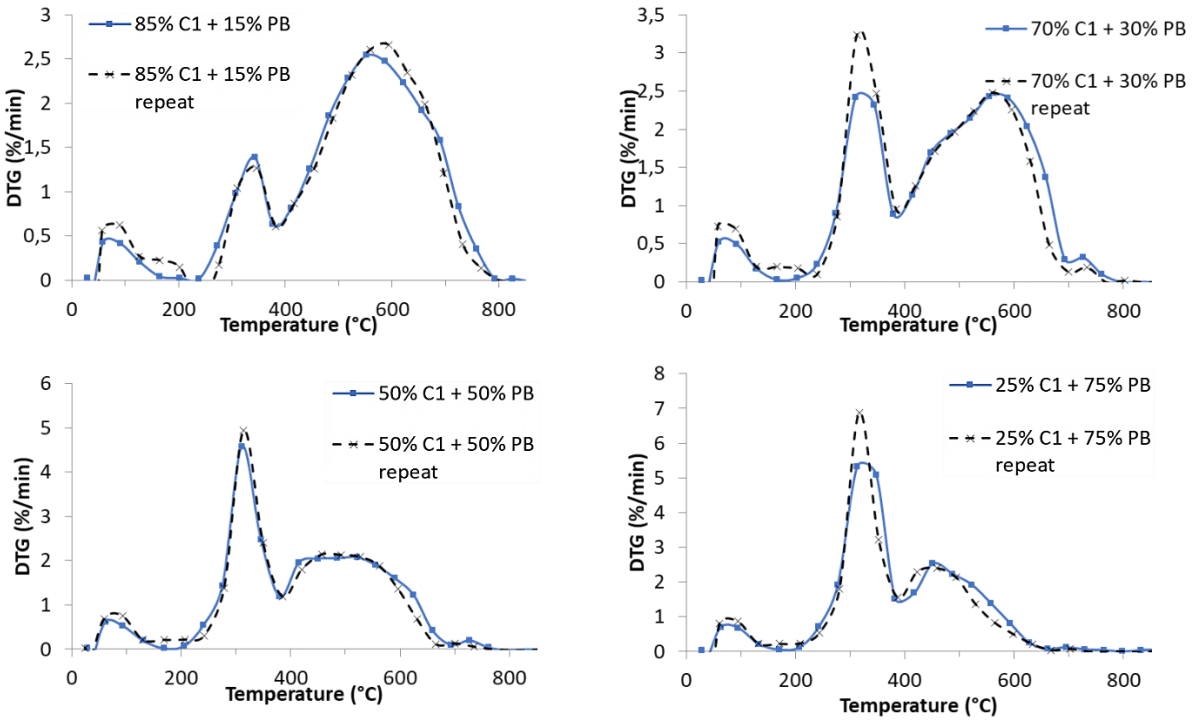

Figure A. 7: Repeat co-combustion tests of C1 and PB

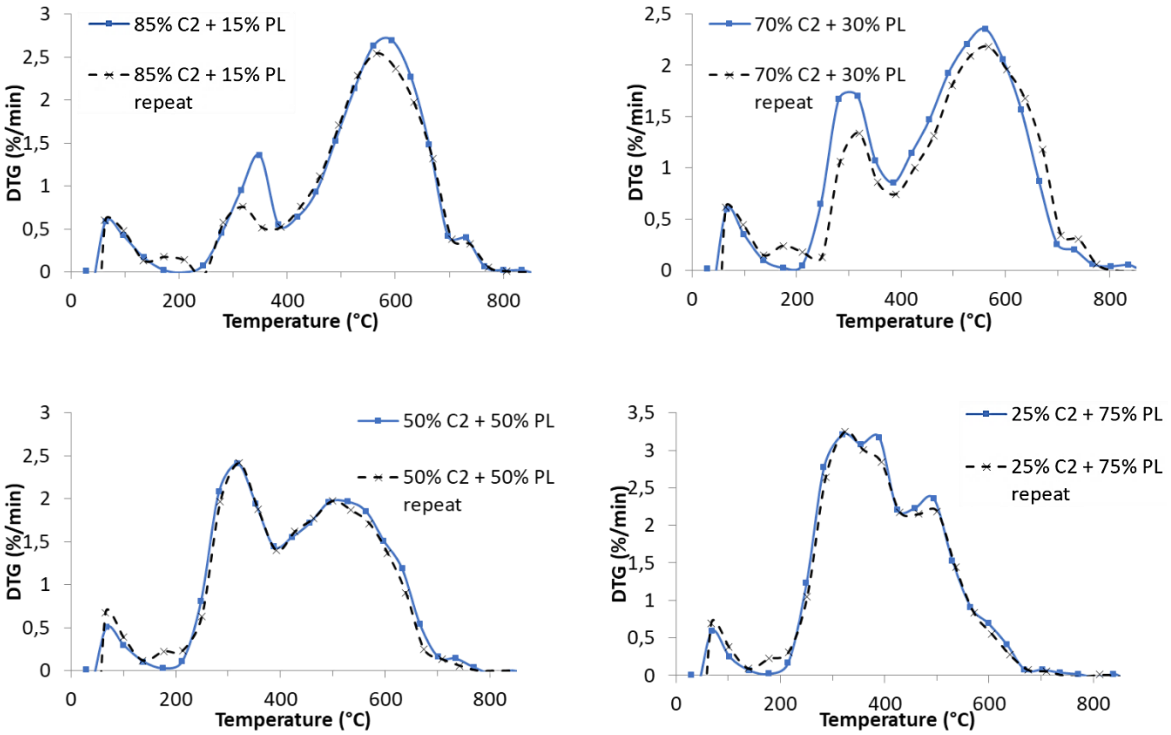

Figure A. 8: Repeat co-combustion tests of C2 and PL

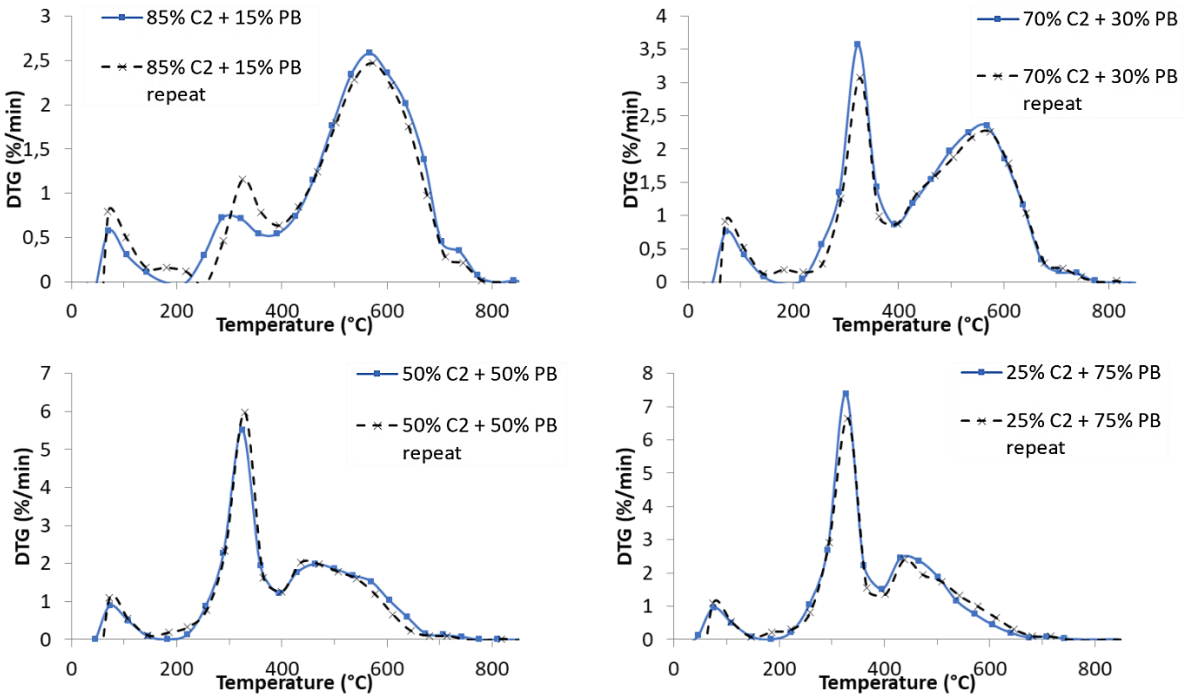

Figure A. 9: Repeat co-combustion tests of C2 and PB

APPENDIX B

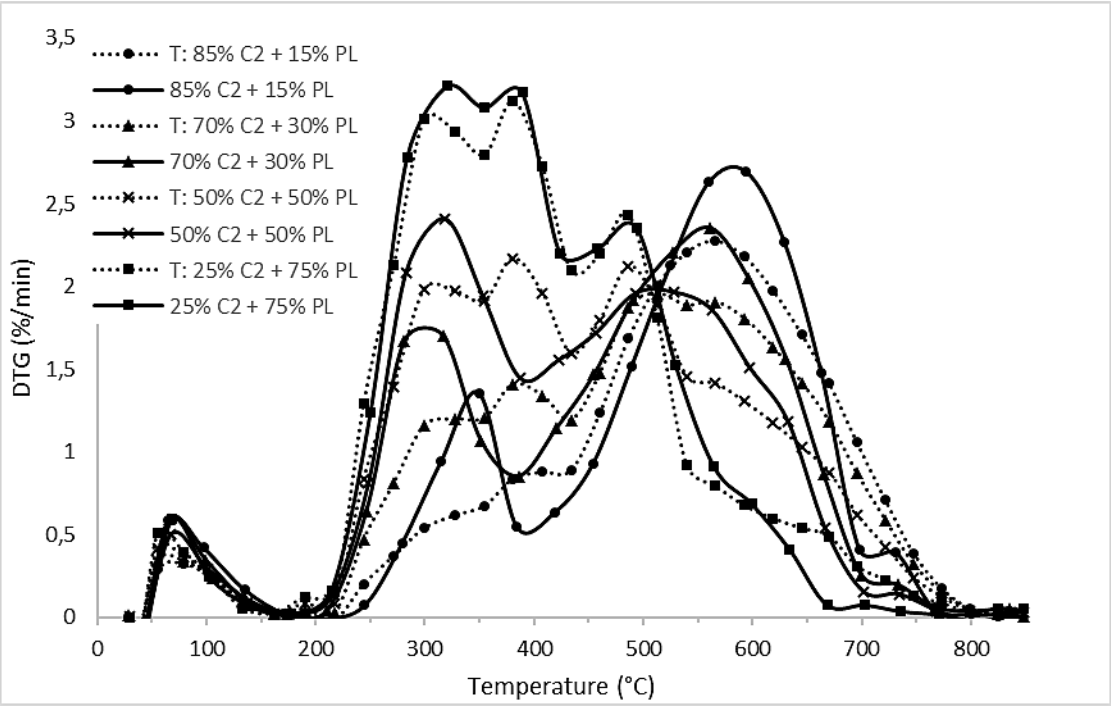

Figure B. 1: The theoretical and experimental DTG plots of C2 and RDF PL

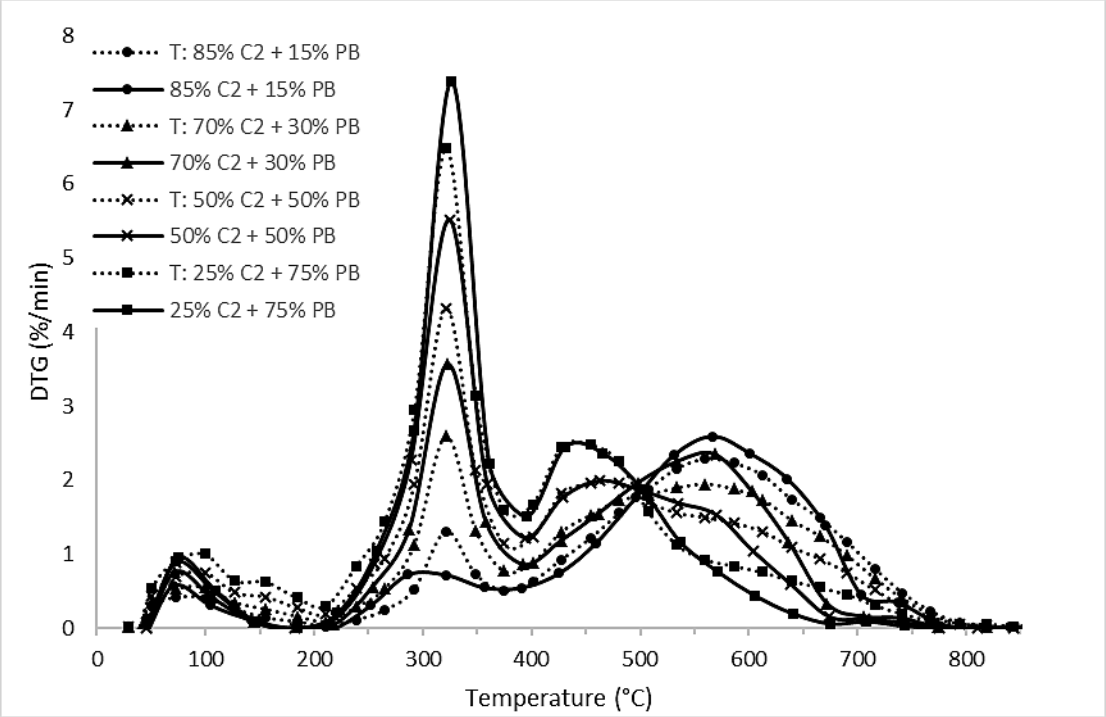

Figure B. 2: The theoretical and experimental DTG plots of C2 and RDF PB

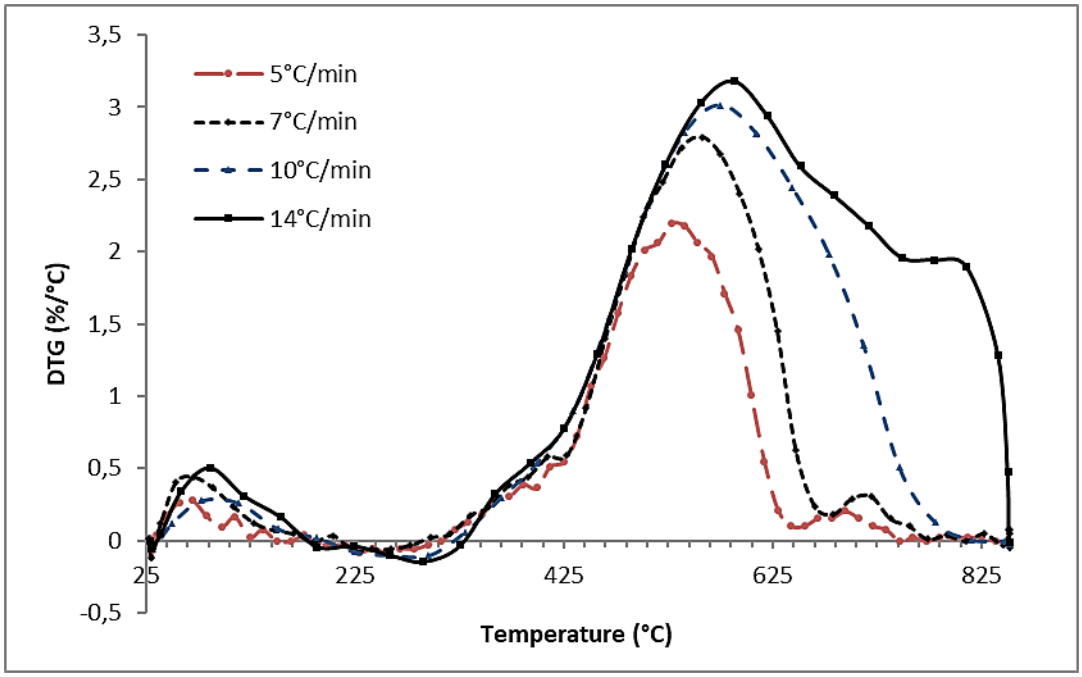

Figure B. 3: C1 combustion profile at different heating rates

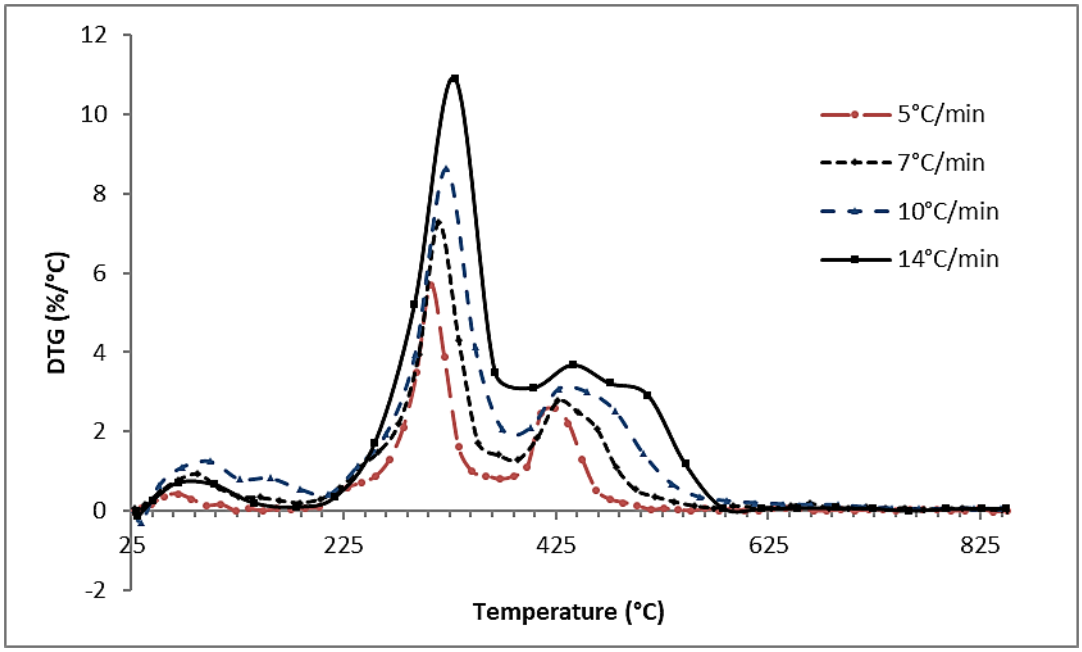

Figure B. 4: PB combustion profile at different heating rates

APPENDIX C

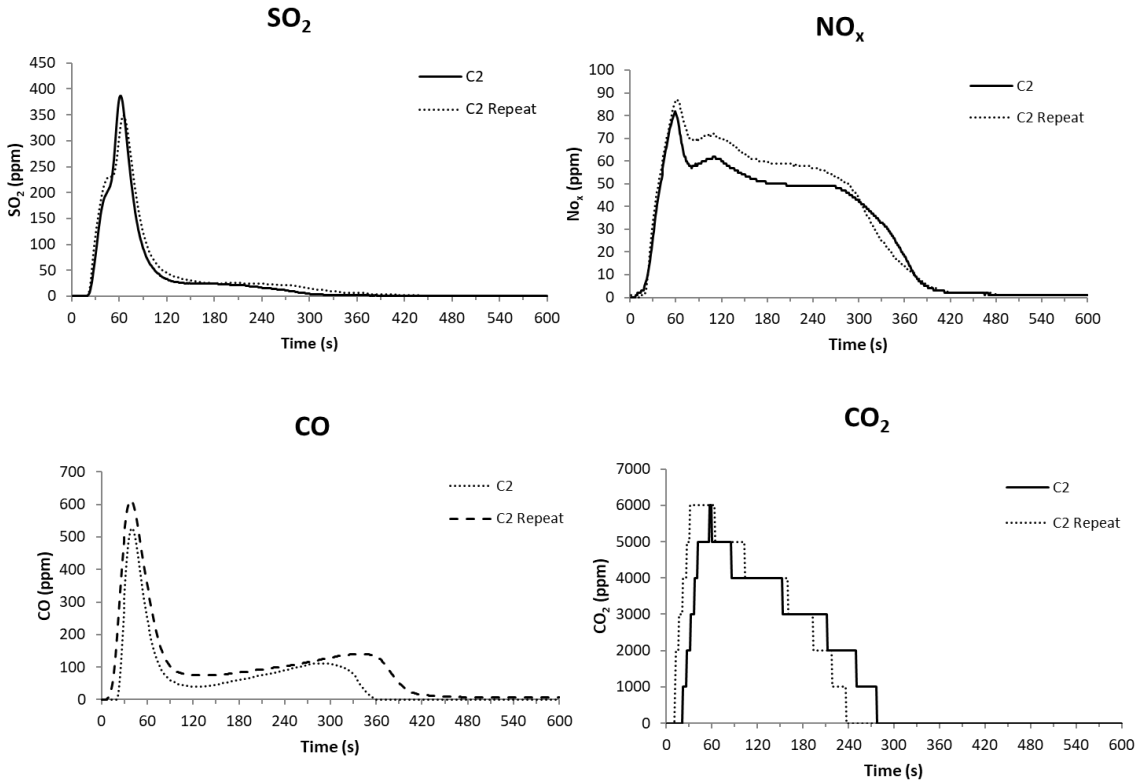

Figure C. 1: Repeat analysis of gaseous emissions of sample C2

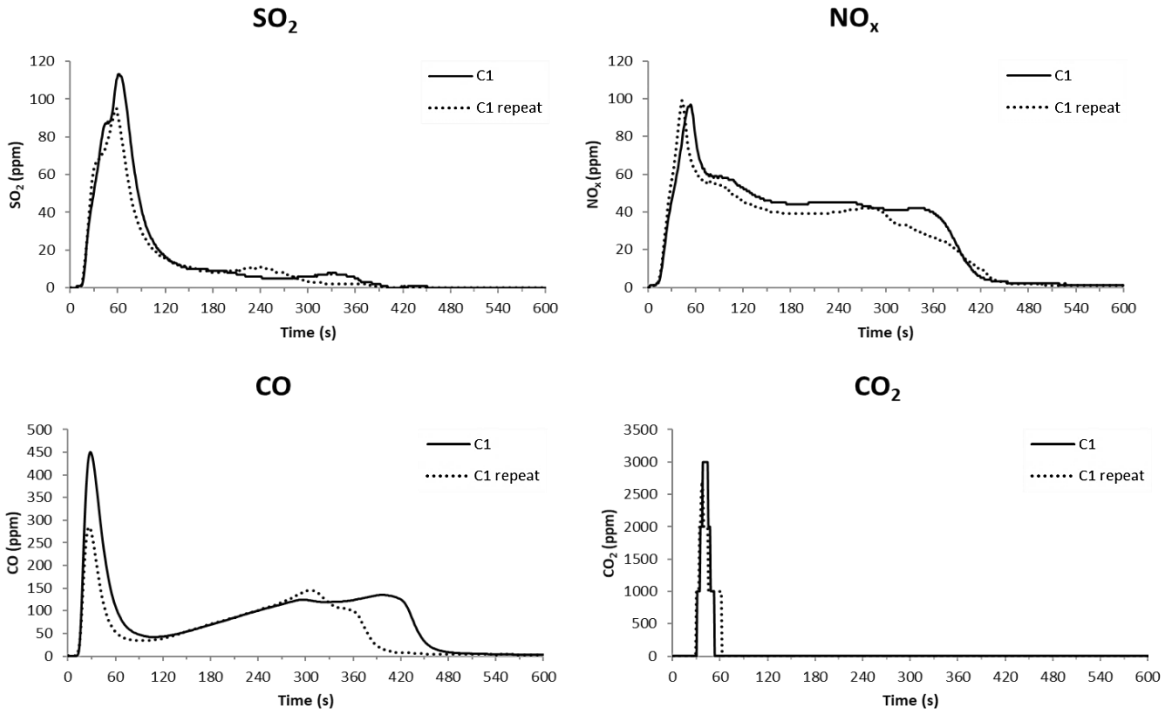

Figure C. 2: Repeat analysis of gaseous emissions of sample C1

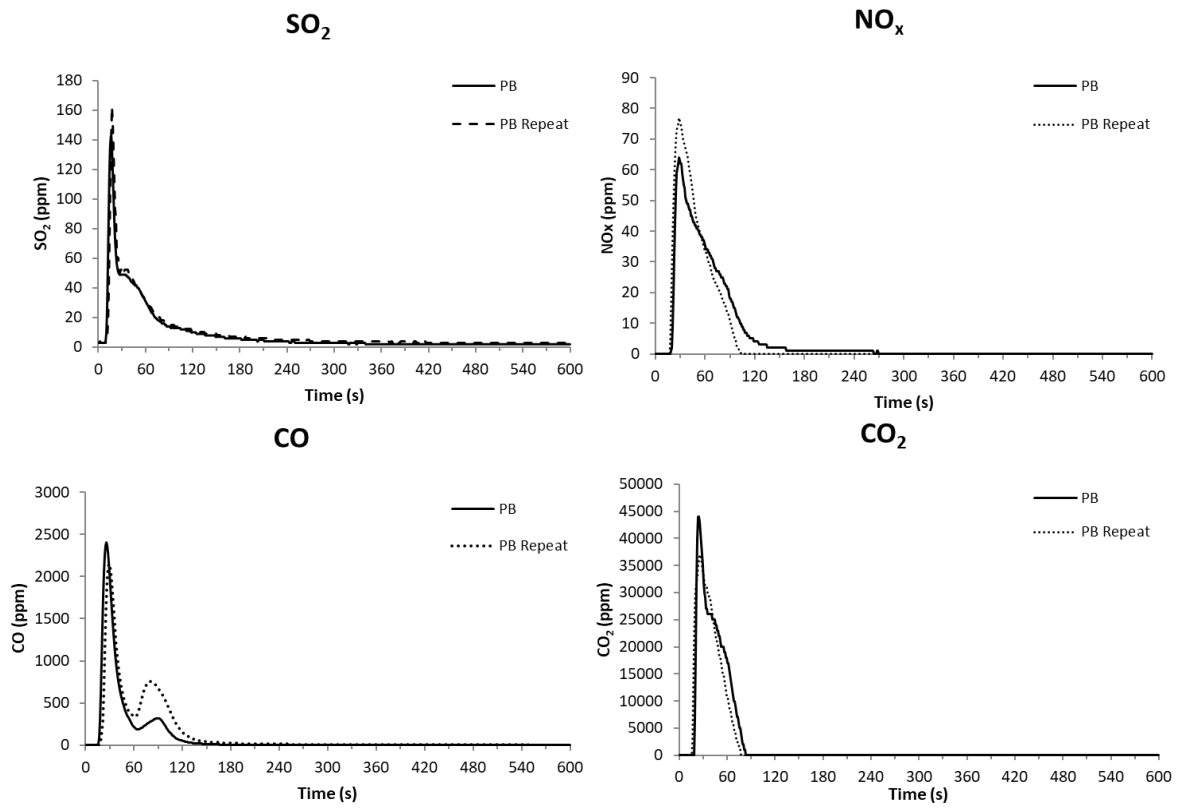

Figure C. 3: Repeat analysis of gaseous emissions of sample PB

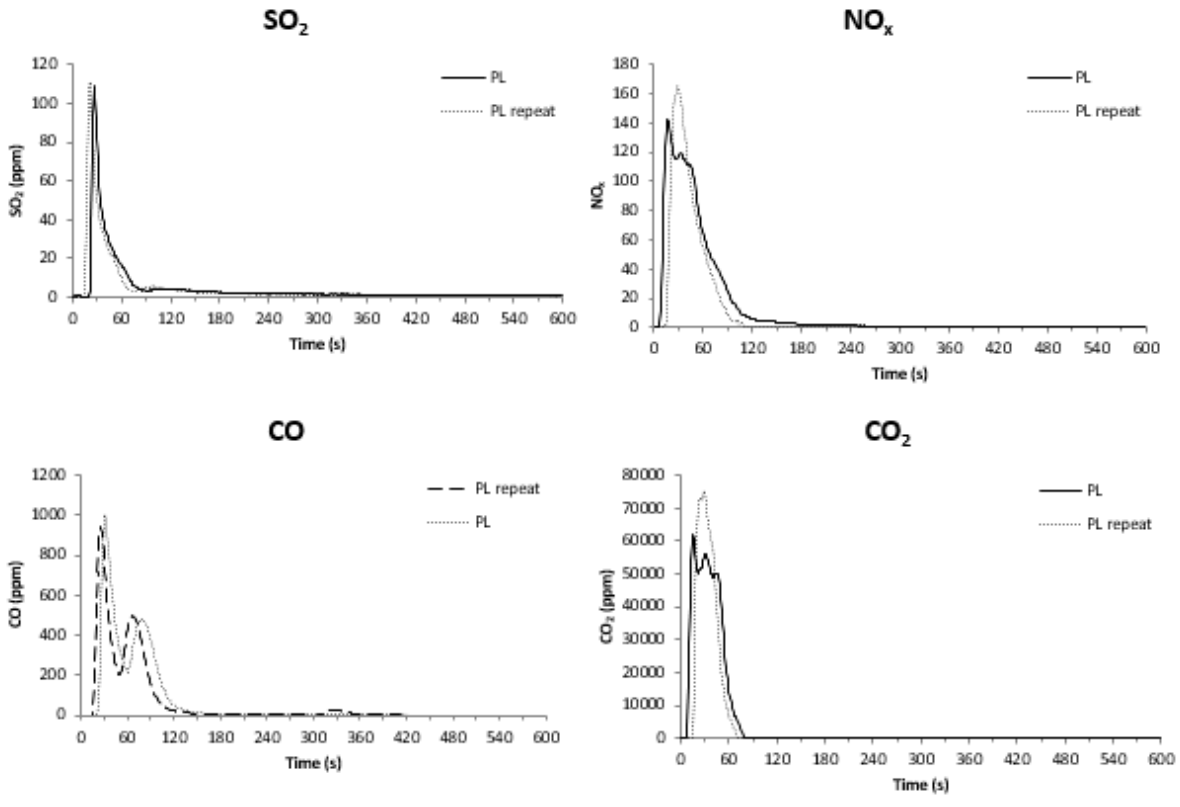

Figure C. 4: Repeat analysis of gaseous emissions of sample PL

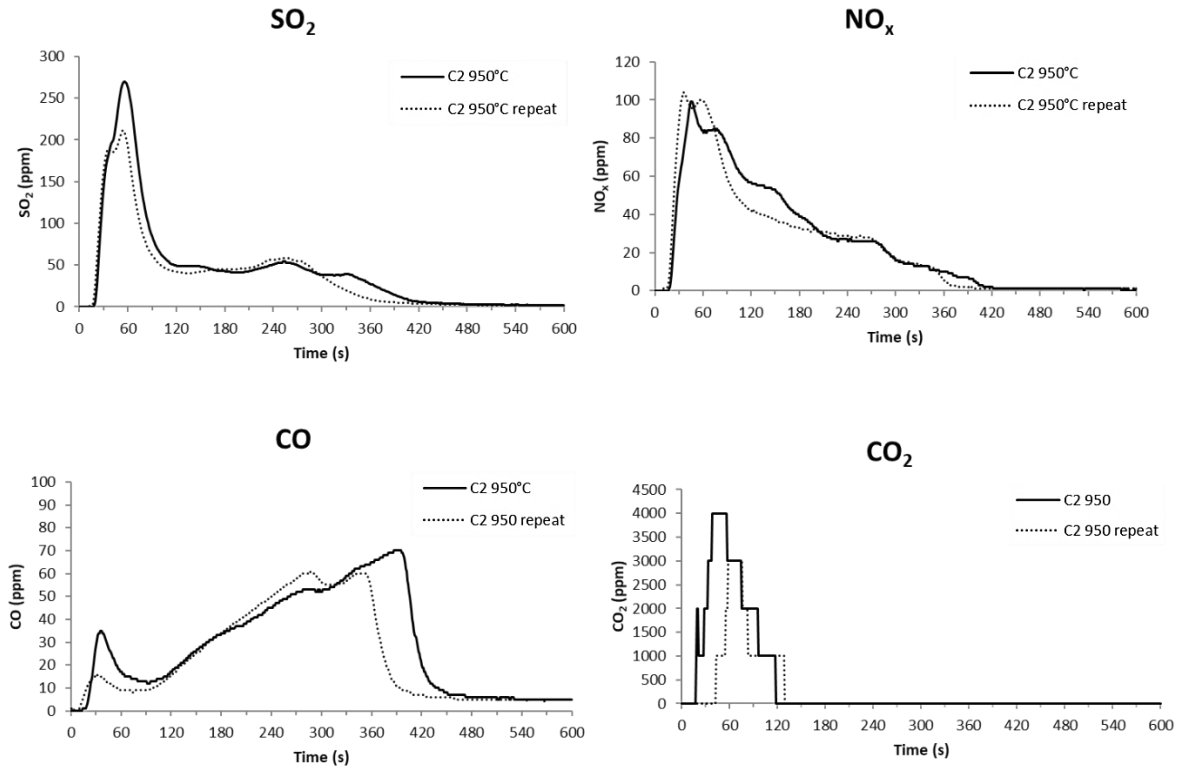

Figure C. 5: Repeat analysis of gaseous emissions of sample C2 at 950°C